Optical Detection of Acetyl Phosphate and Biogenic Amines

DISSERTATION ZUR ERLANGUNG DES DOKTORGRADES DER
NATURWISSENSCHAFTEN (DR. RER. NAT.) DER FAKULTÄT
CHEMIE UND PHARMAZIE DER UNIVERSITÄT REGENSBURG

vorgelegt von

Mark-Steven Steiner

aus Wien (Österreich)

im November 2010

Optical Detection of Acetyl Phosphate
and Biogenic Amines

PhD Thesis

by

Mark-Steven Steiner

Für meine Familie

Diese Doktorarbeit entstand in der Zeit von Oktober 2007 bis November 2010 am Institut für Analytische Chemie, Chemo- und Biosensorik an der Universität Regensburg.

Die Arbeit wurde angeleitet von Prof. Dr. Otto S. Wolfbeis.

Promotionsgesuch eingereicht am:

Kolloquiumstermin: 08.12.2010

Prüfungsausschuss:

Vorsitzender: Prof. Dr. Frank-Michael Matysik

Erstgutachter: Prof. Dr. Otto S. Wolfbeis

Zweitgutachter: Prof. Dr. Joachim Wegener

Drittprüfer: Prof. Dr. Jörg Heilmann

Danksagung

Mein erster Dank gilt besonders Herrn **Prof. Dr. Otto S. Wolfbeis** für die Bereitstellung des interessanten Themas, als auch für die hilfreichen Anregungen, die Betreuung meiner Arbeit und die hervorragenden Arbeitsbedingungen am Lehrstuhl.

Weiterhin möchte ich mich bei Herrn **Dr. Axel Dürkop** für die gute Betreuung und die zahlreichen Diskussionen während meiner Doktorarbeit bedanken.

Außerdem danke ich allen Mitarbeitern des Lehrstuhls für die ausgezeichnete kollegiale Arbeitsatmosphäre, die Hilfestellungen und fortwährende Unterstützung, die zur Vollendung der Dissertation beigetragen haben. Vielen Dank auch an meine ehemaligen Laborkollegen und besonders an **Dr. Christian Spangler** für die stets lockere und angenehme Laborzeit. Dem Kaffeerunden-Team danke ich für willkommene Ablenkung von der täglichen Arbeit und die vielen Übungsstunden in „Zurückhaltung". Spezieller Dank gilt Herrn **Dominik Grögel** für das Teilen desselben harten Schicksals.

Robert Meier gebührt mein Dank für die vielen hübschen bunten Fotos und die technische Hilfe bei der Erstellung des RGB-Messsystems. Für die handwerkliche Arbeit an diesem System danke ich der Elektronik- und Feinmechanikwerkstatt. Herrn **Dr. Alexander Riechers** danke ich für die Bereitstellung von Bis Cyclen und die vielen anregenden Gespräche.

Meinen Azubis **Roxane Harteis**, **Sabine Hofmeister** und **Matthias Hautmann** danke ich recht herzlich für die nette Laborzeit und großartige Hilfe bei der Arbeit – ich hoffe ihr hattet genau so viel Spaß wie ich! Vielen Dank auch an **Johannes Reich** für die geleistete Arbeit während seiner Bachelor Arbeit. Außerdem danke ich Frau **Sarka Bidmanova** und Herrn **Gasser Khairy** für die interessante internationale Zusammenarbeit im Rahmen des Projekts EGY 08/004. Frau **Benz** (ETH Zürich), Herrn **Dr. Stepp** (LFL München) und Herrn **Dr. Schubert** (R-Bio, Darmstadt) danke ich für die gemeinsamen Arbeiten während des Tumor Vision Projekts.

Ganz besonders möchte ich mich bei **Gisela Hierlmeier** und **Barbara Goricnik** für die nie endenden Quellen an Py-1 bzw. Zellen und Bakterien, Geduld und guter Laune bedanken.

Table of Contents

4 Determination of Acetyl Phosphate *via* a Luminescent Ruthenium Ligand Complex   52

1 Introduction and Aim of Work

Over the past decade, the concepts of food control, food safety, and food hygiene have attracted public attention on an unprecedented scale. A number of uncovered incidents throughout the world unsettled the consumers' reliance on the food supply, including bovine spongiform encephalopathy (BSE) in beef[1] and melamine in dairy products from China[2], listeria-tainted meat in Canada[3], dioxins in pork and milk products from Belgium, contamination of foods with pesticides in Japan, tainted Coca Cola in Belgium and France, pesticides in soft drinks in India, and salmonella in peanuts in USA.[4,5] The governments of numerous countries – with the European Union (EU) leading the way – attempted to counteract this loss of confidence by reorganizing their management of food safety issues and food safety-related legislation. Examples are the Codex Alimentarius standards (WHO/FAO), the General Food Law (European Union 2002/178) and the EU BSE Regulations.[6] Further on, food manufacturers and the food-processing industry are using good manufacturing practices (GMPs) as a primary basis to reduce, control, or – at best – eliminate food borne hazards. These concepts are fostered by the Hazard Analysis and Critical Control Point (HACCP) system that was introduced in the US in the 1960s. It provides the means to analyze and target specific steps in food production (critical control points) for prevention, mitigation, or control of food contamination.[7,8] Current EU legislation defines food contaminants as any substance not intentionally added to food, which is present in food as a result of the production, manufacture, processing, preparation, treatment, packaging, transport, or holding of such food, or as a result of environmental contamination. Among those, organic contaminants can be chemicals or biologicals.[9]

The hygienic condition of food is largely influenced by the amount of microorganisms present in the food and their activity. Hence, the presence of them does not relate to a lower food-quality. Fermented food, for example, is processed by the action of microorganism and referred to as hygienically secure. Only a high unwanted activity of microorganism leads to spoilage of food. But even this is not an adequate and general criterion, because delicatessen products, for example, show less or negligible amounts of microorganisms at the end of their durability than the fresh-product, so microbiological stability is pretended to exist.

Microorganisms are ubiquitous in the environment, and they may infect fresh food as well as stored products and also drinking water. Furthermore, several microorganisms produce toxic metabolites. Certain types of microorganisms may also proliferate on entering in gastrointestinal tract, where the specific conditions contribute to their excessive growth.[10,11] Therefore, food borne bacteria represent a twofold problem for food manufacturers and consumers

Up to date, bacterial contamination of food and drinking water is still not only an issue of less industrialized countries. Throughout the past years, major food-borne bacterial targets – *E.Coli*, *Salmonella*, *Listeria, Staphylococus aureus* and *Campylobacter* – have persisted, commanding research and surveillance attention also from government agencies in the industrial countries. These bacterial pathogens together constitute the greatest burden of food-borne illness. Not surprisingly therefore, these diseases also command the majority of public health interest and policy maker awareness in intestinal infectious diseases.[12]

The analysis of food borne bacteria is an important topic that encompasses many disciplines including chemistry, biochemistry and microbiology. The bacterial contamination of food is either determined by direct evaluation of the quantity of bacteria in a given sample. Heterotrophic plate count (HPC) is a procedure used to estimate the number of heterotrophic bacteria that form colonies on agar plates. The HPC analysis presently employed takes 24 to 48 h.[13] HPC is a time consuming process that requires specially equipped laboratories and trained personnel.

The presence of bacteria can also be addressed indirectly by determination of their metabolites. Instrumental analytical methods like high pressure liquid chromatography (HPLC)[14,15], capillary electrophoresis (CE)[16,17], mass spectrometry (MS)[18], and various combinations thereof are used to target a large number of microbial metabolites at a time. These methods are also of use for the determination of unidentified toxins. But again, instrumentation is costly and the process time consuming.

Specific targeting of one analyte or one chemical class of analytes is most often more economic. The development of carbon dioxide for instance is commonly used in hospitals to monitor the sterility and bacterial growth in clinical specimen.[19,20] Measurement of CO_2 using gas chromatography[21,22], radiometric techniques[23], or an infrared CO_2 analyzer[24-26] have all been successfully used in determining the level of

contamination by mesophilic and coliform bacteria in food samples, including hamburger, milk, water, catfish, and bottled juice.

Furthermore, bioluminescence based test kits are commercially available that use the presence of ATP in bacterial contaminated samples. The ATP is converted *via* firefly luciferase so to yield a fluorescent information.[27] The amount of light produced by the firefly luciferase is directly proportional to the amount of ATP in the sample, and hence, also proportional to the amount of bacteria in the sample.[28 -30] This assays can be conducted within 5 min and the test result is automatically evaluated by a handheld device.[31]

Acetyl phosphate (AcP) is another specific analyte in the determination of some prokaryotes. It is primarily used by bacteria to regenerate their ATP pool.[32] Up to date, there is no commercially available assay for the determination of food quality using AcP. However, its metabolic breakdown product acetate is an important target for the quality management of fermented foods like vine, vinegar, and beer.[33,34]

Further on, biogenic amines (BAs) are ubiquitous in animally, herbal and microbiologically metabolic products in a multitude of foods, which also include vegetables and fruits. They can be important indicators of food quality. The amount of histamine, putrescine and cadaverine, for example, can give rapid information on the decomposition of fish, meat, cheese, vine or sauerkraut. High amounts of BA can indicate a risk of health for consumers.[35 - 37]

Reliable, rapid, and simple methods for the determination of these bacterial metabolites are required. On the one hand, new specific and sensitive probes – preferably of the fluorescent or fluorogenic type – need to be developed for in-laboratory analytics of food. On the other hand, there is also a great demand on small and simple test kits – preferably in the test strip format – that are applicable to in-field determination of food quality.

The first major aim of this work was to develop a selective and sensitive fluorescent probe for the determination of the microbial metabolite acetyl phosphate. Detection should be carried out under biocompatible reaction conditions (37 °C, aqueous buffered solution of pH 7) with a short incubation time. In a first step, state-of-the-art probes for acetate and phosphate (the breakdown products of AcP) were to be screened for their spectral responses towards AcP. In a second step, new ruthenium based, and fluorescent probes for the specific determination of AcP were to be designed, synthesized, and characterized with respect to selectivity towards

AcP in organic solvents and highly competitive aqueous solutions and response towards other biologically important anions.

The second major aim of this work was to develop a rapid method for the determination of biogenic amines as they occur as a result of bacterial contamination. This method was to be originated preferably in the test strip format using the amine reactive chameleon probe Py-1. The test strips required to be tested with respect to selectivity towards biogenic amines and sensitivity towards potentially interferents like proteins, ammonia and amino acids and their applicability to real samples.

1.1 References

[1] Miles S, Frewer LJ (2001) Investigating specific concerns about different food hazards. Food Quality and Preference, 12: 47–61.

[2] Barboza D (2008) China's Tainted-Food Inquiry Widens Amid Worries over Animal Feed. The New York Times. November 1st, Available from http://www.nytimes.com/2008/11/01/world/asia/01china.html.

[3] Cribb R (2008) Listeria Reporting Rule Dropped before Crisis; Deaths Preventable, Inspectors Say. The Toronto Star. October 6th, Available from http://www.thestar.com/comment/columnists/article/512306.

[4] Lehotay SJ, Mastovska K, Amirav A, Fialkov AB, Martos PA, Kok AD, Fernández-Alba AR (2008) Identification and confirmation of chemical residues in food by chromatography-mass spectrometry and other techniques. Trends Anal Chem, 27: 1070-1090.

[5] de Jonge J, van Trijp H, Goddard E, Frewer L (2008) Consumer confidence in the safety of food in Canada and the Netherlands: The validation of a generic framework. Food Qual Pref, 19: 439-451.

[6] Trienekens J, Zuurbier P (2008) Quality and safety standards in the food industry, developments and challenges. Int J Product Economics 113: 107-122.

[7] Marvin HJP, Kleter GA, Frewer LJ, Cope S, Wentholt MTA, Rowe G (2009), A working procedure for identifying emerging food safety issues at an early stage: Implications for European and international risk management practices. Food Control, 20: 345-356.

[8] Stringer MF, Hall MN (2007) A generic model of the integrated food supply chain to aid the investigation of food safety breakdowns. Food Control, 18: 755-765.

[9] European Union, Council Directive 92/59/EEC of 29 De June 1992 on General Product Safety, Official Journal L228, 11/08/1992, P.0024–0032, Brussels, 2005.

[10] Beutling DM, Askar AA (1996) Biogene Amine in der Ernährung. Springer Verlag, Berlin 1996.

[11] Chen M-F (2008) Consumer Trust in Food Safety - A Multidisciplinary Approach and Empirical Evidence from Taiwan. Risk Analysis, 28: 1553-1569.

[12] Newell DG, Koopmans M, Verhoef L, Duizer E, Aidara-Kane A, Sprong H, Opsteegh M, Langelaar M, Threfall J, Scheutz F, van der Giessen J, Kruse H (2008) Food-borne diseases - The challenges of 20 years ago still persist while new ones continue to emerge. Int J Food Microbiol, Volume, 139: S3-S15.

[13] Du X-W, Lin C-M, Phu A-T, Cornell JA, Marshall MR, Wei C-I (2002) Development of Biogenic Amines in Yellowfin Tuna (Thunnus albacares): Effect of Storage and Correlation with Decarboxylase-Positive Bacterial Flora. J Food Sci, 67: 292-301.

14   Özdestan Ö, Üren A (2009) A method for benzoyl chloride derivatization of biogenic amines for high performance liquid chromatography. Talanta, 78: 1321-1326.

15   Kirschbaum J, Rebscher K, Brückner H (2000) Liquid chromatographic determination of biogenic amines in fermented foods after derivatization with 3,5-dinitrobenzoyl chloride. J Chromatogr A, 881: 517-530.

16   Juan-García A, Font G, Picó Y (2005) Determination of organic contaminants in food by capillary electrophoresis. J Sep Sci, 28: 793-812.

17   Steiner M-S, Meier RJ, Spangler C, Duerkop A, Wolfbeis OS (2009) Determination of biogenic amines by capillary electrophoresis using a chameleon type of fluorescent stain. Microchim. Acta, 167: 259-266.

18   Santos B, Simonet BM, Ríos A, Valcárcel M (2004) Direct automatic determination of biogenic amines in wine by flow injection-capillary electrophoresis-mass spectrometry. Electrophoresis, 25: 3427-3433.

19   Carricajo A, Fonsale N, Vautrin AC, Aubert G (2001) Evaluation of BacT/Alert 3D liquid culture system for recovery of mycobacteria from clinical specimens using sodium dodecyl (lauryl) sulfate-NaOH decontamination. J Clin Microbiol 39: 3799-3800.

20   Krisher KK, Gibb P, Corbett S, Church D (2001) Comparison of the BacT/Alert PF pediatric FAN blood culture bottle with the standard pediatric blood culture bottle, the Pedi-BacT. J Clin Microbiol 39: 2880-2883.

21   Guerzoni ME, Piva M, Gardini F (1985) Proposal of a rapid HS-GLC method for microbiological control of foods. Lebensm-Wiss Technol, 18:128-132.

22   Basem A, Gardini F, Paparella A, Elisabetta M (1992) Suitability of a rapid gas chromatographic method for total mesophilic bacteria and coliform enumeration in hamburgers. Lett Appl Microbiol, 14 :255-259.

23   Previte JJ (1972) Radiometric detection of some food-borne bacteria. Appl Microbiol, 24: 535-539.

24   Threlkeld CH (1982) Detection of microbial contamination utilizing an infrared CO_2 analyzer. J Food Sci, 47: 1222-1225.

25   Chew S-Y, Hsieh Y-HP (1998) Rapid CO2 evolution method for determining shelf life of refrigerated catfish. J Food Sci, 63: 768–771.

26   Hsieh Y-P, Hsieh Y-HP (1998). Simple system for rapid determination of carbon dioxide evolution rates. J AOAC Int, 81: 652–656.

27   Lundin A, Thore A (1975) Analytical information obtainable by evaluation of the time course of firefly bioluminescence in the assay of ATP. Anal Biochem, 66: 47-63.

28   Deininger RA, Lee JY (2001) Rapid determination of bacteria in drinking water using an ATP assay. Field Analytical Chemistry & Technology, 5: 185-189.

29   Gracias KS, McKillip JL (2004) A review of conventional detection and enumeration methods for pathogenic bacteria in food. Can J Microbiol, 50: 883-890.

30   Luo J , Liu X, Tian Q , Yue W , Zeng J , Chen G , Cai X (2009) Disposable bioluminescence-based biosensor for detection of bacterial count in food. Anal Biochem, 394: 1-6.

31   Lee J, Deininger RA, Fleece RM (2001) Rapid Determination of Bacteria in Pools. J Environ Health, 64: 9-14.

32   Klein AH, Shulla A, Reimann SA, Keating DH, Wolfe AJ (2007) The Intracellular Concentration of Acetyl Phosphate in Escherichia coli Is Sufficient for Direct Phosphorylation of Two-Component Response Regulators. J Bacteriol, 189: 5574-5581.

33   Mizutani F, Sawaguchi T, Sato Y, Yabuki S, Iijima S (2001) Amperometric Determination of Acetic Acid with a Trienzyme/Poly(dimethylsiloxane)-Bilayer-Based Sensor. Anal Chem, 73: 5738-5742.

34   Becker T, Kittsteiner-Eberle R, Luck T, Schmidt H-L (1993) On-line determination of acetic acid in a continuous production of Acetobacter aceticus. J Biotech, 31: 267-275.

35   Silla Santos MH (1996) Biogenic amines: their importance in foods. Int J Food Microbiol, 29: 213-231.

36 Önal A (2007) A review: Current analytical methods for the determination of biogenic amines in foods. Food Chem, 103: 1475-1486.

37 Latorre-Moratalla ML, Bosch-Fusté J, Lavizzari T, Bover-Cid S, Veciana-Nogués MT, Vidal-Carou MC (2009) Validation of an ultra high pressure liquid chromatographic method for the determination of biologically active amines in food. J Chromatogr A, 1216: 7715-7720.

2 Background

2.1 Basic Principles of Luminescent Chemosensors – Recognition and Signalling

Luminescence is the spontaneous emission of radiation from an electronically excited state. The means of excitation can be a chemical reaction (chemoluminescence), biological reactions (bioluminescence), electrical energy (electroluminescence), acoustic waves (sonoluminescence), or mechanical stress just to name a few. Two major luminescence phenomenona are to be distinguished: (1) Fluorescence occurs when the excited singlet state of the molecule results in a molecular state with the same spin multiplicity but with lower energy. This process occurs rapidly by the emission of radiation and is spin-allowed. (2) In contrast, phosphorescence occurs as an emission from an excited triplet state of the molecule with a change in spin multiplicity being involved. This process is slower than fluorescence because it is spin-forbidden. The almost instantaneous emission of light occurs at a longer wavelength than the wavelength of the excitation light.[1]

Fluorescence has been widely used as a tool for the specific and especially sensitive detection and determination of target molecules in life sciences and analytical chemistry.[2,3] This becomes obvious when looking at Parker's law (for solutions of low absorbance):

$$F = I \cdot \varepsilon \cdot c \cdot l \cdot QY \cdot k \tag{1}$$

where F is the fluorescence intensity measured, I is the intensity of the photo-exciting light, ε, c and l are the parameters known from the Lambert-Beer law, QY is the quantum yield, and k is a factor that accounts for the specific instrumental geometry. Equ. (1) shows that fluorescence intensity is directly proportional to the concentration of the fluorescent probe and also directly proportional to the intensity of the incident light. Therefore, fluorescence based methods show a sensitivity that is at least three orders of magnitude higher compared to other optical methods such as absorbance.[4]

Organic anions like inorganic phosphate (Pi), acetate (Ac), dicarboxylates (DC) and pyrophosphate (PP) play a crucial role in biological processes, as described in detail in Chapter 3. Section 2 of this chapter focuses on fluorescence based anion detection because determination of analytes *via* measurement of fluorescence intensity was used throughout the present work.

The principal and most frequently used design for successful sensing of anions (and cations) *via* fluorogenic chemosensors is the so called binding site-signalling subunit approach which is schematically shown in fig. 2.1.[5] First of all, the binding site (receptor) must have a shape and dimension suitable for hosting the target analyte (substrate). Furthermore, abilities for the interaction with the substrate such as coordinative or electrostatic interactions, hydrogen bonds, or π-interactions must be present in the receptor moiety.[6,7] This part of the chemosensor is responsible for the selectivity towards the substrate. Nevertheless, the signalling subunit is essential so to report the recognition event to the external operator *via* transduction of the chemical information into a fluorescent signal. This fluorescent response can be (a) an increase in intensity, (b) quenching, (c) a shift of the emission maximum, (d) a decrease in anisotropy, or (e) a change in the time-resolved anisotropy. Hence, the signalling subunit accounts for the sensitivity of the sensing molecule.[8,9]

Signaling

Signalling subunit/ Fluorophore

Binding subunit/ Receptor (free)

Binding subunit/ Receptor (occupied)
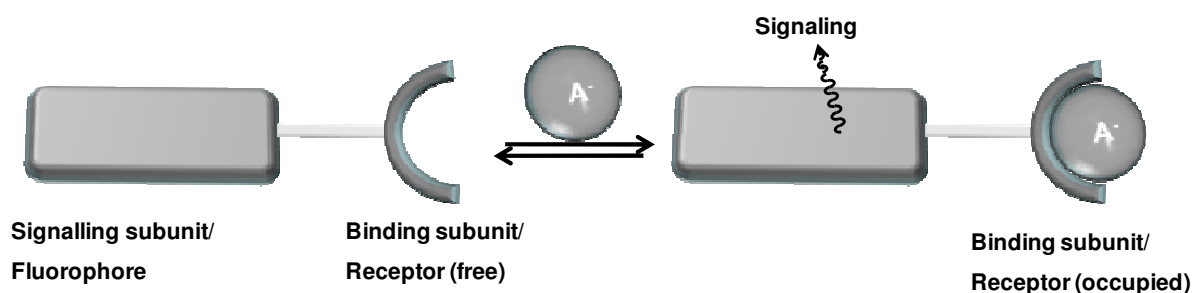
Fig. 2.1 Schematic of the binding site-signalling subunit approach.

The most common photophysical principles used for sensing (signalling) of anions are summarized in the following sections. All of these effects are clearly dependent on the charge, size and to some extent also on the basicity of the anion. Therefore, selectivity towards a certain target molecule or a group of structurally similar molecules can be induced not only by the receptor, but also to some degree by the signalling subunit.

2.1.1 Photoinduced Electron Transfer (PET)

This type of photoinduced process has been widely exploited for the sensing of anions as well as for cations.[5,8,10,11] In principle, fluorescence from a molecule is observed when an excited electron from the lowest unoccupied molecular orbital (LUMO) returns to the highest occupied molecular orbital (HOMO). Hence, excess of energy between both energy levels is released as light. In a PET-based chemosensor another part of the sensor molecule (mostly the receptor moiety) possesses an orbital with an energy level between HOMO and LUMO of the fluorescent signalling unit. When this "alien" orbital is fully occupied, a PET from this orbital to the HOMO of the excited fluorophore can occur followed by an electron transfer from the LUMO to the "alien" orbital (fig. 2.2 A). This results in a nonradiative restoration of the stable ground state of the fluorophore. Consequently, the operator observes a decrease in fluorescence intensity or no fluorescence at all. Similarly, if the external orbital is empty an electron transfer from the LUMO of the excited fluorophore moiety to the "alien" orbital can occur followed by another nonradiative transfer to the HOMO (fig. 2.2 B). PET-based chemosensors are naturally "all or none" switches. They are designed in a way that the external orbital either is induced or removed upon the recognition event resulting in a quenching (ON-OFF)[12,13] or an enhancement (OFF-ON)[14,15] of fluorescence, respectively.
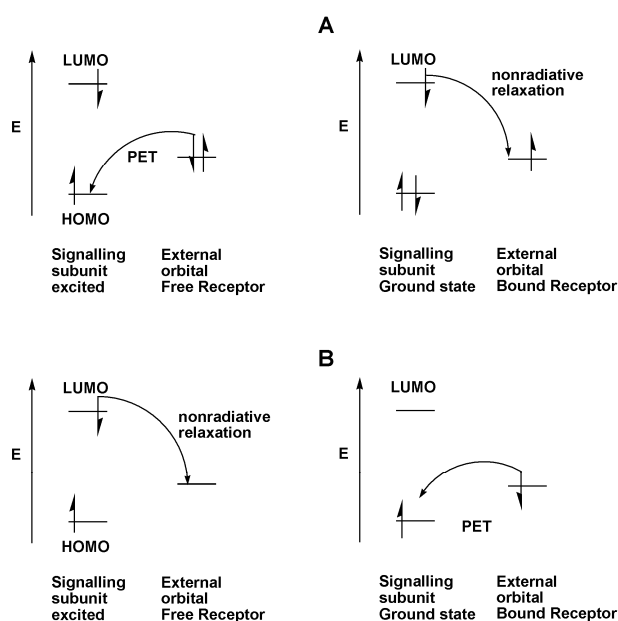
Fig. 2.2 Frontier orbital energy diagram of PET effect. **A:** Filled external orbital. **B:** Empty external orbital.

2.1.2 Internal Charge Transfer (ICT)

Major disadvantages of many PET-based probes are that their emission often is peaking well below 550 nm and anion recognition is merely signalled *via* fluorescence quenching.[16,17] This is unfavorable for determination of anions in biological matrices due to the pronounced autofluorescence between 400 and 600 nm found in these samples. These problems can be adequately circumvented by anion probes based on the photoinduced internal charge transfer (ICT) effect.[18-20] ICT based anion probes most often contain a proton-donating (also electron-donating) group such as an amino, amide, or hydroxy group as binding site. This group is conjugated to the fluorophore (signalling moiety) containing preferably an electron-withdrawing group (fig. 2.3), resulting in an electron donor-acceptor (D-A) system.[21] The probe then undergoes internal charge transfer from the donor to the acceptor upon excitation by light. These molecules have different dipole moments in their ground and excited states and therefore they are sensitive to changes in their micro-environment. Upon addition of anions – that can exert stronger electric effects than solvent molecules – solvent molecules are displaced from the binding site. The anions increase the electron donating character of the receptor group, resulting in an increased ICT which is expected as red shift in the absorption spectrum together with an increased and also red-shifted emission.[22] In addition, also changes in decay times and quantum yields are often observed. Contrarily, if the probe is designed as acceptor-donor-acceptor system (A-D-A), anions that are bound to the receptor (electron acceptor) induce a blue shifted and increased emission.[23]
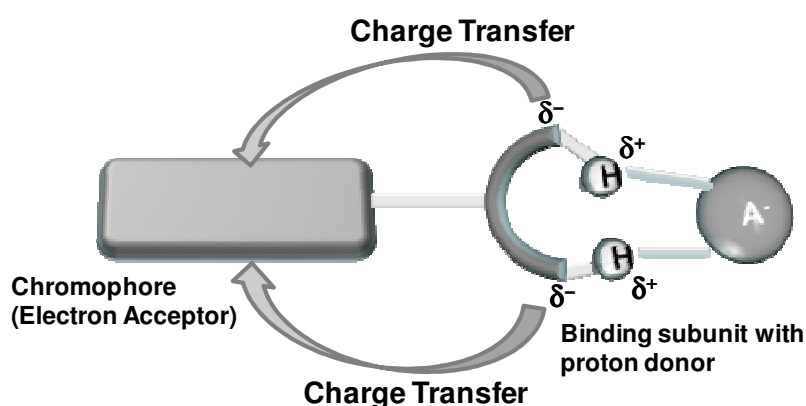
Fig. 2.3 Schematic of anion recognition and signalling by a donor-acceptor ICT based anion probe.

2.1.3 Excimer/Exciplex Formation

The formation of excimers – in contrast to PET and ICT – is a process that demands interaction of at least two fluorophores in close proximity. Most often structures containing pyrene[24] or anthracene[25] moieties are used for excimer based anion probes because of their plain π-systems allowing for strong π-stacking interaction and pronounced excited state lifetimes that favor excimer formation.[26] In principle, a monomer in excited state associates with a ground state monomer to generate an intramolecular excimer state. This is shown schematically in fig. 2.4. The emission of the monomer, and additionally a red shifted, typically broad emission band are observed in the emission spectrum of the excimer formed.[5] This dual emission allows for self-referenced determination of anions. The sensing molecule is either designed as fluorophore-anion receptor structure[25] as shown in fig. 2.4 A or as fluorophore-receptor-fluorophore structure[27,28] (Fig 2.4 B). Various excimer based anion probes known in literature show pronounced selectivity towards pyrophosphate.[29] Binding of anions may either promote or hinder excimer formation. The major disadvantage of most excimer based probes is that their emission is peaking well below 550 nm.[5,8]
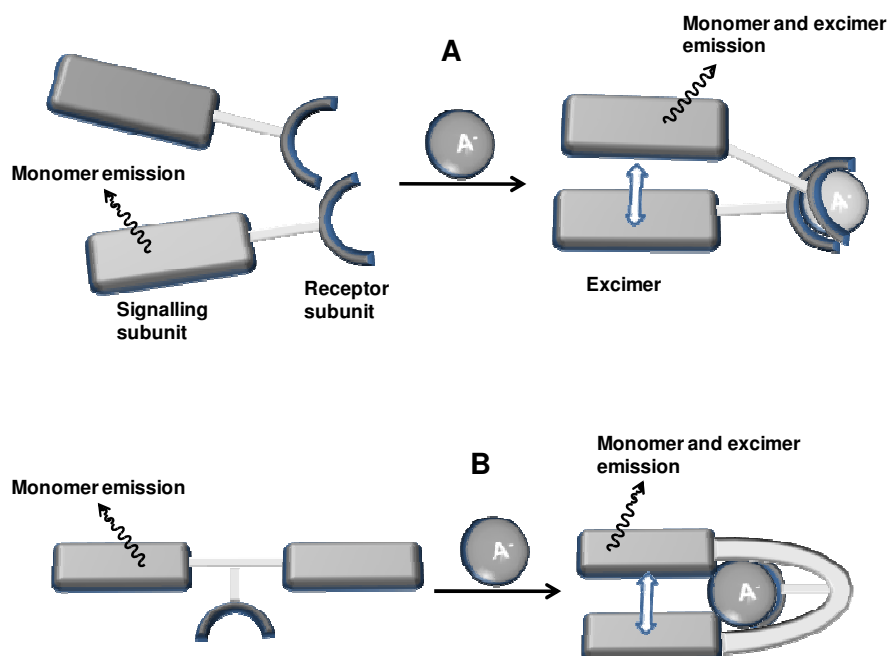
Fig. 2.4 Schematic of anion recognition and signalling by (**A**) fluorophore-receptor anion induced excimer formation and by (**B**) fluorophore-receptor-fluorophore anion induced excimer formation.

2.1.4 Förster Resonance Energy Transfer (FRET)

The Förster (or fluorescence) resonance energy transfer (FRET) is another photophysical effect used for the determination of anions. It is dependent on the interaction of two fluorophores as is the formation of excimers.[1] This effect is well studied and known to be sensitive, selective, and adjustable.[30,31] However, literature on FRET based anion sensing is rare.[32,33] Resonance energy transfer occurs between two dissimilar fluorophores in close proximity. The excited state of one fluorophore (the donor) is transferred (nonradiatively) to the other fluorophore (the acceptor). Thereby, the donor returns to its electronic ground state and emission is observed from the acceptor.[2] Effective resonance energy transfer is dependent on: (1) the distance between both fluorophores (<10 nm); (2) the spectral overlap between the emission spectrum of the donor and the absorbance spectrum of the acceptor; (3) the efficiency of the donor-dipol-acceptor-dipol-coupling.[1,34,35] Hence, a FRET based anion probe is designed in a way that binding of an anion either reduces the distance between to fluorophore moieties of the sensing molecule resulting in FRET "ON" behaviour (fig. 2.5); alternatively, substrate recognition may also induce separation of a FRET pair resulting in FRET "OFF" behavior.
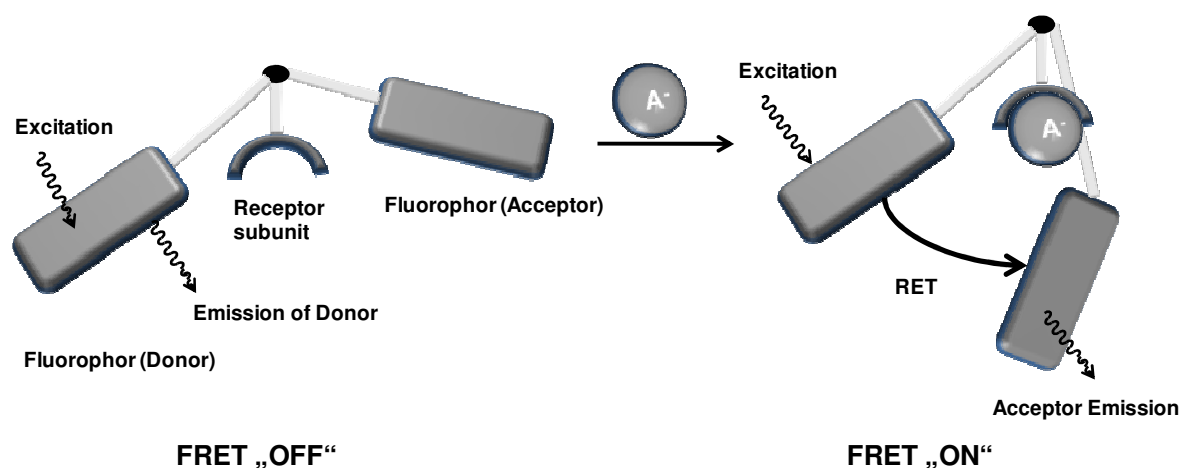
Fig. 2.5 Schematic of anion recognition and signalling *via* FRET. Binding of an anion to the receptor subunit reduces the distance between donor and acceptor enabling a resonance energy transfer.

2.1.5 Other Less Common Mechanisms

An often utilized – yet doubtful – effect for the explanation of enhancement of fluorescence upon anion binding is the so called rigidity effect.[5] Conformational restriction and overall rigidity of the complex is enhanced due to coordination of the anion. Thus, nonradiative decay from the excited singlet state to the ground state is less probable giving rise to fluorescence. Other less common mechanisms like the heavy atom effect or excited state proton transfer (ESPT) have also been reported.[36-38]

2.1.6 Dynamic Quenching by (Pseudo)halides

It is well known that the fluorescence of fluorophores like rhodamine[39], fluorescein[40], acridine[41,42], coumarine[43] and quinine[44] derivatives is effectively quenched by halides and some *pseudo*halides. This dynamic quenching effect occurs upon contact of fluorophore and halide during the lifetime of the excited state. The fluorophore then returns radiationless to the ground state. Consequently, decreased fluorescence intensity or life times are observed and can be directly related to the halide concentration.[45]

2.2 Ruthenium Ligand Complexes (RMLC)

2.2.1 Metal to Ligand Charge Transfer (MLCT) – Mechanism of Emission of Luminescence

Another photophysical effect that is exploited for signalling a noncovalent[46,47] or covalent[48] recognition event is the metal to ligand charge transfer (MLCT) effect. MLCT is observed in numerous metal-organic complexes[5,26] but will only be described in detail for ruthenium metal-ligand complexes (RMLC) in this thesis. RMLC are defined in this context as complexes containing a ruthenium (II) center ion and one or more diimine ligands. These complexes show colors ranging from dark violet ($Ru(bpy)_2Cl_2$) to bright orange ($[Ru(bpy)_3]^{2+}$) (bpy = 2,2'-bipyridine), with these spectroscopic properties originating from the electronic state of the center ion. Typically the d orbitals of the primary coordination sphere of the ruthenium cation are split – arising from the ligand field – into three equivalent energetically low-lying t_{2g} orbitals and two (also energetically equivalent) e_g orbitals with higher energy.[49] The

absolute value of the energetic difference of these orbitals is dependent on the crystal field strength Δ and, therefore, directly linked to the ligands coordinated (fig. 2.6 A).

The six d-electrons of Ru(II) populate the t_{2g} orbitals in the electronic ground state. Electron transition between the d orbitals is formally forbidden, resulting in low probability of radiative transition and quenching of emission. Furthermore, excited d-d states are destabilized due to the antibonding character of the e_g orbitals. Hence, stability and spectroscopic properties of RMLC arise from transitions beyond the d-d states. Namely, the ligands introduce new orbitals into the energetic gap between the metal d orbitals of the metal. As a result, a new electron transfer, the so called metal to ligand charge transfer (MLCT), between the HOMO of ruthenium (II) d(t_{2g}) and the LUMO of the ligands π^*(L) is observed after photoexcitation (fig. 2.6 B).[50] Thereby, electrons undergo rapid and highly efficient intersystem crossing (ISC) from the singlet ground state to the triplet MLCT state.[51] Emission from these states is formally described as phosphorescence but shows shorter lifetimes (ca $10^2 - 10^3$ ns) compared to normal phosphorescence states ($>10^3$ ns).[52] The MLCT excited state of RMLC can also be described as a ruthenium (III) and a radical anion of a diimine ligand.[47] This accounts for strong bonds between the ruthenium center and the ligands leading to high chemical stability of RMLC and negligible dissociation of ligands from the center ion under the typical conditions required for synthetic organic chemistry.
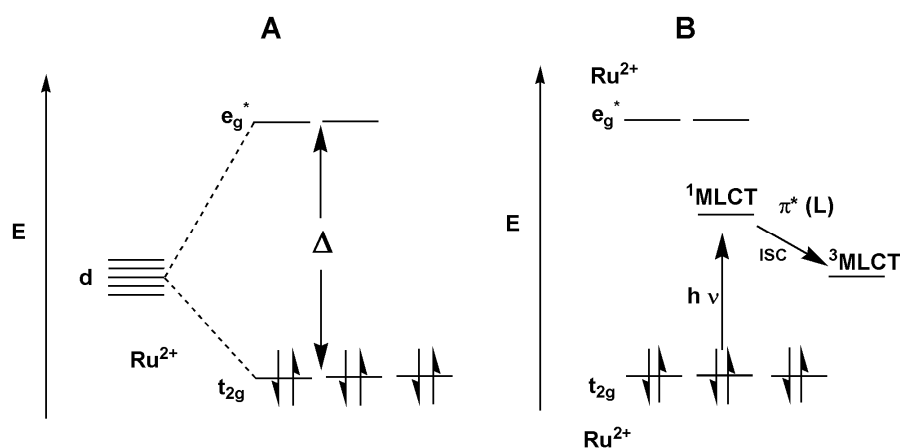
Fig. 2.6 (A) Schematic of the orbital state of the d orbitals of Ru^{2+}. The orbitals are energetically split because of the crystal field of the ligands. **(B)** Schematic of the metal to ligand charge transfer upon photoexcitation. L = Ligand such as bipyridine.

2.2.2 Spectral properties of RMLC

RMLC display intense and broad absorption bands peaking at about 450 nm and emission located at around 610 nm as a result of the MLCT (fig. 2.7). Furthermore, extinction coefficients in the range from 7000 to 35000 M^{-1} cm^{-1} are found, depending on the properties of the coordinated ligands. Obviously, these values are not comparable to extinction coefficients of classical all-organic dyes such as fluorescein (92000 M^{-1} cm^{-1})[53] but they are sufficient for measurements in biological matrices. Excitation light and emission of the RMLC are easily separable *via* cut-off or band pass filters because of their large Stokes' shift. Excitation *via* intense UV-light is disadvantageous for cell analysis due to the harmful nature of this radiation on biological systems.[54] The excitation light of RMLC in the visible region is more biocompatible and also compatible to the often employed argon ion laser (λ_{em} = 488 nm). Further on, numerous biological compounds are excitable by UV light with emissions peaking up to 500 nm.[55] The orange to red emission of ruthenium ligand complexes is well separated from the so called autofluorescence range of biological matrices allowing for luminescence determination against almost zero background. Therefore, RMLC are interesting candidates as luminescent biophysical probes. Other spectral properties of RMLC such as their rather long luminescence lifetimes[56,57], strongly polarized emission (on coordination of nonidentical ligands to the ruthenium center)[58-60], and microenvironment dependent anisotropy[61,62] have been widely exploited for measurements within biological background. Only luminescence intensity has been used throughout the present work for determination of biologically important analytes.
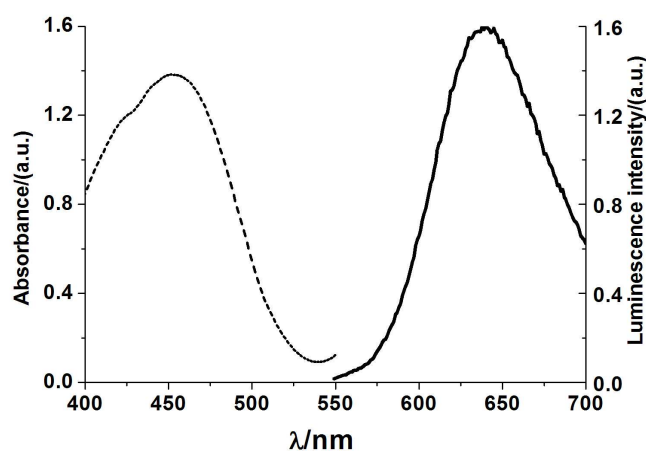
Fig. 2.7 Absorption (dashed line) and emission (solid line) spectra of the probe RuPDO.

2.3 Optical Instrumental Evaluation of Test Strips

2.3.1 Evaluation by Reflectometry

Reflection spectroscopy investigates the spectral properties of light that is remitted from a solid. Two effects contribute to the phenomenon of reflection: (1) Specular reflection occurs at the same angle as the incident light. Therefore, it is also referred to as mirror-like reflection (fig. 2.8 *left*). (2) Diffuse reflection is observed at many angels (fig. 2.8 *right*). The most general mechanism involves the surface where a part of the incident light is partially reflected by surface particles (so called micro-mirrors); hence, most of the reflected light is contributed by internal scattering centers beneath the surface. De facto, always both reflection effects concur if reflection is observed from a surface.[63,64]
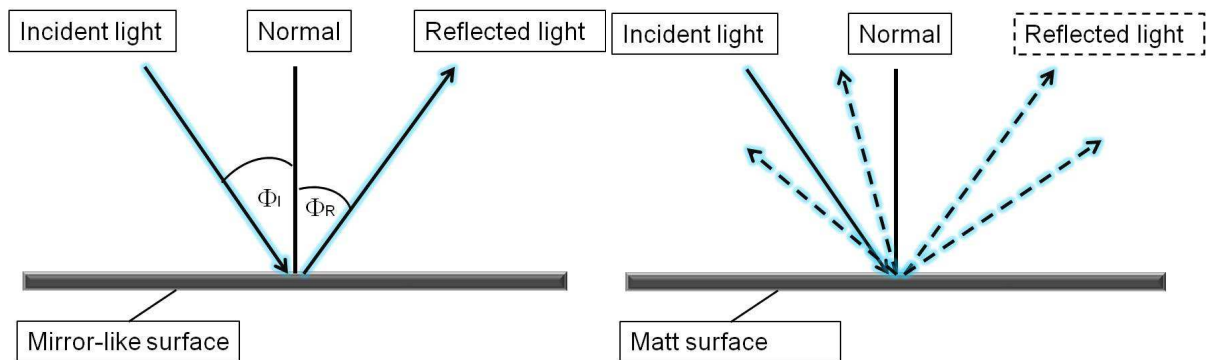
Fig. 2.8 *left:* Specular reflection; *right:* Diffuse reflection.

The theoretical fundament of reflection spectroscopy is a variation of the two-stream-approximation known as Kubelka-Munk-approximation (Eqn. (2)).[65]

$$F(R_\infty) = \frac{(1-R_\infty)^2}{2R_\infty} = \frac{K}{S}$$

(2)

where $F(R_\infty)$ is the Kubelka-Munk-function, R_∞ is the reflectivity of a infinite thick sample, K is the absorption coefficient of the sample and S is the scattering coefficient. It is presumed that the incident light is monochromatic and the reflected light is isotropic.

Diffuse reflection is measured for the reflectometric evaluation of test strips.[66] A test strip is defined (within the scope of the presented work) as a rapid dry chemistry test comprising a solid piece of material that is coated with a reagent that specifically develops a certain concentration dependent color in the presence of an analyte. The incident light is of a color that is capable to be absorbed by the reagent. Hence, the measured reflection decreases with increasing analyte concentration in the sample.

Colorimetric test strips are commercially available for a great number of analytes: pH, ethanol, nitrate, nitrite, glucose, ammonia, water hardness, iron, phosphate and oxygen, just to name a few.[67-69] These strips can be evaluated in small handheld devices like the Merck Reflectoquant or the Roche Accu-Chek within seconds. In principle, inexpensive light emitting devices (LEDs) with appropriate color are used as illuminating source rather than monochromators or optical filters. The reflected diffuse light is collected in a small integrating sphere covered with highly scattering material, like MgO or $BaSO_4$, and determined with a photoresistance or a photodiode.[70] The area of application is the rapid and semi-quantitative determination of the analyte. Therefore, these test strips are limited to the determination of analyte concentrations from the high µM to the mM range.

2.3.2 Evaluation with Red-Green-Blue (RGB) Readout of a Digital Camera

More recently, the groups of Suslick[71-73] and Filippini[74,75] described new approaches in the field of sensor technology by using so called "familiar devices". They used computer screens or polychromatic mobile phone screens as programmable light sources for their multi component analysis *via* colorimetric sensor arrays (CSA). Detection was accomplished with low-tech web cams or mobile phone cameras. As a matter of fact, the sensitivity of this approach is limited. However, the major advantages like low costs, saving of time, and ease of application, can not be denied, and may compensate for the handicaps of these methods.

A further development of this approach was introduced by Wang and Meier in 2010.[76] They used an unsophisticated setup composed of an array of high power LEDs and a commercially available digital camera for the sensitive "photographing of oxygen". The oxygen sensor is a polymeric matrix containing two dyes: an oxygen sensitive, red emitting platinum(II) complex and an oxygen insensitive, green emitting naphthalimide dye, serving as reference.

The basic principle behind this setup is that almost all modern commercially available digital cameras are using CCD (charge-coupled device) or CMOS (complementary metal-oxide-semiconductor) chips for generating a picture. Scheme 1 shows a typical CMOS sensor.

Scheme 1 CMOS Sensor
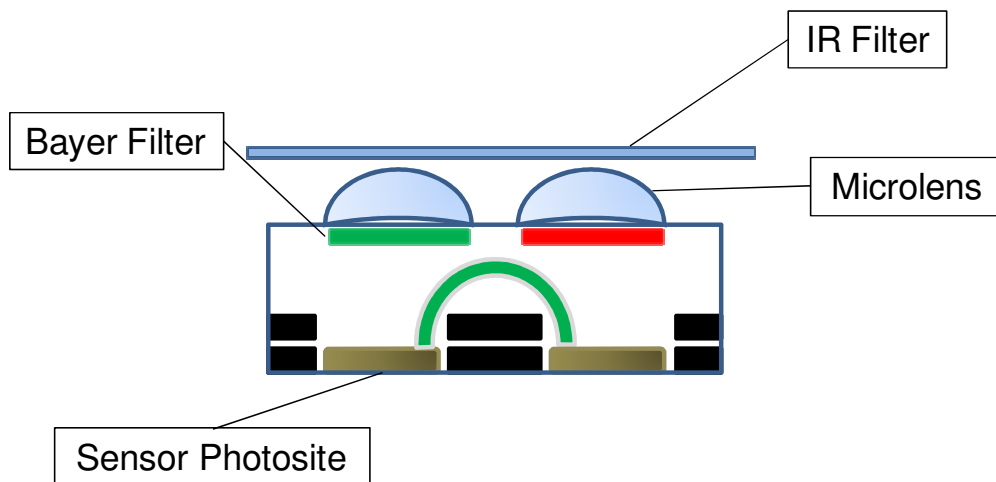
The sensor consists of small spots (pixels) with defined areas that are sensitive to light (sensor-photosite). Here, the incident light (filtered from IR light) is transduced into a proportional charge. The signal yielded by this procedure would only produce a greyscale picture. Therefore, in front of every pixel a so-called Bayer filter is mounted (Scheme 2). This filter either transmits only red, green, or blue (RGB) light to the respective pixel. The total distribution of red, green, and blue pixels is not equal. Actually, the sensor mimics the wavelength-sensitivity of the human eye, i.e. double amount of green pixels than red, or blue pixels.

Scheme 2 Bayer Filter
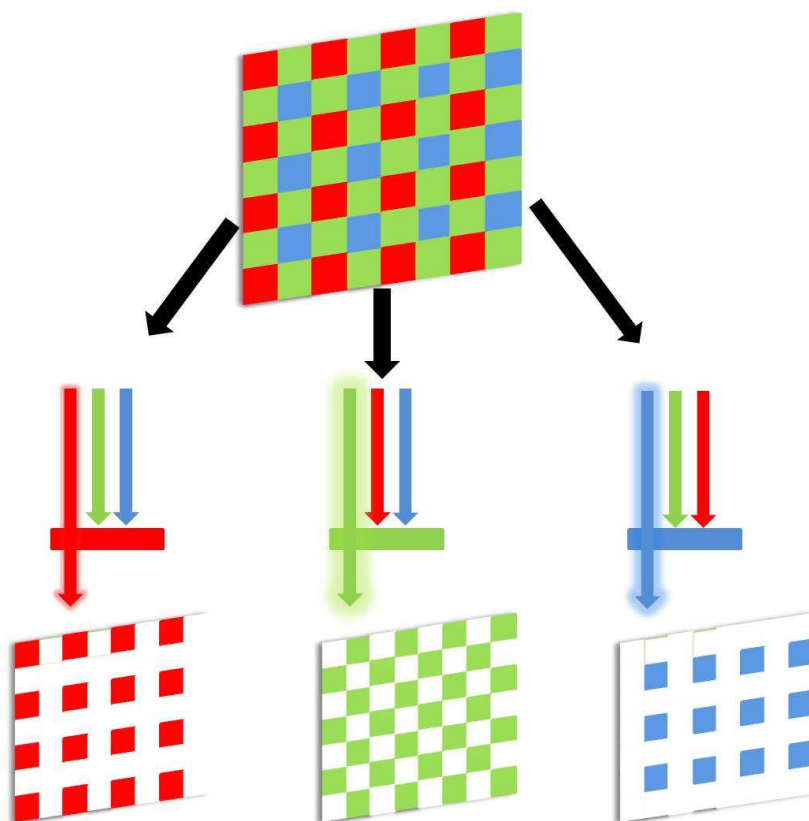
In sum, the resulting picture is composed within the software of the camera of the three virtually independent RGB data sets. The respective brightness of the color is stored in the RGB channel information and is accessible in the form of histograms.

The conversion of the red-green-blue information into a photographic picture is a reversible process, i.e. the color information can be re-extracted with suitable software. Photoshop and ImageJ were used for this purpose in the present work. Up to three independent analytical parameters (for example oxygen pressure, temperature, and pH) can be evaluated from one single picture with the appropriate spectral choice of the sensing dyes, if each of their emissions matches one of the color channels of the CMOS chips.

This principle was also exploited for the sensing stripes presented here (see Chapter 6). An amine reactive dye (Py-1) was used with an emission that is matching the red channel of the camera. Additionally, a green reference dye (fluorescein) was employed matching the green channel. This allows for ratiometric measurements and is described in detail in Chapter 6. The spectral properties of the sensing strips and the measurement setup are shown in fig. 2.9.
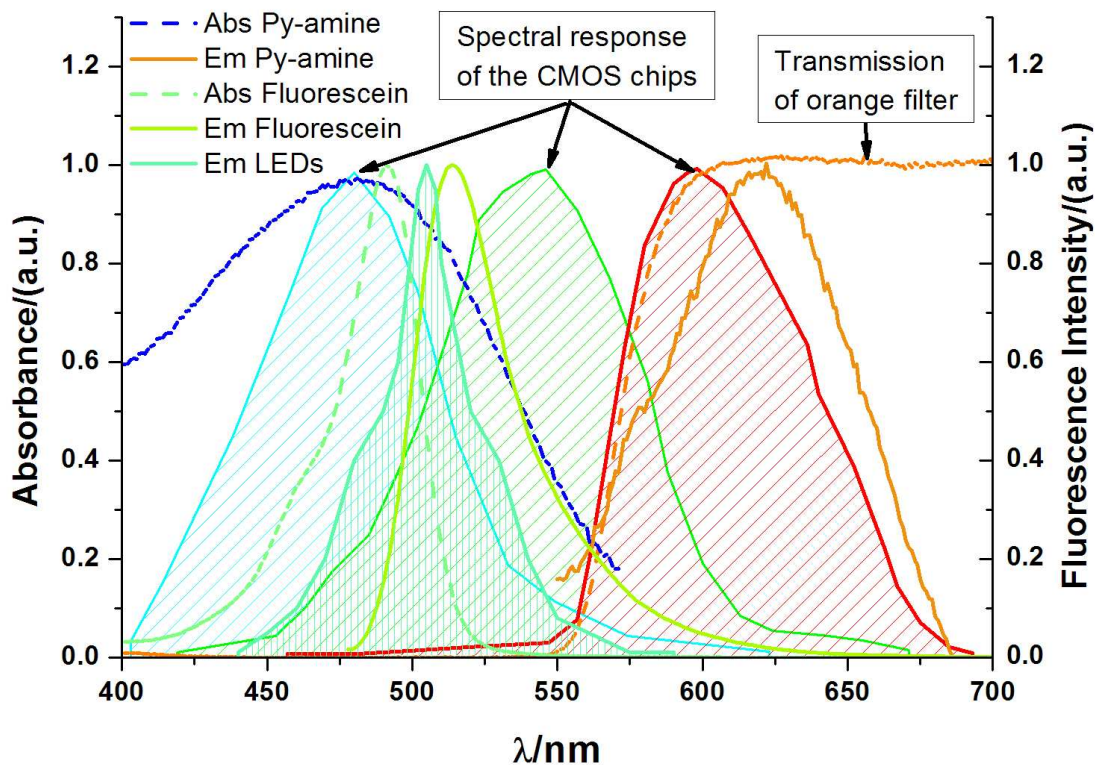
Fig. 2.9 Absorption spectra of Py-1-amine conjugate (dashed, deep blue line) and fluorescein (dashed lines, green line); emission spectra of Py-1-amine conjugate (solid, orange line) and fluorescein (solid, yellow line); transmission of the orange filter (dashed, orange line); emission of LEDs (shaded, turquoise plot); spectral response of CMOS chips (shaded, blue, green, red plots). For details, see Chapter 6.

It can be seen that the emissions of the dyes are closely matching the respective color channel. Both dyes are excitable with the employed 505 nm-LEDs. An orange glass filer was mounted in front of the objective of the camera in order to block the excitation light. Intentionally, the rather strong fluorescence of fluorescein is reduced so to equal the emission of the Py-1-amine conjugate.

2.4 References

[1] Lakowicz JR (1999) Principles of fluorescence spectroscopy. Kluwer Academic/Plenum Publishers.

[2] Valeur B, Brochon JC (2001) New trends in fluorescence spectroscopy: applications to chemical and life sciences. Springer Berlin.

[3] Ishii Y, Yanagida T (2000) Single Molecule Detection in Life Science. Single Mol 1, 1: 5-16.

[4] Beard NP, Edel JB, deMello AJ (2004) Integrated on-chip derivatization and electrophoresis for the rapid analysis of biogenic amines. Electrophoresis, 25: 2363-2373.

[5] Martínez-Máñez R, Sancenón F (2003) Fluorogenic and Chromogenic Chemosensors and Reagents for Anions. Chem Rev, 103:4419-4476.

[6] Gale AG (2000) Anion coordination and anion-directed assembly: highlights from 1997 and 1998. Coord Chem Rev, 199: 181-233.

[7] Fabbrizzi L, Licchelli M, Rabaioli G, Taglietti A (2000) The design of luminescent sensors for anions and ionisable analytes. Coord Chem Rev, 205: 85-108.

[8] Valeur B, Leray I (2000) Design principles of fluorescent molecular sensors for cation recognition. Coord Chem Rev, 205: 3-40.

[9] Fabbrizzi L, Poggi A (1995) Sensors and Switches from Supramolecular Chemistry. Chem Soc Rev, 24: 197-202.

[10] Bryan AJ, de Silva AP, de Silva SA, Rupasinghe RADD, Sandanayake KRAS (1989) Photo-induced Electron Transfer as a General Design Logic for Fluorescent Molecular Sensors for Cations. Biosensors 4: 169-179.

[11] de Silva AP, Moody TS, Wright GD (2009) Fluorescent PET (Photoinduced Electron Transfer) sensors as potent analytical tools. Analyst, 134: 2385-2393.

[12] Swinburne AN, Paterson MJ, Beeby A, Steed JW (2010) A quinolinium-derived turn-off fluorescent anion sensor. Org Biomol Chem, 8:1010-1016.

[13] Shao J, Lin H, Cai Z-S, Lin H (2009) A simple colorimetric and ON–OFF fluorescent chemosensor for biologically important anions based on amide moieties. J Photochem Photobiol B Biol, 95: 1-5.

[14] Kim HJ, Bhuniya S, Mahajan RK, Puri R, Liu H, Ko KC, Lee JY, Kim JS (2009) Fluorescence turn-on sensors for HSO_4^-. Chem Commun, 7128–7130.

[15] Wang H, Wang D, Wang Q, Li X, Schalley CA (2010) Nickel(II) and iron(III) selective off-on-type fluorescence probes based on perylene tetracarboxylic diimide. Org Biomol Chem, 8: 1017-1026.

[16] Kavarnos GJ, Turro NJ (1986) Photosensitization by Reversible Electron Transfer: Theories, Experimental Evidence, and Examples. Chem Rev, 86: 401-449.

[17] Gunnlaugsson T, Davis AP, Hussey GM, Tierney J, Glynn M (2004) Design, synthesis and photophysical studies of simple fluorescent anion PET sensors using charge neutral thiourea receptors. Org Biomol Chem, 2: 1856-1863.

[18] Kovalchuk A, Bricks JL, Reck G, Rurack K, Schulz B, Szumnac A, Weißhoff H (2004) A charge transfer-type fluorescent molecular sensor that "lights up" in the visible upon hydrogen bond-assisted complexation of anions. Chem Commun, 1946-1947.

[19] Su G, Liu Z, Xie Z, Qian F, He W, Guo Z (2009) A visible light excitable fluorescent sensor for triphosphate/pyrophosphate based on a $diZn^{2+}$ complex bearing an intramolecular charge transfer fluorophore. Dalton Trans, 7888-7890.

[20] Kumar V, Kaushik MP, Srivastava AK, Pratap A, Thiruvenkatam V, Guru Row TN (2010) Thiourea based novel chromogenic sensor for selective detection of fluoride and cyanide anions in organic and aqueous media. Anal Chim Acta, 663: 77-84.

[21] Shao J, Lin H, Lin H (2008) Rational design of a colorimetric and ratiometric fluorescent chemosensor based on intramolecular charge transfer (ICT). Talanta, 77: 273-277.

22   Raad FS , El-Ballouli AO , Moustafa RM, Al-Sayah MH, Kaafarani BR (2010) Novel quinoxalinophenanthrophenazine-based molecules as sensors for anions: synthesis and binding investigations. Tetrahedron, 66: 2944-2952.

23   Jamkratoke M, Ruangpornvisuti V, Tumcharern G, Tuntulani T, Tomapatanaget B (2009) A-D-A Sensors Based on Naphthoimidazoledione and Boronic Acid as Turn-On Cyanide Probes in Water. J Org Chem, 74: 3919-3922.

24   Winnik FM (1993) Photophysics of Preassociated Pyrenes in Aqueous Polymer Solutions and in Other Organized Media. Chem Rev, 93: 587-614.

25   Huang X-H, He Y-B, Hu C-G, Chen Z-H (2009) A Selective Metal–Ligand Fluorescent Chemosensor for Dihydrogen Phosphate via Intermolecular Excimer Formation in Water. Eur J Org Chem, 1549-1553.

26   de Silva AP, Gunaratne NHQ, Gunnlaugsson T, Huxley AJM,. McCoy CP, Rademacher JT, Rice TE (1997) Signaling Recognition Events with Fluorescent Sensors and Switches. Chem Rev, 97: 1515-1566.

27   Filby MH, Dickson SJ, Zaccheroni N, Prodi L, Bonacchi S, Montalti M, Paterson MJ, Humphries TD, Chiorboli C, Steed JW (2008) Induced Fit Interanion Discrimination by Binding-Induced Excimer Formation. J Am Chem Soc, 130: 4105-4113.

28   Pramanik A, Das G (2009) An efficient phosphate sensor: tripodal quinoline excimer transduction. Tetrahedron, 65: 2196-2200.

29   Kim SK, Lee DH, Hong J-I, Yoon J (2009) Chemosensors for Pyrophosphate. Acc Chem Res, 42: 23-31.

30   Tsien RY, Miyawak A (1998) Seeing the Machinery of Live Cells. Science, 280: 1954-1955.

31   Weiss S (1999) Fluorescence Spectroscopy of Single Biomolecules. Science, 283: 1676-1683.

32   Lee MH, Quang DT, Jung HS, Yoon J, Lee C-H, Kim JS (2007) Ion-Induced FRET On Off in Fluorescent Calix[4]arene. J Org Chem, 72: 4242 4245.

33   Pohl R, Aldakov D, Kubát P, Jursíková K, Marquez M; Anzenbacher Jr P (2004) Strategies toward improving the performance of fluorescence-based sensors for inorganic anions. Chem Commun, 1282-1283.

34   Stryer L, Haugland RP (1967) Energy Transfer: A Spectroscopic Ruler. Proc Natl Acad Sci USA, 58: 719-726.

35   Kim JS, Quang DT (2007) Calixarene-Derived Fluorescent Probes. Chem Rev, 107: 3780-3799.

36   Beer PD (1997) Transition-Metal Receptor Systems for the Selective Recognition and Sensing of Anionic Guest Species. Acc Chem Res, 31: 71 80.

37   Nie L, Li Z, Han J, Zhang X, Yang R, Liu W-X, Wu F-Y, Xie J-W, Zhao Y-F, Jiang Y-B (2004) Development of N-Benzamidothioureas as a New Generation of Thiourea-Based Receptors for Anion Recognition and Sensing. J Org Chem, 69: 6449-6454.

38   Choi K, Hamilton AD (2001) A Dual Channel Fluorescence Chemosensor for Anions Involving Intermolecular Excited State Proton Transfer. Angew Chem Int Ed, 40: 3912-3915.

39   Wyatt WA, Bright FV, Hieftje GM (1987) Characterization and comparison of three fiber-optic sensors for iodide determination based on dynamic fluorescence quenching of Rhodamine 6G. Anal Chem, 59: 2272-2276.

40   Naim JO, Lanzafame RJ, Blackman JR, Hinshaw RJ (1986) The in vitro quenching effects of iron and iodine on fluorescein fluorescence. J Surg Res, 40: 225-228.

41   Werner T, Fähnrich K, Huber C, Wolfbeis OS (1999) Anion-Induced Fluorescence Quenching of a New Zwitterionic Biacridine Derivative. Photochem Photobiol, 70: 585-589.

42   Huber C, Klimant I, Krause C, Werner T, Mayr T, Wolfbeis OS (2000) Optical sensor for seawater salinity. Fresenius J Anal Chem, 368: 196-202.

43   Moriya T (1988) Excited-State Reactions of Coumarins in Aqueous Solutions. VI. Fluorescence Quenching of 7-Hydroxycoumarins by Chloride Ions in Acidic Solutions. Bull Chem Soc Jpn, 61: 753-759.

44   Geddes CD, Apperson K, Karolin J, Birch DJS (2001) Chloride-Sensitive Fluorescent Indicators. Anal Biochem, 293: 60-66.

45   Geddes CD (2001) Optical halide sensing using fluorescence quenching: theory, simulations and applications – a review. Meas Sci Technol, 12: 53-88.

46   Beer PD, Mortimer RJ, Stradiotto NR, Szemes F, Weightman JS (1995) Electrochemical and spectral recognition of chloride ions by novel acyclic ruthenium(II) bipyridyl receptor complexes. Anal Proc, 32: 419-421.

47   Yang H-X, Liu Y-J, Zhao L, Wang K-Z (2010) Highly selective acetate optical sensing of a ruthenium(II) complex carrying imidazole and indole groups. Spectrochim Acta A, 76: 146-149.

48   Weh J, Duerkop A, Wolfbeis OS (2007) A Resonance Energy Transfer Immunoassay Based on a Thiol-Reactive Ruthenium Donor Dye and a Longwave-Emitting Acceptor. Chem Bio Chem, 8: 122-128.

49   Endicott JF, Uddin J, Schlegel HB (2002) Some spectroscopic aspects of electron transfer in ruthenium(II) polypyridyl complexes. Res Chem Intermed, 28: 761-777.

50   Lainé PP, Campagna S, Loiseau F (2008) Conformationally gated photoinduced processes within photosensitizer–acceptor dyads based on ruthenium(II) and osmium(II) polypyridyl complexes with an appended pyridinium group. Coord Chem Rev, 252: 2552-2571.

51   Endicott JF, Chen Y-J (2007) Charge transfer-excited state emission spectra of mono- and bi-metallic coordination complexes: Band shapes, reorganizational energies and lifetimes. Coord Chem Rev 251: 328–350.

52   Baldo MA, Thompson ME, Forrest SR (1999) Phosphorescent materials for application to organic light emitting devices. Pure Appl Chem, 71: 2095-2106.

53   Resch-Genger U, Grabolle M, Cavaliere-Jaricot S, Nitschke R, Nann T (2008) Quantum dots versus organic dyes as fluorescent labels. Nat Methods, 5: 763-775.

54   Kielbassa C, Roza L, Epe B (1997) Wavelength dependence of oxidative DNA damage induced by UV and visible light. Carcinogenesis, 18: 811-816.

55   Soloviev VY, McGinty J, Tahir KB, Neil MAA, Sardini A, Hajnal JV, Arridge SR, French PMW (2007) Fluorescence lifetime tomography of live cells expressing enhanced green fluorescent protein embedded in a scattering medium exhibiting background autofluorescence. Optics Letters, 32: 2034-2036.

56   Medlycott EA, Hanan GS (2005) Designing tridentate ligands for ruthenium(II) complexes with prolonged room temperature luminescence lifetimes. Chem Soc Rev, 34: 133-142.

57   Campagna S, Puntoriero F,·Nastasi F, Bergamini G, Balzani V (2007) Photochemistry and Photophysics of Coordination Compounds: Ruthenium. Top Curr Chem, 280: 117-214.

58   Sharmin A, Darlington RC, Hardcastle KI, Ravera M, Rosenberg E, Ross JBA (2009) Tuning photophysical properties with ancillary ligands in Ru(II) mono-diimine complexes. J Organomet Chem, 694: 988-1000.

59   Li L, Szmacinski H, Lakowicz JR (1997) Synthesis and Luminescence Spectral Characterization of Long-Lifetime Lipid Metal–Ligand Probes. Anal Biochem, 244: 80-85.

60   Terpetschnig E, Szmacinski H, Lakowicz JR (1995) Fluorescence Polarization Immunoassay of a High-Molecular-Weight Antigen Based on a Long-Lifetime Ru-Ligand Complex. Anal Biochem, 227: 140-147.

61   Terpetschnig E, Szmacinski H, Malak H, Lakowicz JR (1995) Metal-ligand complexes as a new class of long-lived fluorophores for protein hydrodynamics. Biophys J, 68: 342-350.

62   Szmacinski H, Terpetschnig E, Lakowicz JR (1996) Synthesis and evaluation of Ru-complexes as anisotropy probes for protein hydrodynamics and immunoassays of high-molecular-weight antigens. Biophys Chem, 62: 109-120.

63   Schmidt W (1994) Optische Spektroskopie; Eine Einführung für Naturwissenschaftler und Techniker. Weinheim, VCH.

[64] Kortüm G, Braun W, Herzog G (1963) Prinzip und Meßmethodik der diffusen Reflektionsspektroskopie. Angew Chem, 75: 653-696.

[65] Kortüm G, Oelkrug D (1966) Reflexionsspektren fester Stoffe.

[66] Kortüm G, Vogel J (1959) Quantitative Auswertung von Papierchromatogrammen durch Reflexionsmessungen. Angew Chem, 71: 451-455.

[67] Schmidhalter U. (2005) Development of a quick on-farm test to determine nitrate levels in soil. J Plant Nutr Soil Sci, 168:432-438.

[68] Mayo S, Acevedo D, Quiñones-Torrelo C, Canõs I, Sancho M (2008) Clinical Laboratory Automated Urinalysis: Comparison Among Automated Microscopy, Flow Cytometry, Two Test Strips Analyzers, and Manual Microscopic Examination of the Urine Sediments. J Clin Lab Anal, 22: 262-270.

[69] Newman JD, Turner APF (2005) Home blood glucose biosensors: a commercial perspective. Biosens Bioelectron, 20: 2435-2453.

[70] Lugo-Ospina A, Dao TH, Van Kessel JA, Reeves III JB (2005) Evaluation of quick tests for phosphorus determination in dairy manures. Environ Pollut, 135: 155-162.

[71] Rakow NA, Suslick KS (2000) A colorimetric sensor array for odour visualization. Nature, 406:710-713.

[72] Lim SH, Feng L, Kemling JW, Musto CJ, Suslick KS (2009) An Optoelectronic Nose for Detection of Toxic Gases. Nat Chem, 13; 562-567.

[73] Feng L. Musto CJ, Kemling JW, Lim SH, Suslick KS (2010) A colorimetric sensor array for identification of toxic gases below permissible exposure limits. Chem Commun, 46: 2037-2039.

[74] Alimelli A, Pennazza G, Santonico M, Paolesse R, Filippini D, D'Amico A, Lundström I, Di Natale C (2007) Fish freshness detection by a computer screen photoassisted based gas sensor array. Anal Chim Acta, 582: 320-328.

[75] Filippini D, Alimelli A, Di Natale C, Paolesse R, D'Amico A, Lundström I (2006) Chemical Sensing with Familiar Devices. Angew Chem Int Ed, 118: 3884-3887.

[76] Wang X-D, Meier RJ, Link M, Wolfbeis OS (2010) Photographing Oxygen Distribution. Angew Chem Int Ed, 122: 5027-5029.

3 Determination of Acetyl Phosphate (AcP)

3.1 Introduction

The development of fluorescent artificial receptors for selective recognition and sensing of anions has gained large interest over the past 40 years with the aid of supramolecular chemistry.[1,2] Organic anions like phosphate (Pi), acetate (Ac), dicarboxylates (DC) and pyrophosphate (PP) play a crucial role in biological processes.[3] Other anions are of great interest in medicine, for example maintenance of the sulfate concentration in the plasma of dialysis patients is still an important issue.[4] Further on, the sensitive and rapid detection of phosphate and nitrate caused by environmental pollution from overuse of fertilizers and determination of chromate and dichromate in industrial waste water is another vital topic.[2] The first report of a coordination study of anions, namely halide ions, was published in the late 1960s by Park and Simmons.[5] Other fundamental concepts on anion recognition were exposed by Lehn et al. in the 1970s.[6] They reported on macropolycyclic receptors for chloride and azide ions. The anionic guest was coordinated by ammonium groups of the host through electrostatic interactions and hydrogen bonds.

First of all, these pioneering concepts have found abundant applications in the field of cation recognition.[7] More recently, mainly in the last decade, this approach has been applied to the design of anionic receptors.[2,8,9] There are some important reasons why sensing of anions is far more tedious than sensing cations: (1) Anions are large compared to cations (F^-: 133 pm; Cl^-: 181 pm; Br^-: 196 pm; Li^+: 60 pm; Na^+: 98 pm; K^+: 133 pm). (2) They show a broad variety of geometries: spherical (halides), linear (azide, cyanide, isothiocyanide), planar (nitrate, carbonate, carboxylates), tetrahedral (phosphate, sulfate) and octahedral (complex anions, e.g. $[FeF_6]^{3-}$). (3) Anions display a significant charge delocalization. (4) A large number of anions exhibit pH dependent speciation behavior. Altogether, these characteristics result in a low concentration of effective surface charge. Hence, electrostatic binding of anions is less efficient than binding of cations.

The design of the receptor is crucial for selectivity through preorganization of the anion and the performance of the chemosensor. The most common structural motifs for anion recognition are transition metal cations[10], or hydrogen bonding sites[11] like ammonium[6] or guanidinium[12] moieties. Furthermore, urea[13], thiourea[14], amide[15], phenol[16], and pyrrole[17] subunits are also often used as receptors.

Signal transduction is the second important topic regarding sensor performance. In this respect, colorimetric anion sensing probes are far less sensitive than probes using fluorescence.[18,19] Chemosensors for anions using fluorescence are primarily based on photoinduced electron transfer (PET)[10], internal charge transfer (ICT)[20], excimer/exciplex formation[21], Förster resonance energy transfer (FRET)[22], or increase in the rigidity of the host molecules[23] (see also respective section in the Chapter Background).

Acetyl phosphate (AcP), in addition to above mentioned biologically important anions, is another interesting analyte located in cells (see Chapter 4). It is a high-energy metabolic compound derived from acetic acid and orthophosphoric acid and is itself a dianion at pH 7. Therefore, our intention was either to selectively determine AcP itself or its decomposition products, i.e. acetate and phosphate, *via* anion recognition. The recognition motifs known from the probes N-(2,7-dichlorofluorescein)lactam-N'-phenylthiourea[24] (DCFL) and 6-[1-amino-3-(4-trifluoromethylphenyl)-thiourea]-2-ethylbenzo[*de*]isoquinoline-1,3-dione[17] (EIQD) were used as a starting point. In a parallel approach three ruthenium complexes were synthesized containing either one spirolactam (RuDCFL), two thiourea (RuDPTP) or two amide (RuDAAP) anion recognition sites.

3.2 Results and Discussion

3.2.1 Anion Detection *via* DCFL

The fluorescein based spirolactam probe N-(2,7-dichlorofluorescein)lactam-N'-phenylthiourea (DCFL) was first introduced in 2007 as fluorescent chemosensor for anions like acetate and fluoride. Essentially, this probe is a modification of probes with spirolactam moiety for the determination of Hg^{2+}, Pb^{2+}, Cu^{2+}, etc.[25,26] Furthermore, the authors had claimed that selective determination of Ac over Pi is possible. DCFL was chosen as starting point for the evaluation of probes for the selective recognition of AcP due to its fluorescence OFF-ON behavior. The probe itself is virtually non luminescent (in non competitive media like acetonitrile). Anions are able to induce a ring-opening on coordination to the H-bonding donor (thiourea receptor). This ring-opening restores the fairly strong fluorescence of the fluorescein moiety peaking at 550 nm (λ_{exc} = 520 nm) (in acetonitrile). The structure of DCFL and a proposed reaction mechanism of the probe with anions are shown in figure 3.1.
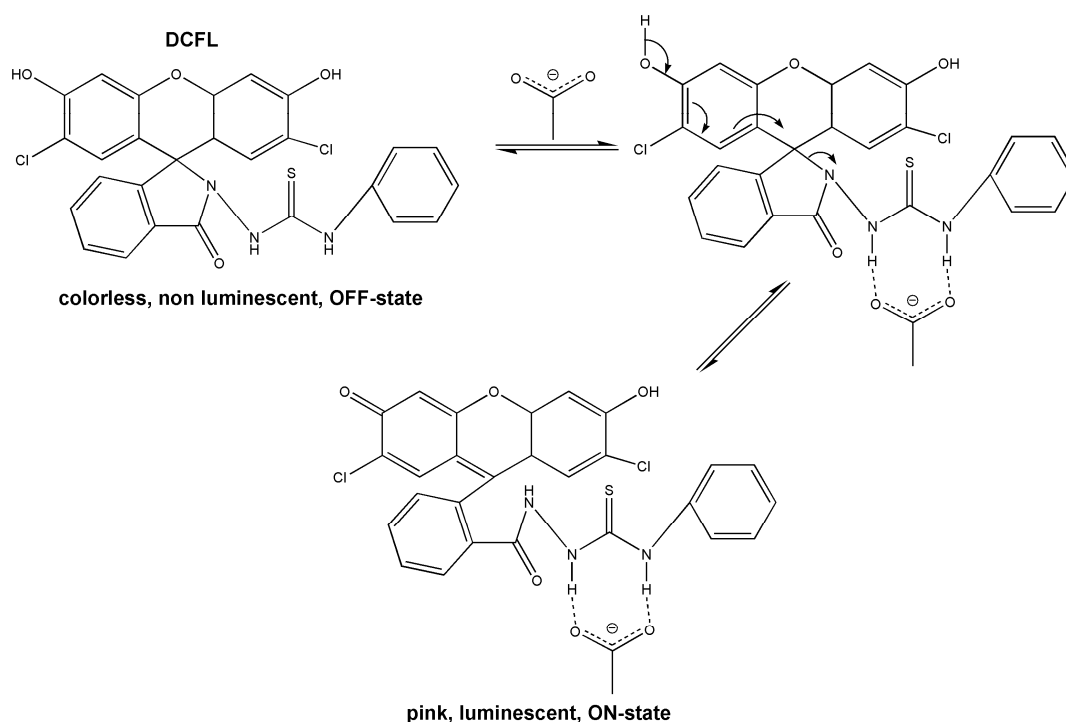
Fig. 3.1 Structure and "Reaction Mechanism" of DCFL.

The response of DCFL towards AcP, Ac, Pi, and PP was first tested in ddH$_2$O and in 10 mM HEPES (4-(2-hydroxyethyl)-1-piperazineethanesulfonic acid) buffer of pH 7.4. Strong fluorescence peaking at 520 nm (λ_{exc} = 504 nm) is observed in both solvents. Neither changes in the absorption spectra nor in the emission spectra occurred on addition of anions (data not shown). Presumably, the spirolactam is mainly present in its ring-open form. This is – not unexpectedly – most likely due to the large free energies of hydration of anions and the competing character of water, a problem which can be observed for most of the anion probes. Therefore, 5% (v/v) of acetonitrile (ACN) was added to the samples. This alters the polarity of the sample sufficiently to enable anion recognition *via* DCFL (fig. 3.2).
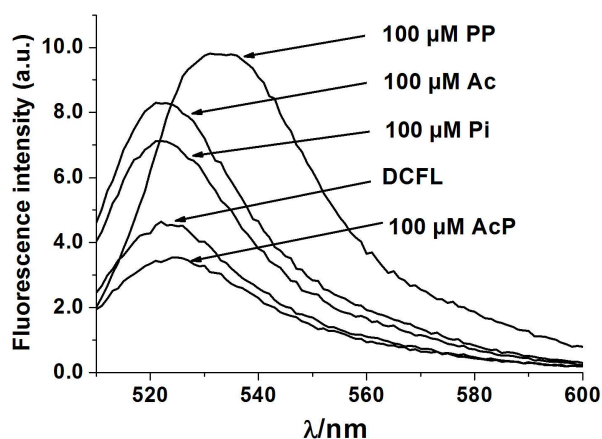
Fig. 3.2 Emission spectra of 10 µM of DCFL in 10 mM HEPES of pH 7.4 with 5% (v/v) ACN. Addition of 100 µM of each AcP, Pi, Ac and PP. Measurement was conducted at room temperature directly after addition of the respective anion.

10 eq. of AcP quench the fluorescence of DCFL by 17%. In the presence of Ac, or Pi a pronounced increase of fluorescence peaking at 522 nm (λ_{exc} = 504 nm) of 100% and 75%, respectively, is observed. Furthermore, a 150% increase of fluorescence intensity is shown after addition of 10 eq. of PP. This increase is accompanied by a red shift of the emission maximum of 10 nm (emission peaking at 523 nm). It is assumed that this effect results from a 2:1 stoichiometry (DCFL:PP). The overall response to the anions is instantaneously observed at room temperature.

The determination of anions *via* DCFL was tested in several other solvent mixtures with the purpose to find more biocompatible conditions. The results are summarized in Table 1.

Table 1 Response of DCFL towards anions in different solvent mixtures

Solvent	Anion	Emission peak	Response F/F_0 [a]
EtOH/ddH$_2$O 1/1	Ac	540 nm	1.50
	Pi	540 nm	1.10
	AcP	533 nm	0.48
	PP	530 nm	0.41
DMSO/ddH$_2$O 1/1	Ac	548 nm	0.90
	Pi	548 nm	0.77
	AcP	537 nm	0.53
	PP	537 nm	0.53
HEPES/DMSO 20/1	Ac	530 nm	1.99
	Pi	530 nm	1.88
	AcP	530 nm	1.73
	PP	530 nm	1.75
HEPES/ACN 20/1	Ac	530 nm	2.00
	Pi	530 nm	1.75
	AcP	530 nm	0.83
	PP	530 nm	2.50

[a] F_0: fluorescence intensity of DCFL without anions; ddH$_2$O: doubly distilled water; EtOH: ethanol; DMSO: dimethyl sulfoxide; ACN: acetonitrile

Only small changes in fluorescence intensity (<20%) and unstable signals were observed on testing of DCFL in mixtures of ethanol and buffers like HEPES, MOPS (3-(N-morpholino)propanesulfonic acid), or TRIS (tris(hydroxymethyl)-aminomethane) (data not shown). Stable signals and strongest fluorescence intensities were measured only in a 5% (v/v) ACN/10 mM HEPES pH 7.4 mixture and in EtOH/ddH$_2$O 1:1 (v/v) (fig. 3.3). The response properties of the probe are slightly altered in the latter unbuffered solvent. Presumably, the difference in response in the solvents is due to pH-effects of the anions. However, the overall trend remains unchanged in buffered and unbuffered solutions: the highest fluorescence signal is achieved in the presence of Ac, followed by Pi. Again, fluorescence is quenched by AcP and unexpectedly, also quenching occurs in the presence of PP.
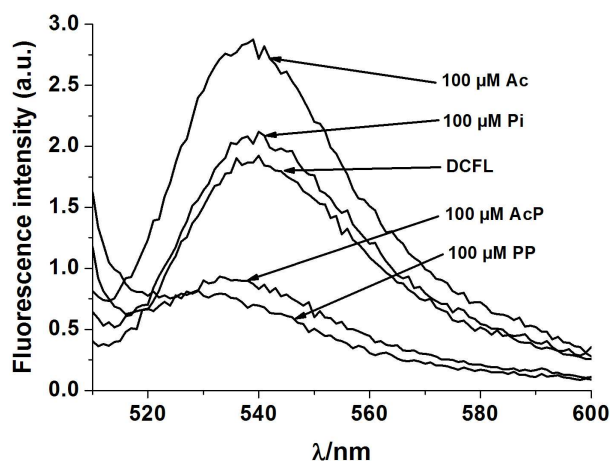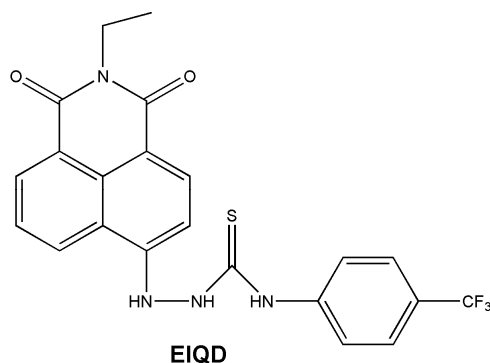
Fig. 3.3 Emission spectra of 10 µM of DCFL in a 1:1 mixture of EtOH and H_2O. Addition of 100 µM of each AcP, Pi, Ac and PP. Measurement was conducted at room temperature directly after addition of the respective anion.

It is obvious from fig. 3.2 and fig. 3.3 that AcP and its decomposition products yield contrary fluorescent signals. This is not suitable for direct determination of AcP. Therefore, other probes were thought for sensing of acetyl phosphate.

3.2.2 Anion Detection *via* EIQD

The naphthalimide based probe 6-[1-amino-3-(4-trifluoromethylphenyl)-thiourea]-2-ethylbenzo[de]isoquinoline-1,3-dione (EIQD) (fig. 3.4) was first introduced in 2005 as colorimetric ICT chemosensor for anions like acetate, phosphate and fluoride.[19] EIQD was chosen as starting point for the evaluation of anion probes for the selective recognition of AcP because the applicability in competitive solvents had been claimed by the authors. The probe itself has a sallow color in a 1:1 mixture of EtOH:H_2O and displays fairly strong fluorescence. Anions are able to coordinate to the thiourea moiety and accessorily to the 4-amino group. This coordination gives rise to ICT which is seen in the absorption spectra. The absorbance of the probe at 410 nm decreases upon addition of anions like Ac, Pi, AcP, and PP, whereas new absorption bands occur peaking at 342 nm and 544 nm. The sample shows a violet color as a result. In addition, the fluorescence of the probe peaking at 527 nm (λ_{exc} = 410 nm) is quenched in the presence of phosphates by up to 50% (fig. 3.5 and 3.6). No fluorescent response to Ac was observed.

Fig. 3.4 Molecular structure of EIQD.

The response of EIQD towards AcP, Ac, Pi, and PP was also tested in buffered (10 mM HEPES buffer pH 7.4) ethanolic solutions. No selective response to anions was observed in these solvents because even the blank sample without analyte turned violet at once. Obviously, also the buffer molecules are capable of induce a ICT. EIQD was discarded for further tests due to these findings.
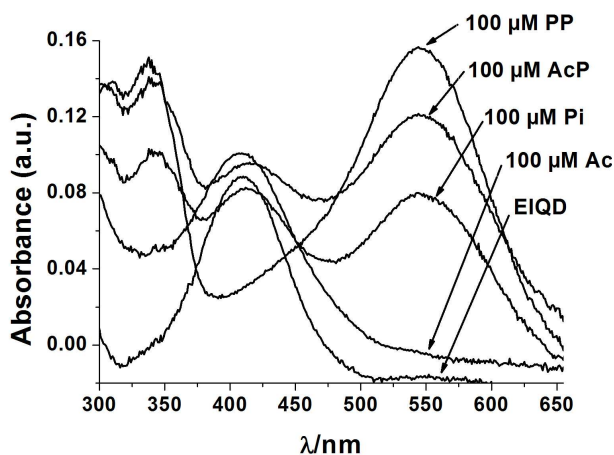
Fig. 3.5 Absorbance spectra of 10 µM of EIQD in EtOH/ddH$_2$0 1/1. Addition of 100 µM of each AcP, Pi, Ac and PP. Measurement was conducted at room temperature directly after addition of the respective anion.
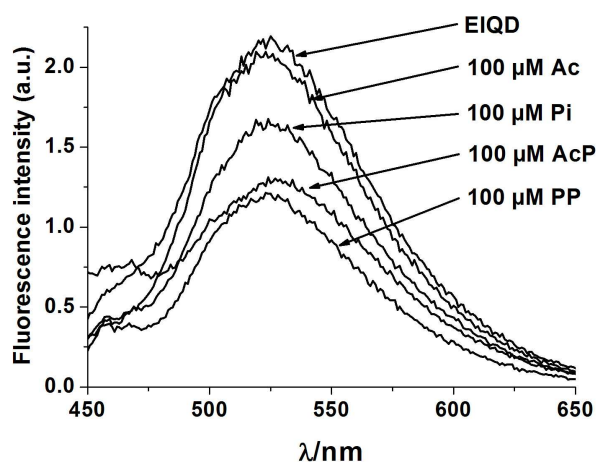
Fig. 3.6 Emission spectra (λ_{exc} = 410 nm) of 10 µM of EIQD in EtOH/ddH$_2$0 1/1. Addition of 100 µM of each AcP, Pi, Ac and PP. Measurement was conducted at room temperature directly after addition of the respective anion.

3.2.3 Anion Detection *via* new Ruthenium Complexes: RuDCFL

Encouraged by the results achieved with the probe DCFL, we tried to transfer the luminescence OFF-ON-concept from the all-organic fluorescein-based dye to a ruthenium complex. The advantages of these complexes are described in detail in the Background Section. A straightforward reaction of 2,7-dichlorofluorescein hydrazide with bis(2,2′-bipyridine)-(5-isothiocyanato-phenanthroline)ruthenium (II) was chosen as pathway for the synthesis. It delivered the dark red colored complex in 75% yield. The structure of the ruthenium probe is shown in fig. 3.7. The luminescence OFF-ON mechanism is identical to that of DCFL. The response of the probe towards Ac, Pi, and AcP was tested in DMSO and in a highly competitive mixture of 10% (v/v) DMSO in ddH$_2$O (fig. 3.8 and fig. 3.9).
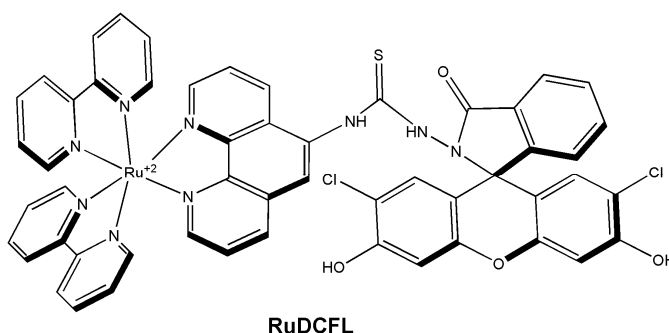
Fig. 3.7 Molecular structure of RuDCFL .

The probe shows dual emission behavior in both solvents tested. Two distinctive emission maxima peaking at 550 nm and 610 nm are observed in DMSO (λ_{exc} = 450 nm). The first emission peak is ascribable to the fluorescein moiety, the latter peak is characteristic for ruthenium complexes with bipyridine ligands.[27,28] The luminescence intensity at 550 nm increases after addition of Ac, Pi or AcP by ca. 60%. However, the MLCT-emission of the complex at 610 nm decreases on addition of these anions by about 60%. This allows for ratiometric sensing. Furthermore, the dual emission characteristic of RuDCFL is also preserved in the highly competitive mixture of 10% (v/v) DMSO and ddH$_2$O. However, the luminescent response of the probe towards anions is decreased. The emission maxima are blue-shifted by 23 nm and 8 nm, respectively. The emission peaks at 527 nm and 602 nm increase non-selectively by ca. 32% and ca.15%, respectively, after addition of anions to the sample. This answer on anions in aqueous organic samples was unsatisfactory and hence, the probe was discarded for further tests.

Fig. 3.8 Emission spectra of 10 µM of RuDCFL in DMSO. Addition of 100 µM of each AcP, Pi and Ac. Measurement was conducted at room temperature directly after addition of the respective anion.
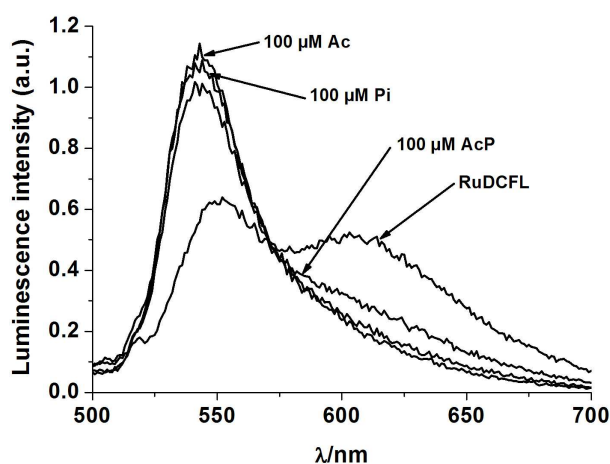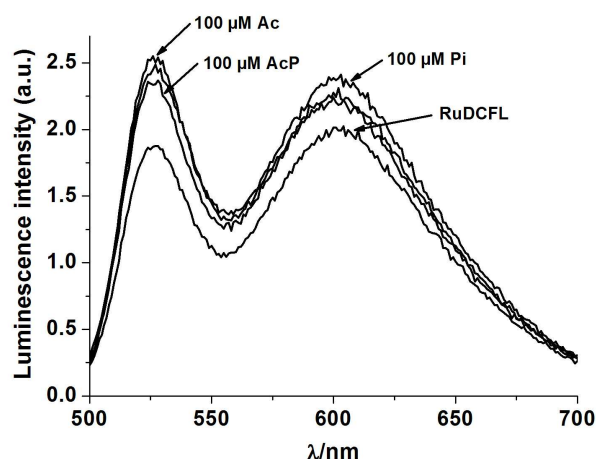
Fig. 3.9 Emission spectra of 10 µM of RuDCFL in a mixture of 10 % (v/v) DMSO in ddH$_2$O. Addition of 100 µM of each AcP, Pi and Ac. Measurement was conducted at room temperature directly after addition of the respective anion.

3.2.4 Anion Detection *via* new Ruthenium Complexes: RuDPTP

The thiourea moiety is a common receptor motif for anion recognition. Therefore, it was obvious to transfer this recognition element also to a ruthenium based metal organic complex. Again, the reaction of an isothiocyanate (phenylisothiocyanate) with a primary amine ((bpy)$_2$-(5,6-diaminophenanthroline)Ru(II)) was chosen as pathway for the synthesis of bis(2,2'-bipyridin)-(5,6-diphenylthiourea-phenanthroline)Ru(II). It delivered the red colored complex in 80% yield. It was assumed that two recognition moieties would result in a stronger response (higher luminescence increase/decrease) than one. Further on, a more stable signal in competitive solvents due to the increased hydrophobic character of the "binding side" was expected. The molecular structure of the ruthenium probe is shown in figure 3.10. The luminescence of the probe is quenched in the presence of anions due to the occurrence of a PET. The response of the probe towards Ac, Pi, and AcP was tested in DMSO and in a highly competitive mixture of 10% (v/v) DMSO in ddH$_2$O (fig. 3.11 and fig. 3.12).

RuDPTP

Fig. 3.10 Molecular structure of RuDPTP.

The probe shows an emission peaking at 620 nm in DMSO and 603 nm in the mixture of 10% (v/v) DMSO in ddH$_2$O (λ_{exc} = 469 nm), respectively. The luminescence intensity is nonselectively quenched after addition of Ac, Pi and AcP by about 53% in DMSO. The decrease in luminescence is less pronounced in the competitive solvent (ca. 30%). The probe was not further investigated due to these findings.

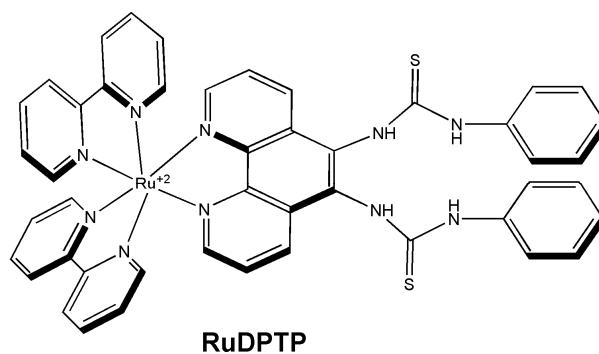**Fig. 3.11** Emission spectra of 10 µM of RuDPTP in DMSO. Addition of 100 µM of each AcP, Pi and Ac. Measurement was conducted at room temperature directly after addition of the respective anion.
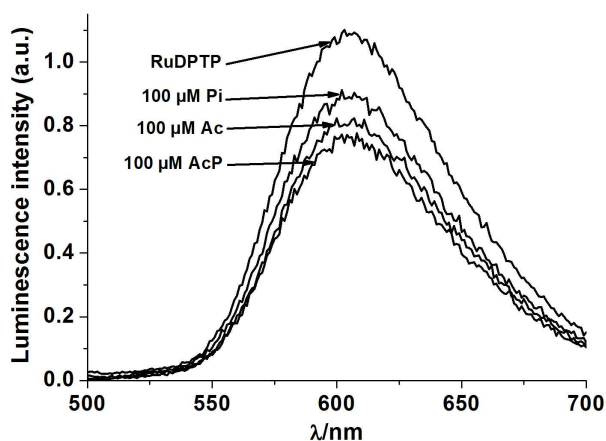
Fig. 3.12 Emission spectra of 10 µM of RuDPTP in a mixture of 10 % (v/v) DMSO in ddH$_2$O. Addition of 100 µM of each AcP, Pi and Ac. Measurement was conducted at room temperature directly after addition of the respective anion.
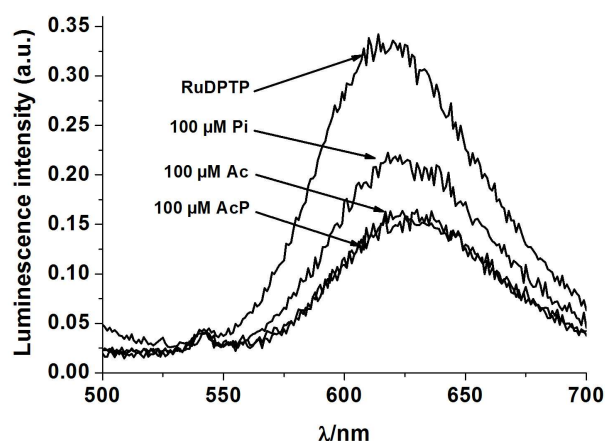
3.2.5 Anion Detection *via* new Ruthenium Complexes: RuDAAP

The amide moiety is another common recognition motif for anion detection. Therefore, it seemed to be apparent to transfer this receptor element also to a ruthenium complex. The structure of the ruthenium probe is shown in fig. 3.13. The luminescence of the probe is quenched in the presence of anions due to the occurrence of a PET. The response of the probe towards Ac, Pi, and AcP was tested in DMSO and in a highly competitive mixture of 10% (v/v) DMSO in ddH$_2$O (fig. 3.14 and fig. 3.15).
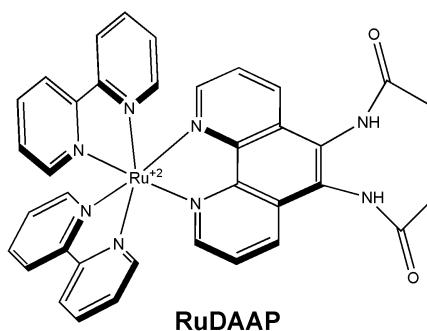

RuDAAP

Fig. 3.13 Molecular structure of RuDAAP.

The probe shows an emission peaking at 615 nm in DMSO and 605 nm in the mixture of 10% (v/v) DMSO in ddH$_2$O (λ_{exc} = 469 nm), respectively. The luminescence intensity is quenched after addition of Ac, Pi and AcP by about 60%, 22%, and 44%, respectively, in DMSO. This suggests that carboxylic compounds show stronger binding to the amide receptor than phosphates. The decrease in luminescence is less pronounced in the competitive solvent. Pi shows virtually no effect on the emission of the probe, whereas both Ac and AcP yield a quenching of the emission of about 31%. The probe was discarded due to these findings.
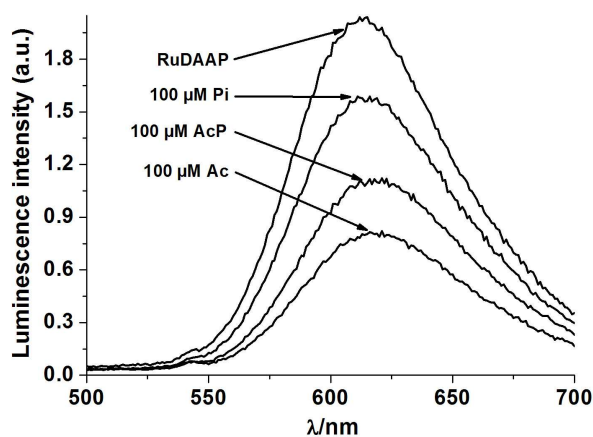
Fig. 3.14 Emission spectra of 10 µM of RuDAAP in DMSO in presence of 100 µM of each AcP, Pi and Ac. Measurement was conducted at room temperature directly after addition of the respective anion.
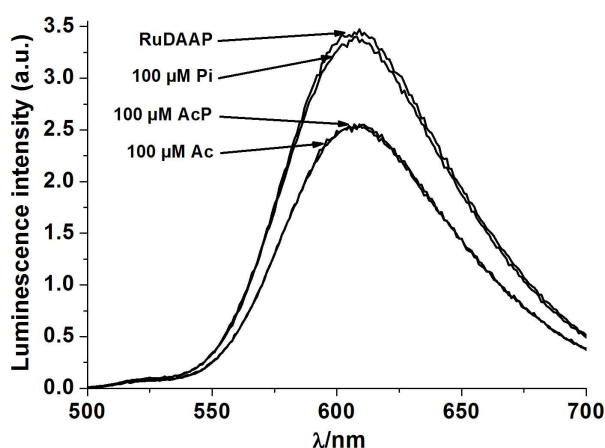
Fig. 3.15 Emission spectra of 10 µM of RuDAAP in a mixture of 10 % (v/v) DMSO in ddH$_2$O. Addition of 100 µM of each AcP, Pi and Ac. Measurement was conducted at room temperature directly after addition of the respective anion.

The probes of the ruthenium type and EIQD were not used for further experiments as their anion recognition properties in highly competitive solvents and under biocompatible conditions do not meet the demands of selectivity for AcP or its decomposition products. Furthermore, the probes are not applicable in purely aqueous buffers and show only a small signal change in competitive samples.

Table 2 Summary of the probes

Probe	$\lambda_{exc\,/\,em}$ /nm	Response to 10eq of anion (F/F$_0$)			
		Ac	Pi	AcP	PP
DCFL	504/530-540[a]	1.5	1.1	0.48	0.41
EIQD	410/527[a]	1.0	0.75	0.55	0.50
RuDCFL	450/550,610[b]	1.8/0.40	1.7/0.40	1.5/0.50	-
	450/527,602[c]	1.4/1.3	1.4/1.4	1.4/1.3	-
RuDPTP	469/620[b]	0.43	0.57	0.43	0.31
	469/603[c]	0.73	0.83	0.71	0.33
RuDAAP	469/615[b]	0.40	0.78	0.54	0.67
	469/605[c]	0.71	1.0	0.71	0.84

[a] H$_2$O/ethanol 1/1; [b] DMSO; [c] H$_2$O/DMSO 9/1

3.2.6 Determination of AcP: Combination of DCFL and Hydrolysis Promoter Bis-Cyclen (BC)

Finally, only DCFL was selected for further testing, because it is fully applicable in highly competitive solvents such as in 10 mM HEPES buffer of pH 7.4 containing 5% (v/v) acetonitrile, in a H$_2$O:DMSO 1:1 mixture, and in a H$_2$O:EtOH 1:1 mixture (Table 1). The latter solvent was selected as reaction medium for all following tests as admission to the measurement design (microtiter plates). Furthermore, the fluorescence of DCFL in this solvent is quenched by AcP. However, a pronounced increase of fluorescence is observed after addition of acetate or phosphate (Table 1). It was assumed that acetyl phosphate can be selectively determined *via* the products of its hydrolysis, namely acetate and phosphate. Despite of AcP being a relatively labile anhydride (ΔG^0: -43 kJ/mol)[29] it shows a kinetically hindered decomposition of less than 20% in a neutral aqueous solution at 20 °C over 0.5 h.[30] Therefore, it was

necessary to incorporate a catalytic element into the anion determination assay for AcP.

A promoter for the hydrolysis of carboxyesters and phosphodiesters was kindly supplied by the Institute of Organic Chemistry of the University of Regensburg, Research Group Prof. B. König. This promoter is a dinuclear Zn(II) complex of 1,4,7,10-tetrazacyclododecane ([12]aneN4 or cyclen) and its reaction with above mentioned esters has been studied in great detail.[31-33] Its molecular structure is shown in Fig. 3.16. This molecule is referred to as bis-cyclen (BC) in the following.
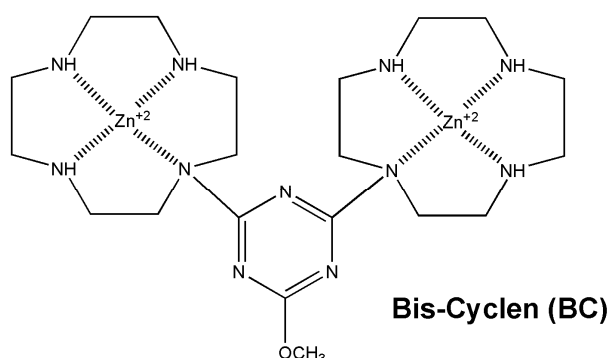
Fig. 3.16 Molecular structure of the hydrolysis promoter bis-cyclen (BC).

The hydrolysis of 100 µM of AcP without promoter and in the presence of 10 µM of BC was studied by monitoring the fluorescence of DCFL (10 µM) at 535 nm (λ_{exc} = 485 nm). Fig. 3.17 shows that the slope of the kinetic plot of AcP in the presence of bis-cyclen (V) is at least two times steeper than the slope of the kinetic plot of AcP without BC (I). This clearly points out that BC promotes the hydrolysis of AcP. Furthermore, the structurally similar compound pyrophosphate (PP) equally displays a pronounced increase of the fluorescence signal in the presence of BC (III). However, even after 90 min the signal of plot III and V is still increasing. This shows that the hydrolysis of AcP and PP is not completed within this prolonged reaction time. In contrast, the slope of the plots of Ac (IV) and Pi (II) in the presence of BC reach a plateau after 10 min. The rather small increase of the signal of plot II and IV is mainly due to evaporation of ethanol during the 90 min of measurement.
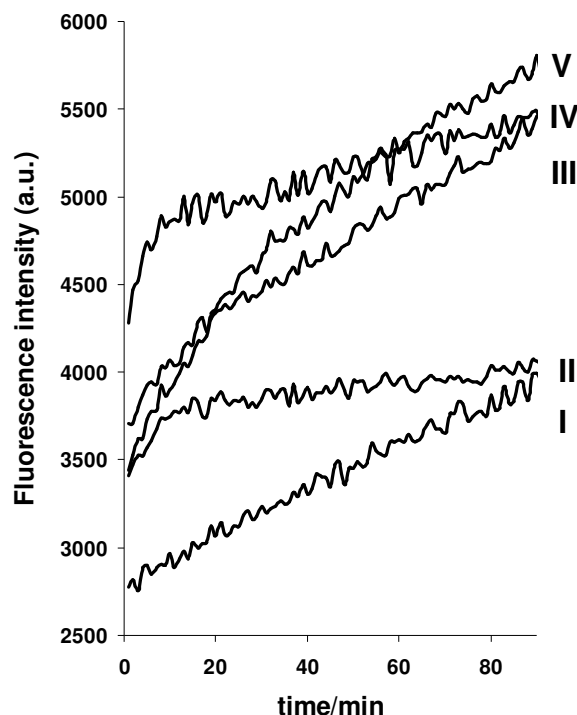
Fig. 3.17 Fluorescence of DCFL in H_2O/EtOH 1:1. 10 µM of DCFL; (I) 100 µM AcP; (II) 100 µM Pi, 10 µM BC; (III) 100 µM PP, 10 µM BC; (IV) 100 µM Ac, 10 µM BC; (V) 100 µM AcP, 10 µM BC. T = 25 °C, (n = 4).

Next, the response of DCFL in the presence of BC and increasing concentrations of AcP was tested. It is obvious from fig. 3.18 that the fluorescence signal of DCFL is increasing with increasing AcP concentration (plot II – V). The signal of DCFL without analyte is stable after 20 min. This is most likely due to a (not further investigated) interaction of DCFL and BC.
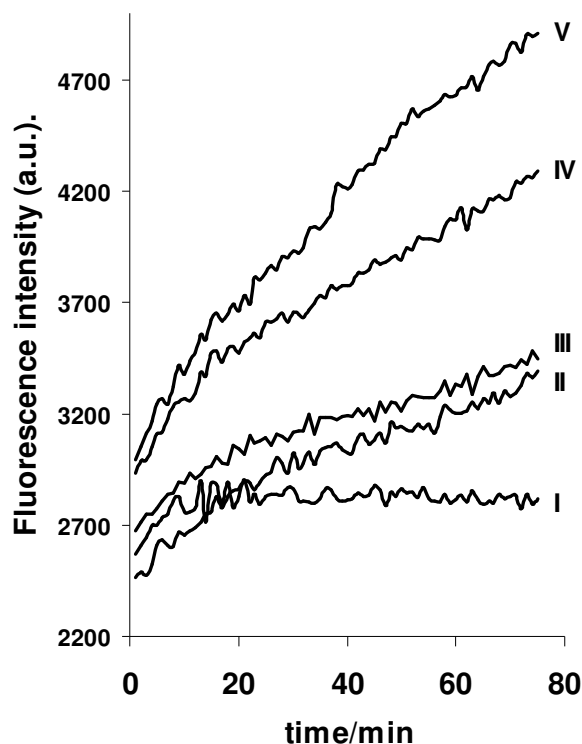
Fig. 3.18 Fluorescence of DCFL in H_2O/EtOH 1:1. 10 µM of DCFL; 10 µM of BC; Increasing concentrations of AcP: (I) 0 mM, (II) 0.1 mM, (III) 0.5 mM, (IV) 1 mM, (V) 2 mM; T = 25 °C, (n = 4).

3.3 Conclusions

In summary, five different anion probes were tested for their anion recognition properties in organic solvents and in highly competitive aqueous solutions. The newly synthesized ruthenium based probes only showed selective anion recognition in organic solvents. The two-recognition-moiety concept could not prove that increased hydrophobic environment around the binding site accounts for a more stable response to anions in competitive solvents. Direct determination of AcP was not successful with the fluorescein based spirolactam probe DCFL. Moreover, the quenching effect of AcP on the fluorescence of DCFL is only small (ca. 20%) and not specific. On the other hand, the decomposition of AcP at room temperature in neutral aqueous solution is slow. Therefore, a hydrolysis promoter of the cyclen type was employed. The hydrolysis of AcP is promoted by BC. AcP was determined successfully and concentration dependent (0.1 mM - 2 mM) in a highly competitive solvent *via* combination of the anion probe DCFL and the hydrolysis promoter BC.

However, a distinct statement about the actual rate of hydrolysis is not possible using this assay. This is due to the fact that the fluorescence signal yielded by DCFL during the hydrolysis of AcP (PP) *via* BC is a combination of the response to Ac, Pi and non-hydrolyzed AcP (Pi and non-hydrolyzed PP, respectively).

3.4 Experimental

3.4.1 Materials

cis-Dichlorobis(2,2'-bipyridine)ruthenium(II) dihydrate (Ru(bpy)$_2$Cl$_2$), and barium carbonate were purchased from ABCR (www.abcr.de). All other common chemicals and solvents, 1,10-phenanthroline-5,6-dione, and 5-amino-1,10-phenanthroline were purchased from Sigma Aldrich (www.sigmaaldrich.com) or Acros Organics (www.acros.be). They were used without further purification. Doubly distilled water was used for the preparation of buffers and stock solutions of anions. Anions were used as the sodium or potassium salts and 10 mM stock solutions thereof were prepared in doubly distilled water shortly before measurement. 40 mM 4-(2-hydroxyethyl)-1-piperazineethanesulfonic acid (HEPES) buffer of pH 7.4 was used for all experiments. Stock solutions of the probes and the hydrolysis promoter bis-cyclen (BC) of a concentration of 1 mM were prepared in DMSO or acetonitrile. The bis-cyclen was kindly supplied by the Institute of Organic Chemistriy, Group of Prof. König.

3.4.2 Methods

10 μL of the probe stock solution (final concentration 10 μM in respective solvent), and additionally 10 μL of the stock solution of BC (final concentration 10 μM in respective solvent) for the hydrolysis experiments, were added to the sample solvent containing at least 100 μM of the respective anion and made up to 1 mL (for tests in cuvettes). One tenth of all volumes were used for microtiter plate-based experiments (final volume 0.1 mL). The same amount of probe was added to the control containing no anions. The absorbance and fluorescence of the samples was measured at 25 °C directly after mixing and shaking.

3.4.3 Instruments

Absorption spectra were recorded on a Cary 50 Bio UV-Vis Spectrophotometer (Varian, Australia, www.varianinc.com). Luminescence spectra were recorded on an Aminco-Bowman AB 2 luminescence spectrometer (www.thermo.com) equipped with a 150 W continuous wave xenon lamp as excitation light source. All spectra are uncorrected. Microtiter plate experiments were performed on a Tecan Genios Plus Reader (www.tecan.de) in clear flat bottom 96-well plates from Greiner Bio One (www.gbo.com). pH was measured with a pH meter CG 842 from Schott (www.schott.com) at room temperature. The ESI mass spectra were taken on a ThermoQuest TSQ 7000 (www.thermo.com) mass spectrometer. ^{1}H-NMR spectra were recorded on a 300 MHz NMR spectrometer (Avance 300 from Bruker BioSpin GmbH; www.bruker-biospin.com). The internal standard was tetramethylsilan (TMS). The chemical shifts are given in ppm. The following abbreviations were used to describe the signals: s = singlet, d = doublet, t = triplet, m = multiplet

3.4.4 Synthesis

Synthesis of N-(2,7-dichlorofluorescein)lactam-N'-phenylthiourea (DCFL)

DCFL was synthesized with slight modifications according to the literature procedure.[23] **(1)** *Synthesis of 2,7-dichlorofluorescein hydrazide:* 0.8 mg (2 mmol) of 2,7-dichlorofluorescein were dissolved in 50 mL of absolute ethanol. After addition of 0.6 mL (11 mmol) of hydrazine monohydrate the mixture turned bilious green. The mixture was heated to reflux for 12 to 48 h until the fluorescence of the solution had disappeared and a strong pink color was observed. After cooling to room temperature the mixture was dissolved in 200 mL of ethyl acetate yielding an orange color. The organic phase was washed four times with ddH$_2$O (100 mL), collected, dried over anhydrous Na$_2$SO$_4$, filtered and the solvent removed by rotary evaporation. **(1)** was used without further purification (0.56 g, 65% yield). R$_f$ = 0.57 (silica, CH$_2$Cl$_2$/methanol = 10/1 (v/v). **(2)** *Synthesis of DCFL:* 0.5 g (1.2 mmol) of **(1)** and 0.5 g (2.6 mmol) of phenyl isothiocyanate were dissolved in 10 mL of dry dimethylformamide (DMF). The mixture was stirred overnight at room temperature yielding a orange-red colored clear solution. The mixture was added to 200 mL of CH$_2$Cl$_2$ and was washed four times with ddH$_2$O (100 mL). The decolorized organic phase was collected, dried, and the solvent was evaporated, yielding a colorless

solid. The crude product was further purified by silica gel chromatography (CH$_2$Cl$_2$/methanol = 10/1 (v/v); R$_f$ = 0.64) to give 0.47 g of DCFL (0.87 mmoL) in 71% yield. *m/z* (ESI) 548.0 ((M-H$^+$)$^-$) C$_{27}$H$_{19}$Cl$_2$N$_3$O$_4$S requires 549.0). ^{1}H NMR (CD$_3$OD, TMS): 8.06-7.97 (t, 2H), 7.81-7.73 (m, 2H), 7.31-7.05 (m, 7H), 6.79 (s, 2H).

Scheme 1 Synthetic route to DCFL.

2,7-Dichlorofluorescein   2,7-Dichlorofluorescein hydrazide

2,7-Dichlorofluorescein hydrazide   DCFL
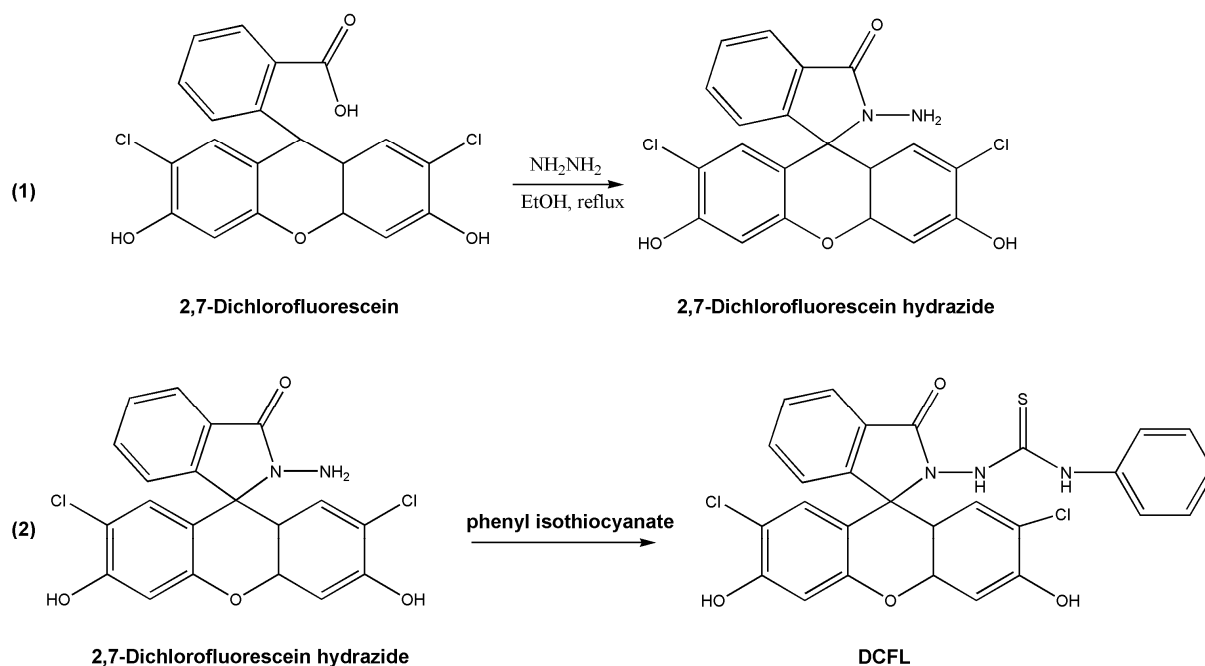
Synthesis of 6-[1-amino-3-(4-trifluoromethylphenyl)-thiourea]-2-ethylbenzo[de]isoquinoline-1,3-dione (EIQD)

EIQD was synthesized with slight modifications according to the literature procedure.[19] **(1)** *Synthesis of 6-Bromo-2-ethylbenzo[de]isoquinoline-1,3-dione:* 1 g (3.6 mmol) of 4-Bromo-1,8-naphthalic anhydride and 0.35 mL (4.3 mmol) of ethylamine (70% solution in water) were refluxed in 1,4-dioxane (90 mL) for 8 h yielding a brownish mixture. The solution was poured into 350 mL of ddH$_2$O after cooling to room temperature to precipitate out a cream-colored solid. The solid was collected by filtration, washed with 20 mL of ddH$_2$O and dried to yield 0.86 g (2.8 mmol; 78% yield). **(2)** *Synthesis of 2-Ethyl-6-hydrazinobenzol[de]isoquinoline-1,3-dione:* 0.60 g (2.0 mmol) of **(1)** and 0.52 mL (10 mmol) of hydrazine monohydrate were dissolved in 15 mL of dry DMF and heated at 130 °C for 2 h. The mixture was then poured into ddH$_2$O to precipitate out a brownish solid. This solid was collected

by filtration, washed with 20 mL of ddH$_2$O and dried as an orange colored solid (0.20 g; 0.8 mmol; 40% yield). **(3)** *Synthesis of EIQD:* 0.19 g (0.76 mmol) of **(2)** and 0.30 g (0.9 mmol) of 4-(trifluoromethyl)phenyl isothiocyanate were dissolved in 3 mL of dry DMF and stirred at room temperature for 24 h. The solvent was evaporated and the brownish residue dissolved in acetonitrile. 10 mL of 0.1 M HCl was added to the solution to precipitate out a brown solid. The solid was washed with 20 mL of ddH$_2$O and dried. (0.04 g; 10% yield). *m/z* (ESI) 457.0 (M-H$^+$). C$_{22}$H$_{17}$F$_3$N$_4$O$_2$S requires 458.0). ^{1}H NMR (d6-DMSO, TMS): 10.36-9.92 (m, 3H), 8.72 (d, 1H), 8.54 (d, 1H), 8.46 (d, 1H), 7.80 (dd, 1H), 7.75-7.68 (m, 4H), 6.92 (d, 1H), 4.03 (m, 2H), 1.16 (t, 3H).

Scheme 2 Synthetic route to EIQD.

45
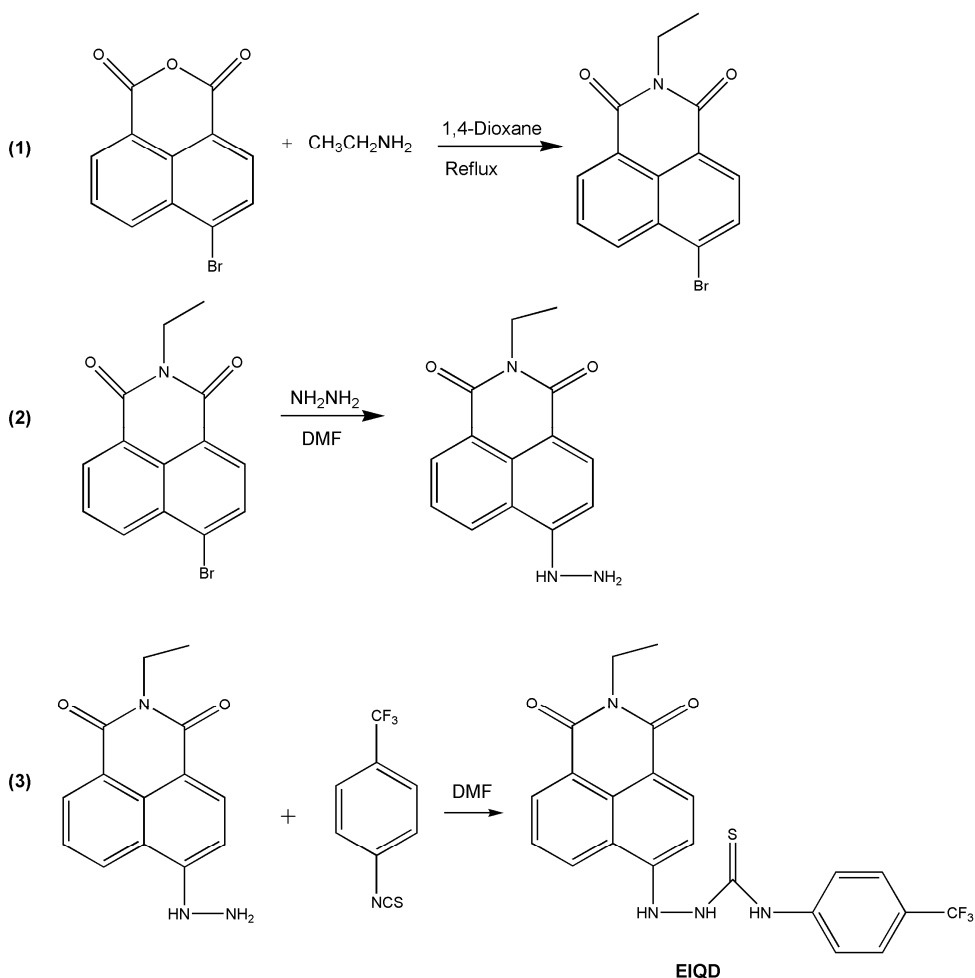
Synthesis of Bis(2,2'-bipyridine)-5(N-(2,7-dichlorofluorescein)lactam-N'-1,10-phenanthroline thiourea) ruthenium(II) bis(hexafluorophosphate) (RuDCFL)

(1) *Synthesis of Bis(2,2'-bipyridine)-(5-amino-1,10-phenanthroline)ruthenium(II) bis(hexafluorophosphate):* 40 mg (0.21 mmol) of 5-Amino-phenanthroline and 100 mg (0.22 mmol) of $Ru(bpy)_2Cl_2$ were refluxed in 10 mL of methanol/water 1:2 (v/v) for 8 h. Methanol was evaporated and an orange precipitate was obtained after addition of excess NH_4PF_6. The precipitate was filtered, washed with 10 mL of ddH_2O and dried (0.20 g; 0.21 mmol; 99% yield). R_f (Al_2O_3, ACN:TOL 2:1 (v/v)): 0.81 **(2)** Synthesis of *Bis(2,2'-bipyridine)-(5-isothiocyanato-1,10-phenanthroline)ruthenium(II) bis(hexafluorophosphate):* 0.19 mg (0.20 mmol) of **(1)** and 0.09 g of $CaCO_3$ were dissolved in 5 mL of dry acetone. 22 µL of thiophosgene (98%) were added and the solution was stirred at room temperature for 1 h. Then, the solution was refluxed for 2.5 h. The mixture was filtered over celite and the solvent was removed by rotary evaporation to yield a red solid (0.24 g; 0.18 mmol; 86% yield). **(3)** *Synthesis of 2,7-dichlorofluorescein hydrazide:* see above. **(4)** *Synthesis of RuDCFL:* 0.13 g (0.13 mmol) of **(2)** and 0.11 g (0.26 mmol) of **(3)** were dissolved in dry DMF and stirred at room temperature for 18 h. The mixture was dissolved in 100 mL of CH_2Cl_2 yielding a deep red colored solution. The organic phase was washed four times with ddH_2O (100 mL), collected, dried over anhydrous Na_2SO_4, filtered and the solvent was removed by rotary evaporation yielding a deep red colored solid. (0.15 mg; 0.11 mmol; 85% yield) R_f (Al_2O_3, H_2O:ACN 2:8 (v/v)): 0.94 ; *m/z* (ESI) 532.6 (M^{2+}); 1210 ($M^{2+}+PF_6^-$). $C_{53}H_{35}Cl_2N_9O_4RuS$ requires 532.5; 1210).

Scheme 3 Synthetic route to RuDCFL.
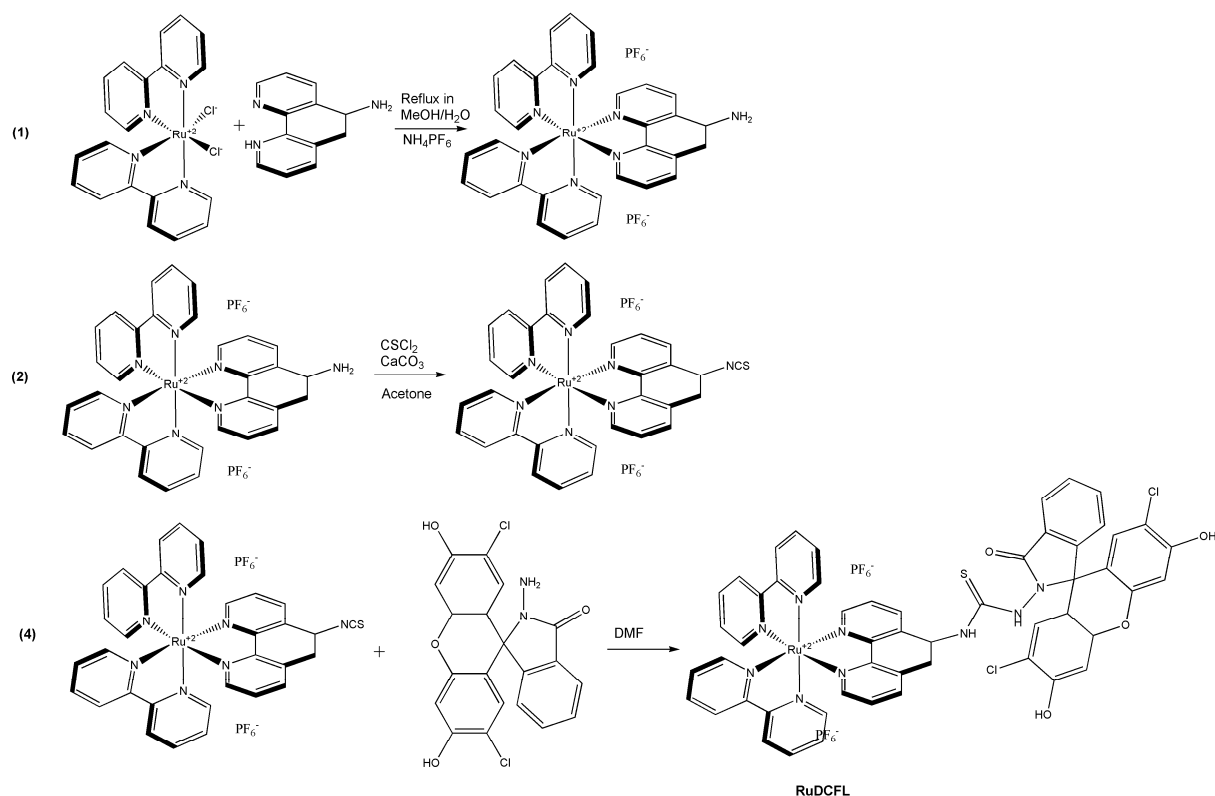
Synthesis of Bis(2,2'-bipyridine)-(5,6-diphenylthiourea-1,10-phenanthroline) ruthenium(II) bis(hexafluorophosphate) (RuDPTP)

(1) *Synthesis of Bis(2,2'-bipyridine)-(5,6-diamino-1,10-phenanthroline)ruthenium(II) bis(hexafluorophosphate) (Ru(bpy)₂phendiamin):* The complex was synthesized with slight modifications according to the literature procedure.[34] **(a)** *Synthesis of Ru(bpy)₂phendione:* 0.1 mg (0.20 mmol) of Ru(bpy)₂Cl₂ and 1,10-phenanthroline-5,6-dione were dissolved in 6 mL of ethanol:H_2O 1/1 (v/v). The mixture was refluxed for 18 h. Ethanol was evaporated and a red precipitate was obtained after addition of excess NH₄PF₆. The precipitate was filtered, washed with 10 mL of ddH₂O and dried (0.18 g; 0.20 mmol; 99% yield). **(b)** *Synthesis of Ru(bpy)₂phendioxime:* 0.18 g (0.20 mmol) of **(a)** and 30 mg of CaCO₃ were dissolved in 5 mL of dry ethanol. The mixture was refluxed for in total 18 h and a solution of 49 mg of NH₂OH HCl in 2 mL of ethanol was added dropwise during the first hour. The solvent was evaporated and the residue was dissolved in 5 mL of ddH₂O. Addition of excess NH₄PF₆ precipitated a red solid which was collected, washed, and dried. (0.17 g; 0.18 mmol; 88% yield). **(c)** *Synthesis of Ru(bpy)₂phendiamine:* the total amount of **(b)** was dissolved in 10

mL of DMSO and 50 mL of ethanol were added. A small portion of Pd/C was added to the mixture and hydrogenated for 24 h with a H_2-pressure of 10 bar. The solvent was evaporated and the residue dried. **(2)** *Synthesis of Bis(2,2'-bipyridine)-(5,6-diphenylthiourea-1,10-phenanthroline)ruthenium(II)bis(hexafluorophosphate) (RuDPTP):* 0.033 mmol of **(c)** and 0.05 mmol of phenyl isothiocyanate were dissolved in dry DMF and stirred at room temperature for 24 h. The solvent was evaporated and the red residue dried. (0.03 g; 0.025 mmol; 76% yield).
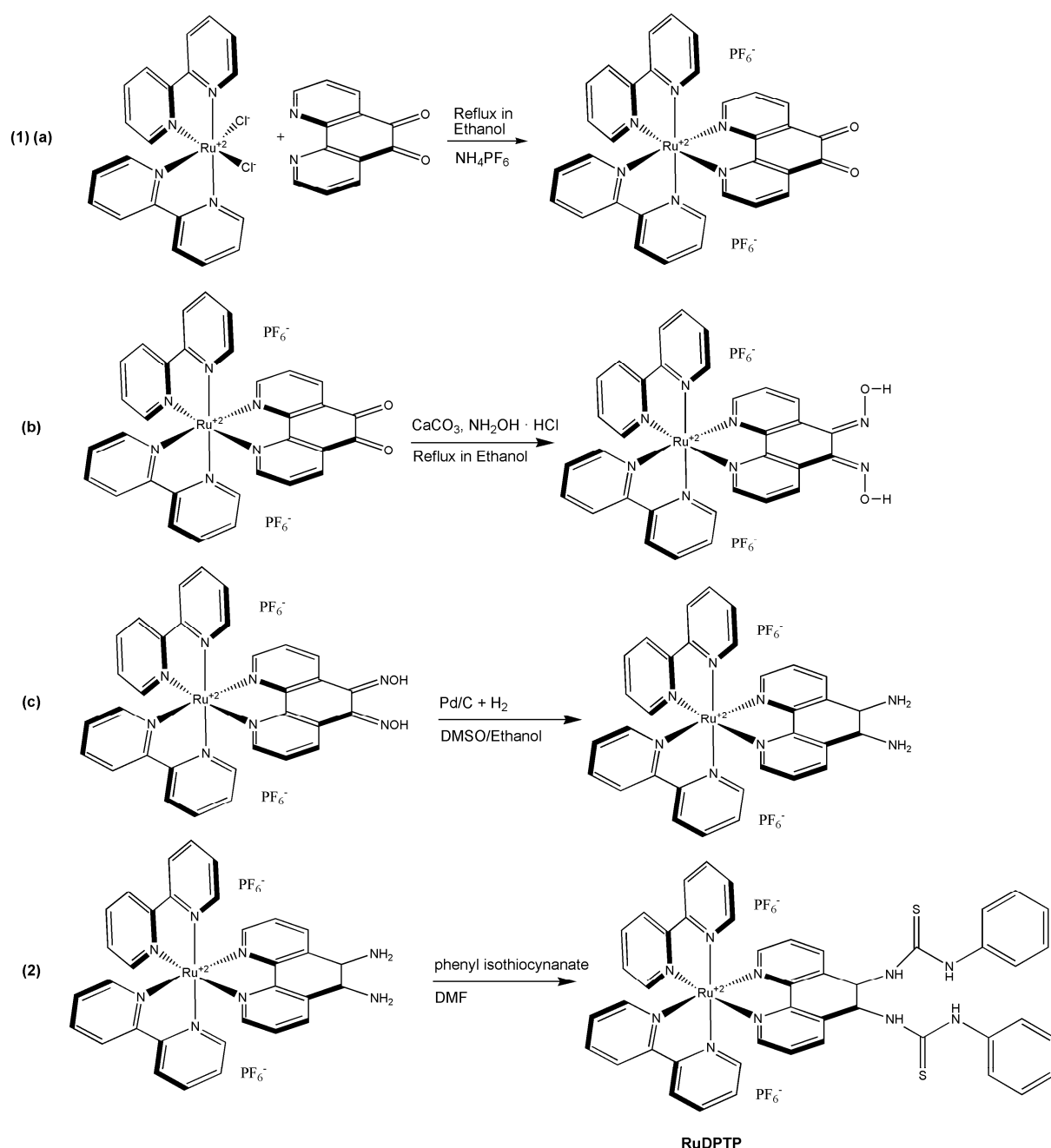
Scheme 4 Synthetic route to RuDPTP.

Synthesis of Bis(2,2'-bipyridine)-(5,6-diacetamido-1,10-phenanthroline) ruthenium(II) bis(hexafluorophosphate) (RuDAAP)

(1) *Synthesis of Bis(2,2'-bipyridine)-(5,6-diamino-1,10-phenanthroline)ruthenium(II) bis(hexafluorophosphate) (Ru(bpy)$_2$phendiamine):* see above. **(2)** *Synthesis of RuDAAP:* 0.5 mmol of **(1)** and 200 μL (2 mmol) of acetic anhydride were dissolved in 30 mL of CHCl$_3$. The mixture was refluxed under N$_2$ for 96 h. The solvent was removed and the brownish residue was dissolved in 3 mL of ddH$_2$O. Excess NH$_4$PF$_6$ was added to precipitate a brown solid that was collected, filtered, washed and dried. (0.16 mg; 0.16 mmol; 32% yield) *m/z* (ESI) 353.6 (M^{2+}); 853.2 (M^{2+}+PF$_6^-$). C$_{36}$H$_{30}$N$_8$O$_2$Ru requires 708.2; 836.0).

Scheme 5 Synthetic route to RuDAAP.

RuDAAP
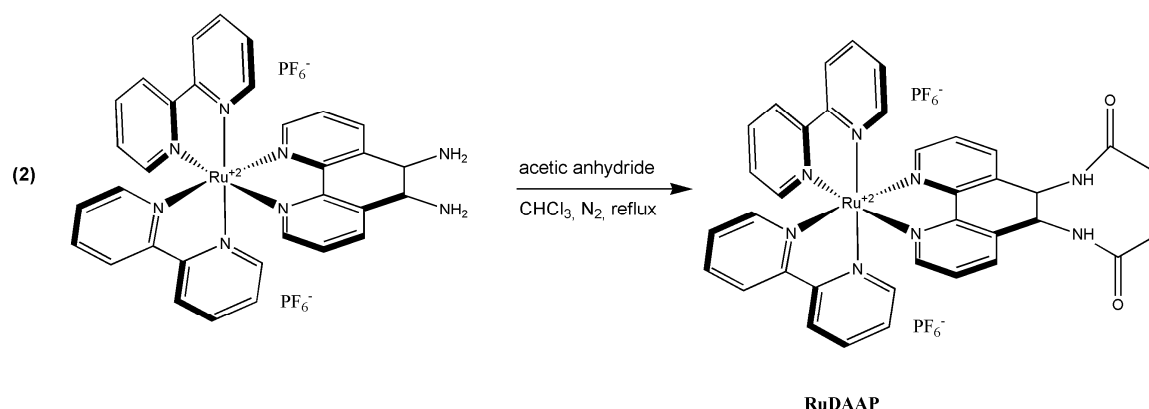
3.5 References

[1] Ng P-L, Lee C-S, Kwong H-L, Chan ASC (2005) Zinc complex of bipyridine crown macrocycle: Luminescence sensing of anions in aqueous media via the cooperative action of metal-ligand and hydrophobic interactions. Inorg Chem Comm, 8: 769-772.

[2] Martínez-Máñez R, Sancenón F (2003) Fluorogenic and Chromogenic Chemosensors and Reagents for Anions. Chem Rev, 103: 4419-4476.

[3] Bianchi A, Bowman-James K; García-España E (Eds.) (1997) Supramolecular Chemistry of Anions. Wiley-VCH: New York.

[4] Brunetti M, Timio L, Saronio P, Capodicasa E (2001) Plasma sulfate concentration and hyperhomocysteinemia in hemodialysis patients. J Nephephrol, 14: 27-31.

[5] Park CH, Simmons HE (1968) Macrobicyclic amines. III. Encapsulation of halide ions by in,in-1,(k + 2)-diazabicyclo[k.l.m.]alkane ammonium ions. J Am Chem Soc, 90: 2431-2432.

[6] Lehn J-M, Sonveaux E, Willard AK, (1978) Molecular recognition. Anion cryptates of a macrobicyclic receptor molecule for linear triatomic species. J Am Chem Soc, 98: 4914-4916.

7   Rurack K (2001) Flipping the light switch 'ON' - the design of sensor molecules that show cation-Induced fluorescence enhancement with heavy and transition metal ions. Spectrochim Acta A, 57: 2161-2195.

8   Czarnik AW (1994) Chemical Communication in Water Using Fluorescent Chemosensors. Acc Chem Res, 27: 302-308.

9   Dietrich B (1993) Design of anion receptors: Applications. Pure & Appl Chem, 65: 1457-1464.

10   O'Neil EJ, Smith BD (2006) Anion recognition using dimetallic coordination complexes. Coord Chem Rev, 250: 3068-3080.

11   Amendola V, Esteban-Gómez D, Fabbrizzi L, Licchelli M (2006) What Anions Do to N H-Containing Receptors. Acc Chem Res, 39: 343-353.

12   Houk RJT, Tobey SL, Anslyn EV (2005) Abiotic Guanidinium Receptors for Anion Molecular Recognition and Sensing. Top Curr Chem, 255: 199-229.

13   Mei M, Wu S (2000) Fluorescent sensor for α,ω-dicarboxylate anions. New J Chem, 25: 471-475.

14   Gunnlaugsson T, Davis AP, O'Brien JE, Glynn M (2005) Synthesis and photophysical evaluation of charge neutral thiourea or urea based fluorescent PET sensors for bis-carboxylates and pyrophosphate. Org Biomol Chem, 3: 48-56.

15   Chmielewski MJ, Jurczak J (2005) Anion Recognition by Neutral Macrocyclic Amides. Chem Eur J, 11: 6080-6094.

16   Libra ER, and Scott MJ (2006) Metal salen complexes incorporating triphenoxymethanes: efficient, size selective anion binding by phenolic donors with a visual report. Chem Commun, 1485-1487.

17   Black CB, Andrioletti B, Try AC, Ruiperez C, Sessler JL (1999) Dipyrrolylquinoxalines: Efficient Sensors for Fluoride Anion in Organic Solution. J Am Chem Soc, 121: 10438-10439.

18   de Silva AP, Gunaratne NHQ, Gunnlaugsson T, Huxley AJM,. McCoy CP, Rademacher JT, Rice TE (1997) Signaling Recognition Events with Fluorescent Sensors and Switches. Chem Rev, 97: 1515-1566.

19   Burdette SC, Walkup GK, Spingler B, Tsien RY, Lippard SJ (2001) Fluorescent Sensors for Zn^{2+} Based on a Fluorescein Platform: Synthesis, Properties and Intracellular Distribution. J Am Chem Soc, 123: 7831-7841.

20   Gunnlaugsson T, Kruger PE, Jensen P, Tierney J, Ali HDP, Hussey GM (2005) Colorimetric „Naked Eye" Sensing of Anions in Aqueous Solution. J Org Chem, 70: 10875-10878.

21   Kim SK, Bok JH, Bartsch RA, Lee JY, Kim JS (2005) A Fluoride-Selective PCT Chemosensor Based on Formation of a Static Pyrene Excimer. Org Lett, 7: 4839-4842.

22   Lee MH, Quang DT, Jung HS, Yoon J, Lee C-H, Kim JS (2007) Ion-Induced FRET On Off in Fluorescent Calix[4]arene. J Org Chem, 72: 4242 4245.

23   Lee DH, Im JH, Lee J-H, Hong J-I (2002) A new fluorescent fluoride chemosensor based on conformational restriction of a biaryl fluorophore. Tetrahedr Lett, 43: 9637-9640.

24   Wu J-S, Kim HJ, Lee MH, Yoon JH, Lee JH, Kim JS (2007) Anion-induced ring-opening of fluorescein spirolactam: fluorescent OFF-ON. Tetrahedr Lett, 48: 3159-3162.

25   Kwon JY, Jang YJ, Lee YJ, Kim KM, Seo MS, Nam W, Yoon J (2005) A Highly Selective Fluorescent Chemosensor for Pb^{2+}. J Am Chem Soc, 127: 10107-10111.

26   Dujols V, Ford F, Czarnik AW (1997) A Long-Wavelength Fluorescent Chemodosimeter Selective for Cu(II) Ion in Water. J Am Chem Soc, 119: 7386-7387.

27   Friedman AE, Chambron JC, Sauvage JP, Turro NJ, Barton KJA (1990) Molecular "Light Switch" for DNA: $Ru(bpy)_2(dppz)^{2+}$. J Am Chem Soc, 112: 4960-4962.

28   Van Houten J, Watts RJ (1976) Temperature Dependence of the Photophysical and Photochemical Properties of the Tris(2,2'-bipyridyl)ruthenium(II) Ion in Aqueous Solution. J Am Chem Soc, 98: 4853-4858.

29   Ferry JG, House CH (2006) The Stepwise Evolution of Early Life Driven by Energy Conservation. Mol Biol Evol, 23: 1286-1292.

30 Lipmann F, Tuttle LC (1944) Acetyl Phosphate: Chemistry, Determination, And Synthesis. J Biol Chem, 153: 571-582.

31 Walenzyka T, Koenig B (2005) Immobilised zinc (II) cyclen complexes as catalytic reagents for phosphodiester hydrolysis. Inorg Chim Acta, 358: 2269-2274.

32 Subat M, Woinaroschy K, Gerstl C, Sarkar B, Kaim W, König B (2008) 1,4,7,10-Tetraazacyclododecane Metal Complexes as Potent Promoters of Phosphodiester Hydrolysis under Physiological Conditions. Inorg Chem, 47: 4661-4668.

33 Subat M, Woinaroschy K, Anthofer S, Malterer B, König B (2007) 1,4,7,10-Tetraazacyclododecane Metal Complexes as Potent Promoters of Carboxyester Hydrolysis under Physiological Conditions. Inorg Chem, 46: 4336–4356.

34 Bodige S, MacDonnell FM (1997) Synthesis of Free and Ruthenium Coordinated 5,6-Diamino-1,10-phenanthroline). Tetrahedr Lett, 38: 8159-8160.

4 Determination of Acetyl Phosphate *via* a Luminescent Ruthenium Ligand Complex

4.1 Introduction

Acetyl phosphate (AcP) is a high-energy metabolic compound derived from acetic acid and orthophosphoric acid. It was discovered by Lipmann in 1944[1] and lad to the discovery of coenzyme A.[2] Acetyl phosphate was also proposed as a primeval form of metabolic energy currency due to its simple chemical structure and high phosphorylation potential (ΔG^0 (AcP): -43 kJ/mol; ΔG^0 (ATP): -31 kJ/mol).[3-5] Therefore, AcP is primarily found in prokaryotes to serve as a regulatory signal transducer, i.e. in the ATP-dependent proteolysis[6], activation of the phosphate regulation[7], in motility and chemotaxis expression[8], or in the initiation of membrane phospholipid synthesis[9] of innumerable microorganisms.

The steady state concentration of AcP in wild type *E.Coli* reaches at least 3 mM.[10] Wolfe et al.[11] proved that acetyl phosphate acts as a global sign in *E.Coli*. AcP is also a non-nucleotide substrate for the Ca-ATPase[12] and an important source for regeneration of ATP[7]. Recently, the presence of an acetate kinase-phosphotransacylase-pathway (involving acetyl phosphate) was also validated for some eukaryotic microbe species.[13] Up to date, there is no clear evidence that AcP is a stable metabolic intermediate in higher living organisms. On the one hand, enzymes permitting the production of acetyl phosphate from citric acid for example are found in animal tissues.[14] On the other hand, also highly active acetylphosphatase is present in these tissues.[15] Furthermore, acetate – the prokaryotic metabolic product of AcP breakdown – is generated endogenously in mammalian cells from acetyl-CoA hydrolase without using AcP.[16]

There might also be a chance of retrieving acetyl phosphate in those cells considering the Warburg-Hypothesis[17] that tumor cells generate their energy mainly by non-oxidative breakdown of glucose followed by lactic acid fermentation. This hypothesis has re-gained some attention in recent years and was supported by a number of research groups.[18] Further assuming that non-malign cells do not produce and preserve AcP in high concentrations, it might be a powerful tumor marker. AcP attracted some attention in the commercial synthesis of ATP *via* acetate kinase. This system also provides an inexpensive and stable source for regeneration of ATP in bacterial batch reactors.[19,20]

Up to date, the most common methods for the determination of acetyl phosphate are the colorimetric hydroxylaminolysis and some acetate kinase (AK) coupled enzymatic methods. The hydroxamate assay was originally developed by Lipmann and Tuttle[21] and frequently optimized, among others by Rose et al.[22] and Pechère et al.[23] Briefly, AcP is reacted with hydroxylamine and the hydroxamic acid formed reacts with ferric ions to form an orange colored complex. This assay is simple and fast but requires strongly acidic pH and high concentrations of hydroxylamine (704 mM). This is not suitable for direct analysis of biological samples. Its limit of detection (LOD) is about 40 µM.

Recently, this assay was coupled to an enzymatic reaction resolving some of these limitations.[24] AcP is hydrolyzed by lowly concentrated hydroxylamine. The inorganic phosphate produced is then determined with a commercially available kit[25] using a purine nucleoside phosphorylase to yield a product absorbing at 330 nm at µM concentrations of AcP. The main drawback of this assay is that the presence of high concentrations of inorganic phosphate (Pi) in samples prevents direct AcP determination. Further on, Prüß and Wolfe[26] presented an AK-based assay wherein the ATP formed is determined by the luciferase reaction.[27] This assay was further improved by Ito et al.[28] and Zhao et al.[29] Another sensitive, yet time consuming method utilizing AK involves the conversion of acetyl phosphate with radioactive [^{3}H]ADP to [^{3}H]ATP, separation by thin layer chromatography (TLC) and scintillation signal readout.[30] As low as 20 nM of AcP were determined. Furthermore, AcP was assayed by supplementing cells with [^{32}Pi] and 2D-TLC of the cell extract.[31] Most of these methods share the characteristics that either they are conducted under non-biocompatible conditions or that they are complicated and time consuming.

The aim of the work reported in this chapter was to develop a luminescent method for the direct determination of AcP under biocompatible conditions. It was intended to transfer the tunable (e.g. by addition of Zn, Cu, Ni, Co) and selective reaction of hydroxylamines or hydroxamic acids[32,33] to a luminescent reporter molecule. Ruthenium complexes are known to have interesting spectral properties, e.g. large Stokes' shift, high photostability and good quantum yields. Hence, it was found that (bpy)$_2$Ru(1,10-phenanthroline-5,6-dione dioxime) (RuPDO) is an interesting candidate for further investigations. It is shown that upon reaction with AcP in the presence of Zn^{2+} or Cu^{2+} a strong increase in luminescence intensity is accompanied by a bathocromic shift. This selective reaction occurs under highly

biocompatible conditions and enables determination of AcP down to the low μM range. Although RuPDO does not emit from an excited singlet state, it is referred to as a fluorogenic probe as this is a much more common term than a luminogenic probe. Furthermore, the high potential of RuPDO for determination of acetyl phosphate in complex biological matrices is demonstrated.

4.2 Results and Discussion

4.2.1 Spectral Properties of RuPDO and Response to AcP

A solution of RuPDO in aqueous buffer displays only weak luminescence ($\lambda_{exc/em}$ at 469/610 nm). For determination of acetyl phosphate, the *vic*-oxime groups of the phenanthroline ligand are activated *in-situ* by addition of cations like Zn^{2+}, Cu^{2+} or Ni^{2+}. The addition of these activators does not alter the emission spectrum of RuPDO. The luminescence spectra of RuPDO with (RuPDO-Zn) and without activator cation (RuPDO) and in the presence of AcP (AcP-RuPDO-Zn) are shown in fig. 4.1 A.

A red shift of the emission of RuPDO of 30 nm (from 610 nm to 640 nm) is observed in the presence of AcP. This is also accompanied by a strong enhancement of fluorescence intensity, increase of quantum yield and change of decay time (see figure 4.1 B and table 1). The wavelength of the excitation maximum remains unchanged. These changes solely occur in the presence of transition metal cations and active acetic acid esters like AcP or 4-nitrophenyl acetate (4 NA). This effect is not observed in the presence of Ca^{2+} or Mg^{2+} (data not shown). Hence, a proposed reaction mechanism is shown in scheme 1 and evidence for the mechanism is given in a later section.

The large Stokes' shift of 141 nm (RuPDO-Zn) and 171 nm (AcP-RuPDO-Zn), respectively, is a further benefit of RuPDO. This warrants excellent blocking of excitation light in filter-based fluorescence instrumentation. The fairly strong red fluorescence of AcP-RuPDO-Zn also permits measurements in biological samples with almost zero background. Furthermore, the reaction product can easily be distinguished from the probe itself as the former shows much stronger and red shifted (by 30 nm) emission.

A
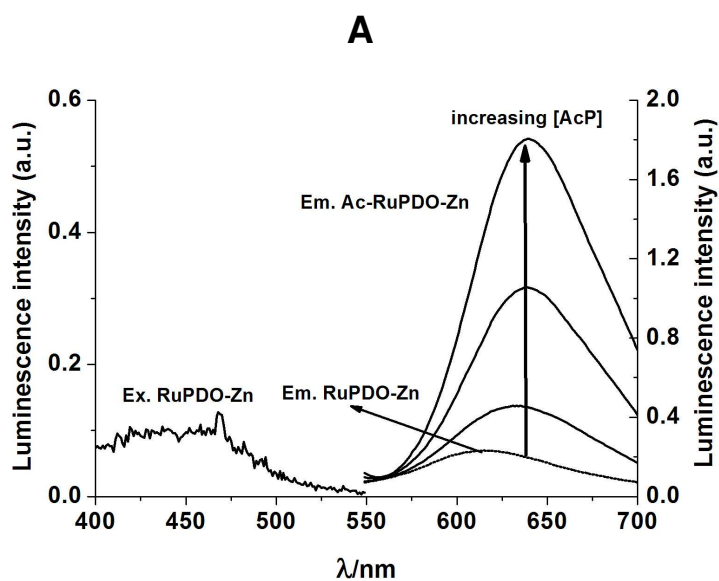
B
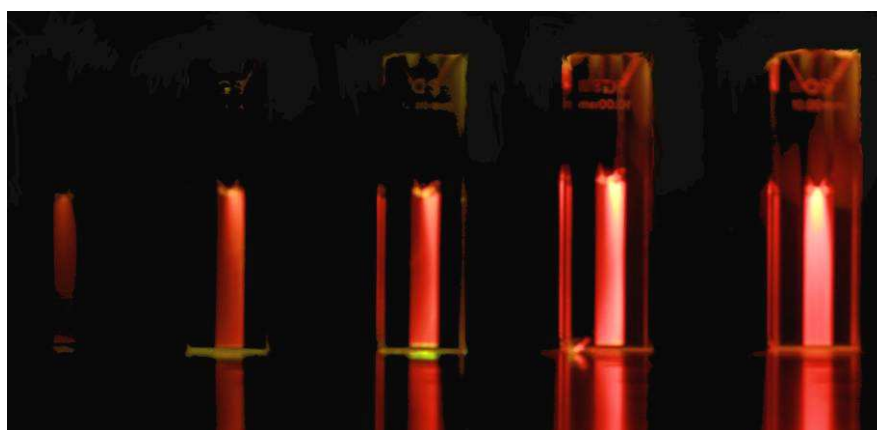
Fig. 4.1 (A) Excitation spectrum of RuPDO-Zn and emission spectra of RuPDO-Zn and the reaction product with AcP (AcP-RuPDO-Zn) after addition of increasing concentrations of AcP; 50 µM RuPDO, 0.5 mM Zn^{2+}, 20 µM, 0.1 mM, 0.5 mM of AcP, respectively, 40 mM HEPES buffer of pH 7.4; 60 min incubation at 37 °C. The emission spectrum of RuPDO closely matches the one of RuPDO-Zn and is almost invisible. **(B)** Photograph of the probe excited with 10 mW argon ion laser. From left to right (increasing concentration of AcP): probe without analyte, 50 µM, 100 µM, 500 µM, 1000 µM AcP.

The longwave emission of AcP-RuPDO-Zn suggests further investigations for detection of AcP *in-vivo*, where emission at >600 nm is a prerequisite to avoid

autofluorescence from tissue and warrants suitable penetration depth (due to reduced absorption of tissue).

Table 1 Spectral properties of RuPDO and the reaction Product with AcP (AcP-RuPDO-Zn)

	RuPDO	AcP-RuPDO-Zn
λ_{exc}/nm	469	469
λ_{em}/nm	610	640
ε_{430}, ε_{469}/L mol^{-1}cm^{-1}	7200, 5800	6300, 4400
Φ [a]	0.64%	4.5%
τ [b]	τ_1: 351 ns (81.6 %) τ_2 : 81 ns (16.3%) (χ^2=2.5)	τ_1: 280 ns (19.6 %) τ_2 : 149 ns (80.4%) (χ^2=2.1)

[a] in air saturated ethanol; Reference: rhodamine 6G (Φ = 0.95)

[b] in air saturated HEPES buffer (40 mM, pH 7.4)
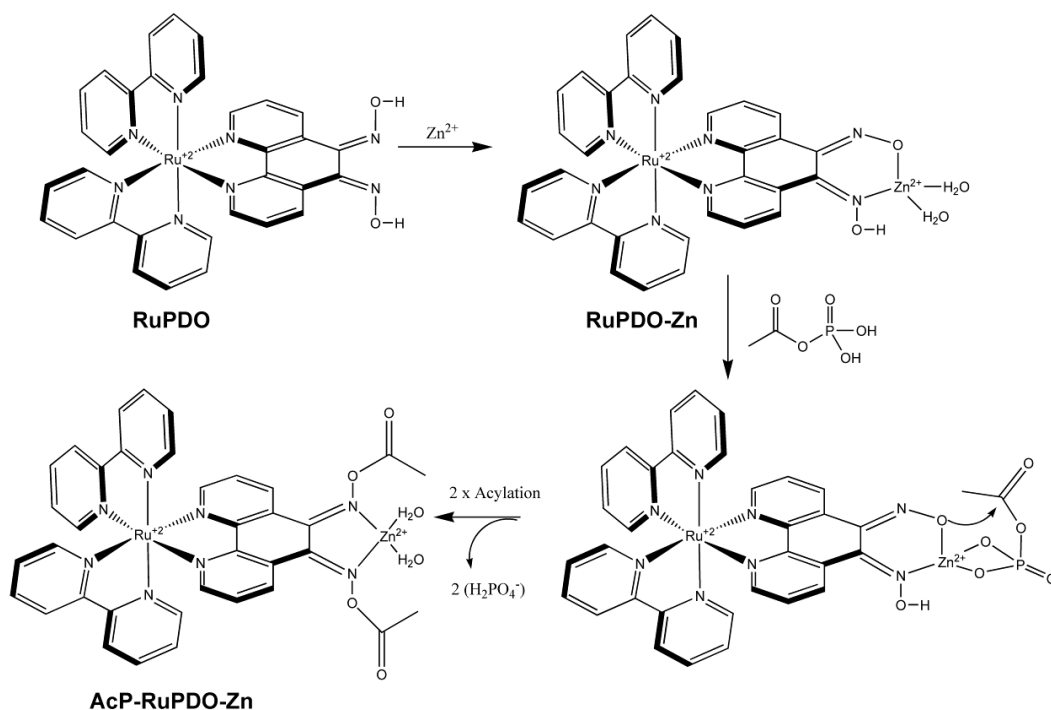
Scheme 1 Reaction mechanism of RuPDO-Zn with AcP.

4.2.2 Choice of Activating Cation

Several cations were screened for their oxime activation properties (Table 2). The reaction of RuPDO with AcP was carried out in HEPES buffer pH 7.4 (40 mM) at 37 °C in the presence of 1 mM of AcP, 0.5 mM of activating cation and 50 µM of RuPDO. The luminescence intensity at 640 nm was referenced with respect to the signal found for Zn^{2+}-activation at 640 nm after 60 min incubation time. Finally, only Zn^{2+} and Cu^{2+} were selected for further investigations due to their higher biocompatibility compared to the other cations tested and the strong response to AcP.

Table 2 Effect of activating cations

Activator Cation	$I_M^{x+}/I_{Zn}^{2+\ a}$	Activator Cation	$I_M^{x+}/I_{Zn}^{2+\ a}$
Zn^{2+}	100%	Ce^{4+}	17%
Cu^+	52%	Ce^{3+}	66%
Cu^{2+}	87%	La^{3+}	39%
Cd^{2+}	51%	Ni^{2+}	86%
Pd^{2+}	13%	Yb^{3+}	54%
Ru^{3+}	13%	Y^{3+}	58%
Cr^{2+}	13%	Tb^{3+}	53%
Ag^+	18%	Eu^{3+}	46%
Co^{2+}	14%		

a) after 60 min incubation time, each

4.2.3 Effect of pH and Reaction Time

The effect of pH on the reaction of Zn^{2+}- and Cu^{2+}-activated RuPDO with AcP was investigated *via* luminescence measurement at 640 nm. The pH dependence of the reaction of RuPDO-Zn and RuPDO-Cu with AcP is shown in Fig 2. It is in good agreement with previous data of Cu^{2+} and Zn^{2+} activated oximes.[34,35] It is possible to determine AcP at physiological pH with RuPDO-Zn as well as with RuPDO-Cu. Therefore, pH 7.4 was chosen as the optimal pH for all further investigations.
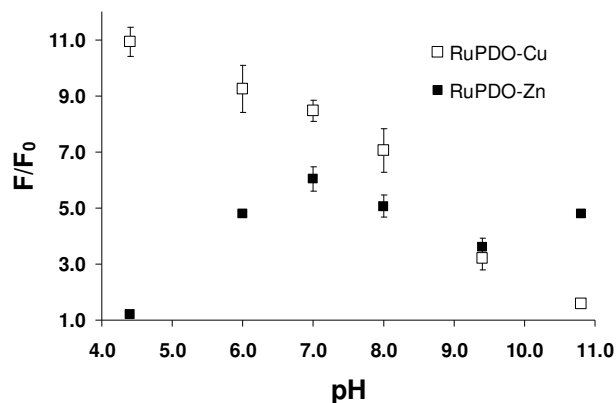
Fig. 4.2 Effect of pH on the reaction of RuPDO-Zn/Cu with AcP.10 mM Piperacine-Glycylglycine buffer; 50 µM RuPDO; 0.5 mM $ZnCl_2$ or $CuCl_2$, respectively; 1 mM AcP; 60 min incubation at 37 °C (n = 4).

The reaction rate of 50 µM RuPDO in the presence of 0.5 mM Zn^{2+} or Cu^{2+} with 0.1, 0.2 and 1 mM of AcP, respectively, was also examined at 37 °C *via* F/F_0 at 640 nm (fig. 4.3). After 60 min incubation, over 90% of the maximum signal is achieved at all concentrations of AcP. Therefore, a 1 h incubation time was chosen for all further investigations.
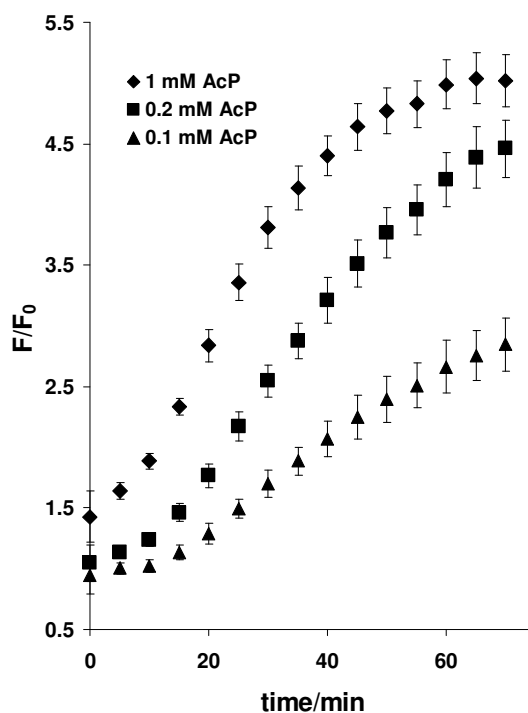
Fig. 4.3 Effect of reaction time on the reaction of RuPDO-Zn with AcP. 40 mM HEPES buffer of pH 7.4; 50 µM RuPDO; 0.5 mM Zn^{2+}; 0.1, 0.2, 1 mM of AcP, respectively; 60 min reaction at 37 °C (n = 4).

4.2.4 Mechanism of Fluorogenic Reaction

We were further interested in the mechanism of the reaction between RuPDO-Zn and AcP. The proposed reaction mechanism (scheme 2) was inspired by the work of Lipmann and Tuttle[21], Weijnen et al.[36] and Mancin et al.[34] The two main possibilities clearly are either an acetylation of the oxime groups or a phosphorylation. Therefore, 4-nitrophenyl acetate (4 NA) was added to a buffered solution of RuPDO-Zn and in another experiment bis(nitrophenyl) phosphate (BNPP). In case of 1 mM 4 NA, the same increase of luminescence intensity peaking at 640 nm was observed as with AcP solution of equal concentration (figure 4.4 B). Additionally, an increase of the absorbance at 400 nm was found due to absorption of the 4-nitrophenolate anion formed during the reaction (figure 4.4 A). Neither the emission spectrum nor the absorption spectrum was affected during the reaction of RuPDO-Zn with BNPP or other biologically relevant phosphates like inorganic phosphate (Pi), pyrophosphate (PP), ATP and ADP. This is clear evidence for the oxime acetylation thesis. Furthermore, the IR spectra of RuPDO prior and after reaction with AcP (AcP-RuPDO-Zn) differ mainly due to the appearance of the new aliphatic C-H stretching vibrations at 2923 and 2853 cm^{-1}, respectively, of the O-Ac group (AcP-RuPDO-Zn).

A   **B**
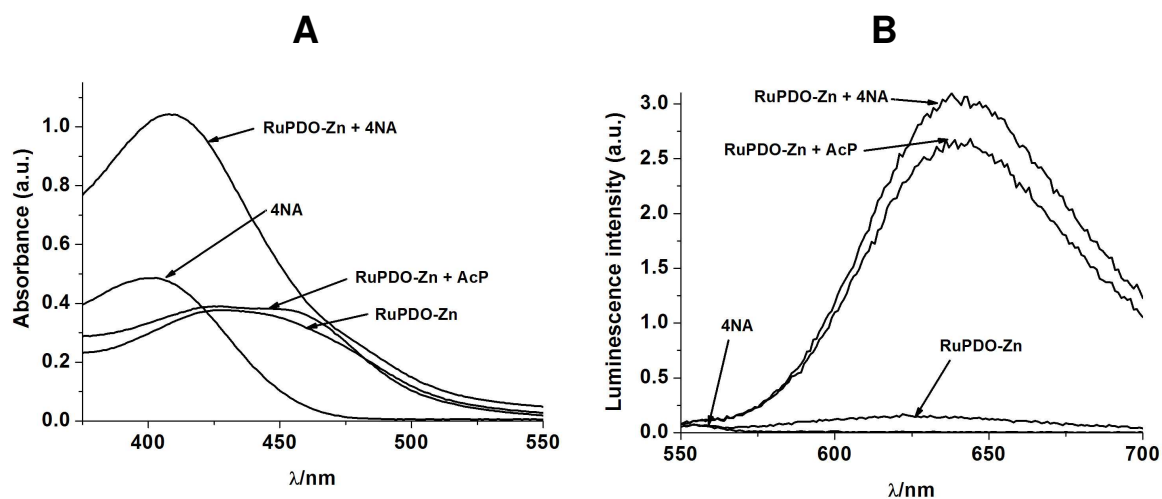
Fig. 4.4 (A) Absorbance spectra of RuPDO-Zn, RuPDO-Zn + AcP, 4 NA, and RuPDO-Zn + 4 NA after 60 min of incubation in 40 mM HEPES buffer of pH 7.4 at 37 °C. **(B)** Emission spectra of RuPDO-Zn, RuPDO-Zn + AcP, 4NA, and RuPDO-Zn + 4NA after 60 min of incubation in 40 mM HEPES buffer of pH 7.4 at 37 °C. [AcP] = 1 mM; [RuPDO] = 50 µM; [Zn^{2+}] = 0.5 mM; [4 NA] = 1 mM.

4.2.5 Complex Stoichiometry and Calibration Plots

The stoichiometry of the reaction was determined *via* Job's method of continuous variation. From figure 4.5, a 1:1 stoichiometry of the reaction of RuPDO-Zn and AcP under the given reaction conditions can be deduced. However, one can assume that in the presence of excess acetyl phosphate both oxime groups of RuPDO will be involved in the reaction. This behavior was observed in the calibration plots in fig. 4.6. The fact that linearity of the calibration plot exceeds equimolar concentrations between AcP and RuPDO suggests the participation of the second oxime reaction site. A linear dynamic range from 10 to 200 µM of AcP and 80 to 400 µM of AcP at a probe concentration of 50 µM is observed for RuPDO-Zn and RuPDO-Cu, respectively (0.5 mM of Zn^{2+}/Cu^{2+}). The regression equation for RuPDO-Zn is $F/F_0 = 16.59$ L mmol^{-1} [AcP] + 1.29 (r = 0.990) and $F/F_0 = 4.28$ L mmol^{-1} [AcP] + 0.74 (r = 0.990) for RuPDO-Cu. The limit of detection of AcP *via* RuPDO-Zn is 3.4 µM. Hence, AcP can be determined at least at 10 times lower concentrations compared to the method of Lipmann.[21]
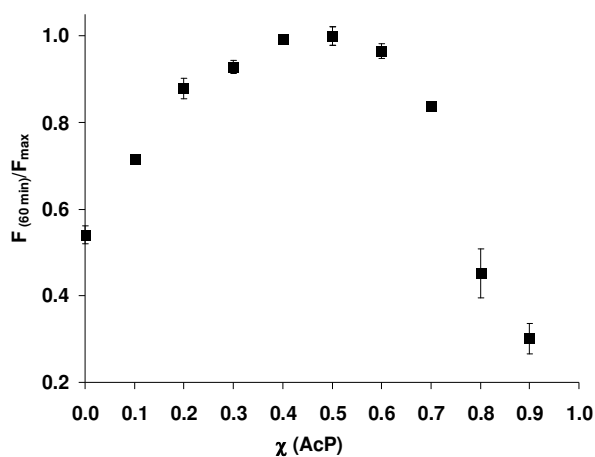
Fig. 4.5 Normalized fluorescence at 640 nm vs. mole fraction AcP. Data collected after 60 min of incubation at 37 °C in 40 mM HEPES of pH 7.4 (n = 4).
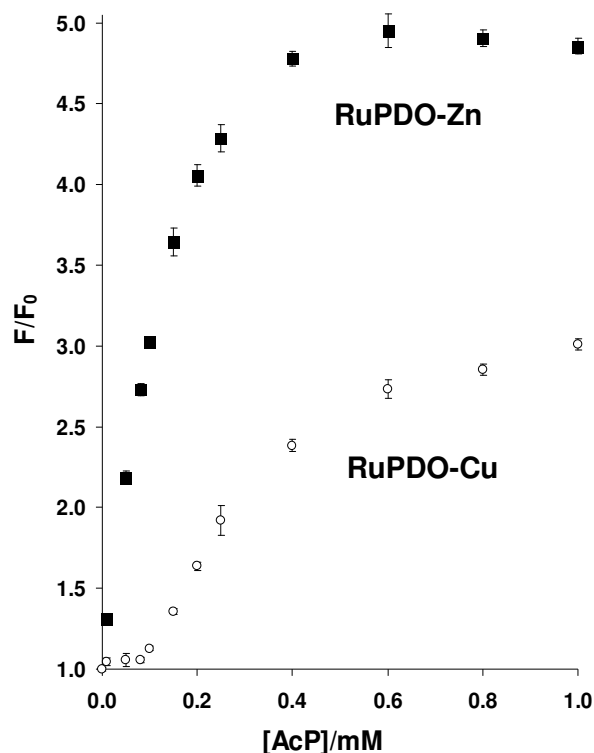
Fig. 4.6 Plot of F/F_0 vs. [AcP] collected after 60 min of incubation at 37 °C in 40 mM HEPES of pH 7.4 (n = 4).

4.2.6 Interference by other Relevant Phosphates

The reaction of RuPDO-Zn with AcP in the presence of equimolar concentrations of inorganic phosphate (Pi), pyrophosphate (PP) and ATP was monitored using luminescence (fig. 4.7). These phosphates slightly quench the luminescence of RuPDO-Zn, probably due to coordination to Zn^{2+}. Within a tolerance limit of ± 10 % the following concentrations of interferents are acceptable: Pi = 1 mM; PP = 0.22 mM and ATP = 0.67 mM. Hence, even in the presence of equimolar concentrations of AcP and phosphate (1 mM as found in DMEM medium, see next section) a pronounced increase of luminescence is detectable. As a result, the slope of a calibration plot for AcP in the presence of equimolar phosphate is slightly reduced. It is assumed that binding of these phosphates to RuPDO-Zn blocks the "binding-site" for AcP, resulting in a lower acetylation rate and therefore a lower luminescence. Addition of phosphate to a reacted solution (90 min) of AcP-RuPDO-Zn does not change the signal (data not shown), substantiating the binding-site-blocking thesis. The binding of phosphates to the probe can adequately be reduced by adding a higher amount of Zn^{2+} to the sample, resulting in higher luminescence intensity due

to complexation of phosphate by free Zn^{2+} in solution. This was tested in detail by adding increasing amounts of Zn^{2+} (50 µM - 5 mM) to solutions containing 1 mM of AcP and 1 mM of Pi. It is obvious from figure 4.8 that higher concentrations of Zn^{2+} are able to overcome the quenching-effect of Pi.
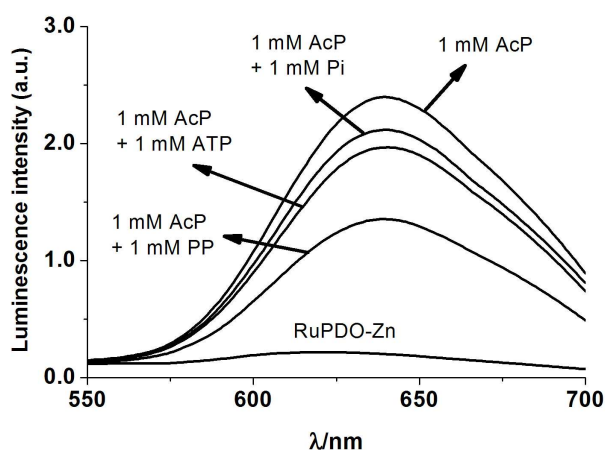
Fig. 4.7 Effect of bio-phosphates on the luminescence of the reaction of RuPDO-Zn with AcP. 40 mM HEPES buffer of pH 7.4; 50 µM RuPDO; 0.5 mM Zn^{2+}; 1 mM of AcP and inorganic phosphate (Pi), pyrophosphate (PP), ATP, each; 60 min reaction at 37 °C.
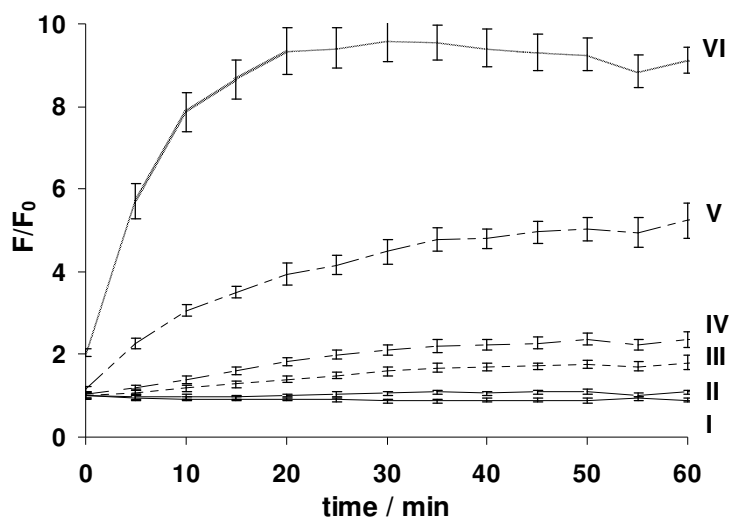
Fig. 4.8 Luminescence of RuPDO-Zn in 40 mM HEPES buffer of pH 7.4 in the presence of 1 mM Pi (RuPDO: 50 µM; AcP: 1 mM). The solid line (I) represents the sample without Zn^{2+}. Zn^{2+}-concentrations: II = 50 µM; III = 250 µM; IV = 0.5 mM; V = 2.5 mM; VI = 5.0 mM.

4.2.7 Tests of RuPDO-Zn in Cell Medium Containing NRK Cells

The reaction of RuPDO-Zn with AcP was examined in Dulbecco's Modified Eagle Medium (DMEM) and also in DMEM medium containing normal rat kidney (NRK) cells in order to test the future applicability of the probe for measurements in biological matrices. DMEM medium used in the experiments contains, among others, high millimolar concentrations of inorganic compounds like $CaCl_2$, NaH_2PO_4 and KCl, various amounts of different amino acids and 10% (w/w) fetal calf serum. NRK cells were grown in DMEM medium for 2 days. During this period the medium is further enriched with products of cell metabolism. Hence, the cell medium used is a complex matrix and served as reaction medium without further workup. The medium together with 50 µM of RuPDO, 0.5 mM of $ZnCl_2$ and various amounts of AcP was incubated at 37 °C and the progress of the reaction was monitored for 90 min by recording the increase of the luminescence intensity at 640 nm. An almost 2.5 fold signal increase in both DMEM medium containing NRK cells (fig. 4.9) and medium without cells (data not shown) was observed on addition of 2 mM of AcP. As a matter of fact, the signal increase is not as high as observed in plain aqueous buffered solution due to the complex matrix. The slope is reduced by a factor of 20 compared to aqueous buffer. However, it is obvious from the calibration plot that determination of AcP from 0.5 to 2 mM is possible with reasonable precision in complex biological matrices using the luminescence of RuPDO-Zn. Importantly, the reaction time in cell medium is much shorter compared to the reaction in aqueous buffer. The maximal luminescence intensity at 640 nm is obtained after 30 min of incubation. This strongly supports the proposed reaction mechanism of RuPDO-Zn. A high amount of RuPDO-Zn is already blocked in the presence of high concentrations of phosphate. Therefore, only few RuPDO-Zn molecules are able to react with AcP, resulting in an decreased luminescence intensity at 640 nm and shorter reaction time compared to a sample in plain buffer.
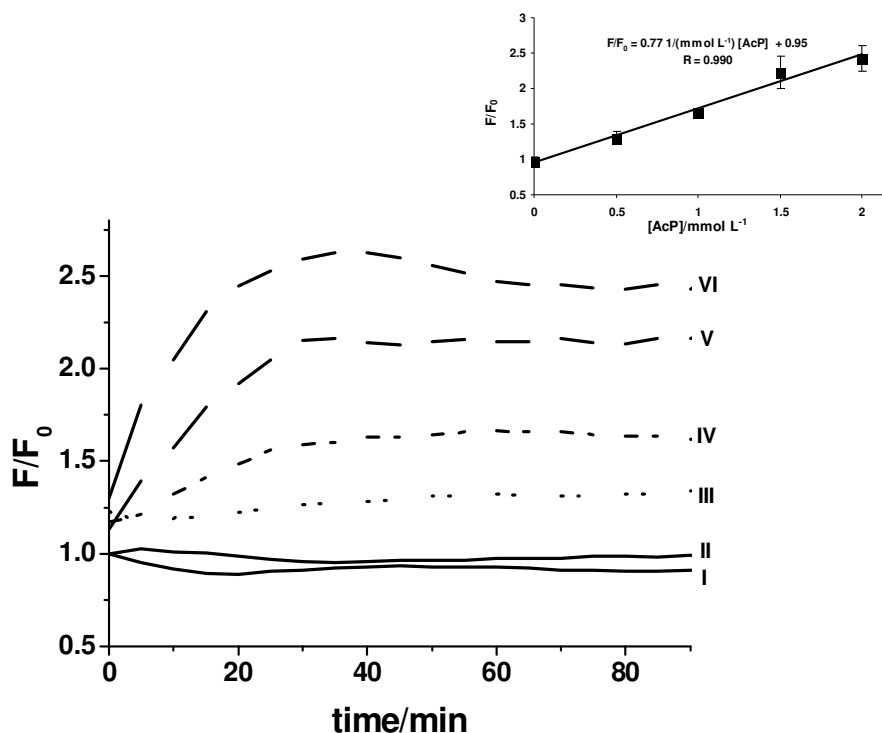
Fig. 4.9 Luminescence of RuPDO-Zn in suspensions of NRK-cells in DMEM cell medium after spiking with AcP. Solid lines (I and II) represent unspiked samples without cells (I) and in the presence of cells (II). Dashed lines (III to VI) represent spiked samples of cell media containing NRK cells. AcP concentration is increasing from 0.5 mM (III) to 2 mM (VI). (n = 4).

4.2.8 RuPDO-Zn in Lysogeny Broth Medium (LB) Containing *E.coli*

Additional tests of RuPDO-Zn were conducted in *E.coli* Lysogeny broth media (LB) without bacteria, in LB media containing *E.coli*, and in LB media containing sonicated *E.coli* (see figures 4.10-4.15). The kinetic of the reaction of RuPDO-Zn with AcP in *E.coli* LB media without bacteria is shown in figure 4.10. The reaction of RuPDO-Zn with AcP is slower than in DMEM medium (figure 4.9). While the increase of luminescence intensity is slower, the slope of the calibration plot is steeper (figure 4.11) than in DMEM medium (inset of figure 4.9).
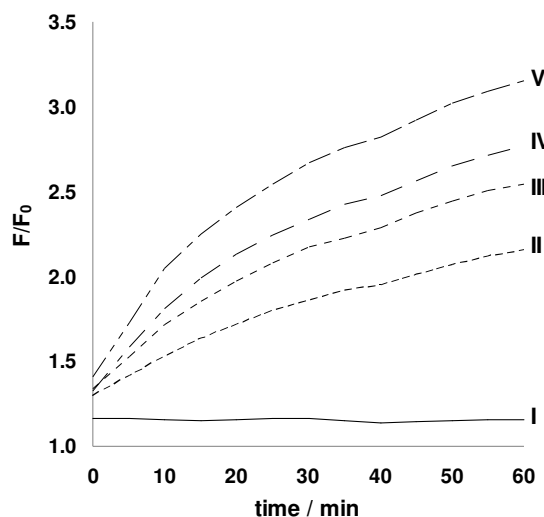
Fig. 4.10 Luminescence of RuPDO-Zn in LB medium after spiking with AcP. Solid line (I) represents unspiked medium. Dashed lines (II to V) represent spiked samples of broth media. AcP concentration is increasing from 0.4 mM (II) to 1 mM (V). (n = 4).
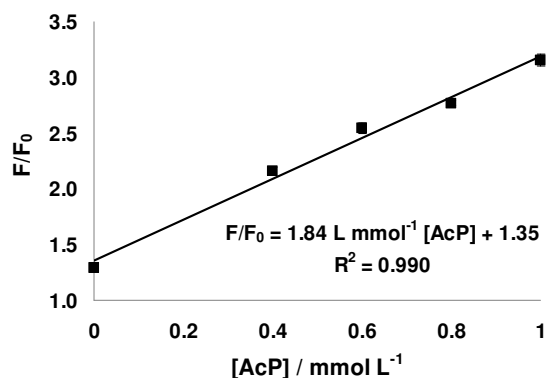
Fig. 4.11 Calibration plot of RuPDO-Zn in LB medium after spiking with AcP. AcP concentration is increasing from 0.4 mM to 1 mM (n = 4).

The kinetics of the reaction of RuPDO-Zn with AcP in LB media containing *E.coli* is shown in figure 4.12. It remains almost unchanged with respect to LB medium without *E.coli* (figure 4.10). The increase of luminescence intensity is lower, resulting in a lower slope of the calibration plot (figure 4.13) than in LB medium without *E.coli* (figure 4.11). This behavior may be expected because cells usually show strong scatter in luminescence measurements.
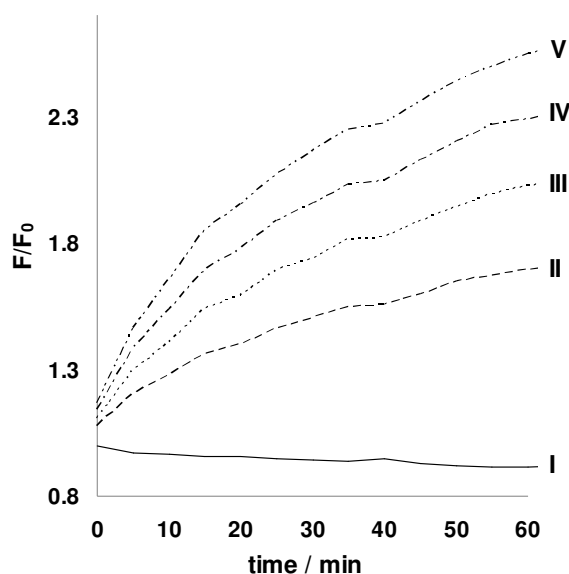
Fig. 4.12 Luminescence of RuPDO-Zn in LB medium containing *E.Coli* after spiking with AcP. Solid line (I) represents unspiked medium with *E.Coli*. Dashed lines (II to V) represent spiked samples of broth media. AcP concentration is increasing from 0.4 mM (II) to 1 mM (V). (n = 4).
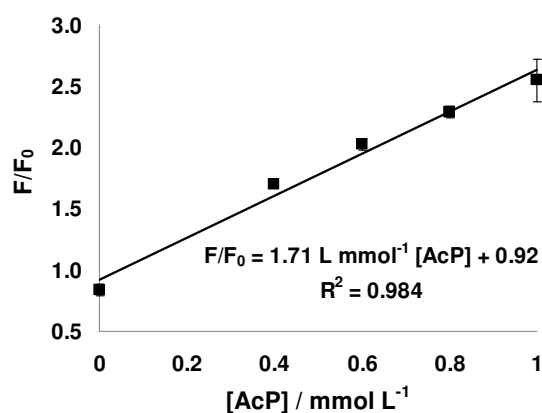
Fig. 4.13 Calibration plot of RuPDO-Zn in LB medium containing sonicated *E.Coli* after spiking with AcP. AcP concentration is increasing from 0.4 mM to 1 mM (n = 4).

The kinetics of the reaction of RuPDO-Zn with AcP in LB media containing sonicated *E.coli* is shown in figure 4.13 and remains almost unchanged with respect to LB medium containing *E.coli* (figure 4.12). Here, the increase of luminescence intensity (figure 4.15) is almost constant with respect to the unlysed cells (figure 4.13). These data clearly show the applicability of the probe in various complex biological matrices.
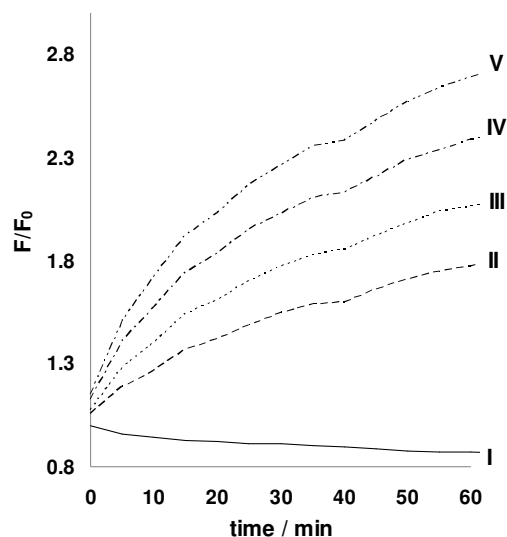
Fig. 4.14 Luminescence of RuPDO-Zn in LB medium containing sonicated *E.Coli* after spiking with AcP. Solid line (I) represents unspiked medium. Dashed lines (II to V) represent spiked samples of broth media containing sonicated *E.Coli*. AcP concentration is increasing from 0.4 mM (II) to 1 mM (V). (n = 4).
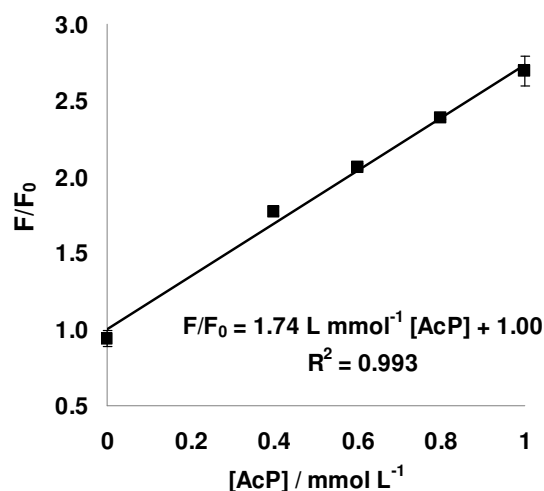
Fig. 4.15 Calibration plot of RuPDO-Zn in LB medium containing *E.Coli* after spiking with AcP. AcP concentration is increasing from 0.4 mM to 1 mM (n = 4).

4.3 Conclusions

The first fluorogenic probe RuPDO is introduced for rapid and direct determination of acetyl phosphate in aqueous solutions at neutral pH. The probe itself is virtually nonluminescent but undergoes strong increase in luminescence accompanied by a 30-nm red-shift in presence of AcP and cations like Zn^{2+} or Cu^{2+}. Unlike in common methods for determination of AcP, the presence of millimolar concentrations of inorganic phosphate only weakly reduces sensitivity and no radioactive waste is produced. Successful determination of AcP in complex biological matrices and the longwave emission of AcP-RuPDO-Zn suggest further investigations for detection of AcP *in-vivo*. A combination of RuPDO with suitable enzymes involved in the formation or conversion of AcP suggest luminescent probing of other biological important analytes like glucose, α-ketoglutarate, and acetate (see Chapter 5).

4.4 Experimental

4.4.1 Materials

cis-Dichlorobis(2,2'-bipyridine)ruthenium(II) dihydrate ($Ru(bpy)_2Cl_2$) was purchased from ABCR (www.abcr.de). All other chemicals and solvents were purchased from Sigma Aldrich (www.sigmaaldrich.com) or Acros Organics (www.acros.be). Stock solutions of acetyl phosphate (10.0 or 1.0 mM) were prepared in HEPES buffer of pH 7.4 (40 mM) shortly before measurements. Stock solutions of RuPDO (1.0 mM) were prepared by pre-dissolving of 0.94 mg of the reagent in 10 µL of DMSO followed by dilution with HEPES buffer to 1.0 mL. The RuPDO stock solution was stored at 4 °C. Stock solutions of $ZnCl_2$ were prepared by dissolving 34.1 mg of the reagent in 50 mL of HEPES buffer.

4.4.2 Methods

50 µL of the RuPDO stock solution (final concentration 50 µM in 40 mM HEPES buffer of pH 7.4) and 100 µL of $ZnCl_2$ (final concentration 0.5 mM) was added to HEPES buffer of pH 7.4 (40 mM) containing at least 0.05 mM of AcP and made up to 1 mL (for tests in cuvettes). One-tenth of all volumes were used for microtiter plate

based experiments (final volume 0.1 mL). The same amount of RuPDO and $ZnCl_2$ was added to the control containing no AcP. The reaction vials were then kept at 37 °C for 60 min before measuring luminescence.

4.4.3 Instrumentation

Absorption spectra were recorded on a Cary 50 Bio UV-Vis Spectrophotometer (Varian, Australia; www.varianinc.com). Luminescence spectra were recorded on an Aminco-Bowman AB 2 luminescence spectrometer (www.thermo.com) equipped with a 150 W continuous wave xenon lamp as excitation light source. All spectra are uncorrected. Lifetime measurements were done on an ISS K2 multifrequency cross-correlation phase modulation fluorimeter (www.iss.com) using an argon ion laser for excitation. Microtiter plate experiments were performed on a Tecan Genios Plus Reader (www.tecan.de) at λ_{exc} = 485 nm and λ_{em} = 635 nm in black flat bottom 96-well plates from Greiner Bio One (www.gbo.com). pH was measured with a pH meter CG 842 from Schott (www.schott.com) at room temperature. The ESI mass spectra were taken on a ThermoQuest TSQ 7000 (www.thermo.com) mass spectrometer. IR Spectra of solids were recorded with a diamond ATR-crystal on a Varian 670-IR spectrometer (www.varianinc.com).

4.4.4 Synthesis

RuPDO was synthesized with slight modifications according to the literature procedure[37,38] in good yields. $Ru(bpy)_2Cl_2$ (74 mg) was dissolved in dry ethanol (10 mL), then 1,10-phenanthroline-5,6-dione (phendione) (29 mg) was added and the violet solution heated to reflux for 5 h under N_2. After cooling to room temperature, the solvent was removed *via* rotary evaporation. $Ru(bpy)_2(phendione)$ was redissolved in ethanol (15 mL), $CaCO_3$ (dried, 34 mg) added and the mixture was heated to 81 °C. A solution of $NH_2OH·HCl$ (53 mg) in 5 mL of ethanol was added dropwise over a period of 1 h, while the orange solution turned to a reddish color. After reflux for 5 h and cooling to room temperature the solvent was evaporated. The remaining orange to red colored solid was dissolved in a small amount of H_2O and the complex was precipitated by adding excess of NH_4PF_6 (Scheme 2). The red precipitate was washed with few mL of water and diethyl ether. The crude product (60% yield) was recrystallized from acetone (50% yield). (Found: C, 38.85; H, 3.21;

N, 11.51. $C_{32}H_{24}F_{12}N_8O_2P_2Ru \cdot 3\ H_2O$ requires C, 38.53; H, 3.03; N, 11.23 %); *m/z* (ESI) 326.8 (M^{2+}. $C_{32}H_{24}N_8O_2Ru$ requires 327.1).

Scheme 2 Synthetic route to RuPDO.
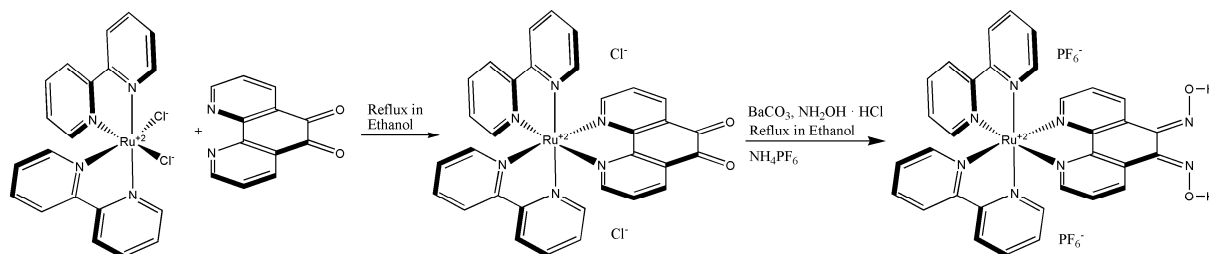
4.5 References

[1] Lipmann F, Tuttle CL (1944) Acetyl Phosphate: Chemistry, Determination, and Synthesis. J Biol Chem, 153: 571-582.

[2] Kresge N, Simoni RD, Hill RL (2005) Fritz Lipmann and the Discovery of Coenzyme A. J Biol Chem, 280: e18.

[3] Ferry JG, House CH (2006) The stepwise evolution of early life driven by energy conservation. Mol Biol Evol, 23: 1286-1292.

[4] de Duve C (2003) A Research Proposal on the Origin of Life. Orig Life Evol Biosph, 33: 559-574.

[5] Martin W, Russell MJ (2007) On the origin of biochemistry at an alkaline hydrothermal vent. Phil Trans R Soc Lond B, 362: 1887-1926.

[6] Mizrahi I, Biran D, Ron EZ (2006) Requirement for the acetyl phosphate pathway in Escherichia coli ATP-dependent proteolysis. Mol Microbiol, 62: 201-211.

[7] Kim SK, Wilmes-Riesenberg MR, Wanner BL (1996) Involvement of the sensor kinase EnvZ in the in vivo activation of the response-regulator PhoB by acetyl phosphate. Mol Microbiol, 22: 135-147.

[8] Gueriri I, Bay S, Dubrac S, Cyncynatus C, Msadek T (2008) The Pta–AckA pathway controlling acetyl phosphate levels and the phosphorylation state of the DegU orphan response regulator both play a role in regulating Listeria monocytogenes motility and chemotaxis. Mol Microbiol, 70: 1342-1357.

[9] Lu YJ, Zhang YM, Grimes KD, Qi J, Lee RE, Rock CO (2006) Acyl-Phosphates Initiate Membrane Phospholipid Synthesis in Gram-Positive Pathogens. Mol Cell, 23: 765-772.

[10] Klein AH, Shulla A, Reimann SA, Keating DH, Wolfe AJ (2007) The Intracellular Concentration of Acetyl Phosphate in Escherichia coli Is Sufficient for Direct Phosphorylation of Two-Component Response Regulators. J Bacteriol, 189: 5574-5581.

[11] Wolfe AJ (2010) Physiologically relevant small phosphodonors link metabolism to signal transduction. Curr Opin Microbiol, 13: 204-209.

[12] Soler F, Fortea MI, Lax A, Fernández-Belda F (2002) Dissecting the hydrolytic activities of sarcoplasmic reticulum ATPase in the presence of acetyl phosphate. J Biol Chem, 277: 38127-38132.

[13] Ingram-Smith C, Martin SR, Smith KS (2006) Acetate kinase: not just a bacterial enzyme. Trends Microbiol, 14: 249-253.

[14] Guly MF, Pechenova TN, Matusevich LI (1966) Pathway and Enzymes of Conversion of Citric Acid into Acetyl Phosphate in Animal Tissues. Nature, 212: 36-37.

[15] Shapiro B, Wertheimer E (1945) Acetylphosphatase in Animal Tissues. Nature, 156: 690.

[16] Crabtree B, Souter MJ, Anderson SE (1989) Evidence that the production of acetate in rat hepatocytes is a predominantly cytoplasmic process. Biochem J, 257: 673-678.

[17] Warburg O, Wind F, Negelein E (1926) Über den Stoffwechsel von Tumoren im Körper. J Mol Med, 5: 829-832.

[18] a) Engler I, Atzmüller C, Donic V, Steinhäusler F (2009) Reactive oxygen species, especially O_2^{+*} in cancer mechanisms. J Exp Ther Oncol, 8: 157-165; b) Schulz TJ, Thierbach R, Voigt A, Drewes G, Mietzner B, Steinberg P, Pfeiffer AFH, Ristow M (2006) Induction of Oxidative Metabolism by Mitochondrial Frataxin Inhibits Cancer Growth: Otto Warburg Revisited. J Biol Chem, 281: 977-981; c) Thierbach R, Schulz TJ, Isken F, Voigt A, Mietzner B, Drewes G, von Kleist-Retzow J-C, Wiesner RJ, Magnuson MA, Puccio H, Pfeiffer AFH, Steinberg P, Ristow M (2005) Targeted Disruption of Hepatic Frataxin Expression Causes Impaired Mitochondrial Function, Decreased Life Span and Tumor Growth in Mice. Human Molecular Genetics, 14: 3857-3864; d) Langbein S, Zerilli M, zur Hausen A, Staiger W, Rensch-Boschert K, Lukan N, Popa J, Ternullo MP, Steidler A, Weiss C, Grobholz R, Willeke F, Alken P, Stassi G, Schubert P, Coy JF (2006) Expression of transketolase TKTL1 predicts colon and urothelial cancer patient survival: Warburg effect reinterpreted. British Journal of Cancer, 94: 578-585.

[19] Baughn RL, Adalsteinsson O, Whitesides GM (1987) Large-scale enzyme-catalyzed synthesis of ATP from adenosine and acetyl phosphate. Regeneration of ATP from AMP. J Am Chem Soc, 100: 304-306.

[20] Ryabova LA, Vinokurov LM, Shekhovtsova EA, Alakhov YB, Spirin AS (1995) Acetyl phosphate as an energy source for bacterial cell-free translation systems. Anal Biochem, 226: 184-186.

[21] Lipmann F, Tuttle LC (1945) A Specific Micromethod for the Determination of acyl phosphates. J Biol Chem, 159: 21-28.

[22] Rose IA (1955) Acetate kinase of bacteria (acetokinase). Methods Enzymol, 1, 591-595.

[23] Pechère JF, Capony JP (1968) On the colorimetric determination of acyl phosphates. Anal Biochem, 22: 536-539.

[24] Mukhopadhyay S, Hasson MS, Sanders DA (2008) A continuous assay of acetate kinase activity: Measurement of inorganic phosphate release generated by hydroxylaminolysis of acetyl phosphate. Bioorg Chem, 36: 65-69.

[25] Webb MR (1992) A continuous spectrophotometric assay for inorganic phosphate and for measuring phosphate release kinetics in biological systems. Proc Natl Acad Sci USA, 1: 4884-4887.

[26] Prüß BM, Wolfe AJ (1994) Regulation of acetyl phosphate synthesis and degradation, and the control of flagellar expression in Escherichia coli. Mol Microbiol, 12: 973-984.

[27] Lundin A, Thore A (1975) Analytical information obtainable by evaluation of the time course of firefly bioluminescence in the assay of ATP. Anal Biochem, 66: 47-63.

[28] Ito K, Nakagawa K, Murakami S, Arakawa H, Maeda M (2003) Highly sensitive simultaneous bioluminescent measurement of acetate kinase and pyruvate phosphate dikinase activities using a firefly luciferase-luciferin reaction and its application to a tandem bioluminescent enzyme immunoassay. Anal Sci, 19: 105-109.

[29] Zhao Y, Tomas CA, Rudolph FB, Papoutsakis ET, Bennett GN (2005) Intracellular Butyryl Phosphate and Acetyl Phosphate Concentrations in Clostridium acetobutylicum and Their Implications for Solvent Formation. Appl Environ Microbiol, 71: 530-537.

[30] Hunt AG, Hong JS (1980) A micromethod for the measurement of acetyl phosphate and acetyl coenzyme A. Anal Biochem, 108: 290-294.

31 Keating DH, Shulla A, Klein AH, Wolfe AJ (2008) Optimized two-dimensional thin layer chromatography to monitor the intracellular concentration of acetyl phosphate and other small phosphorylated molecules. Biol Proced Online, 10: 36-46.

32 Oestreich CH, Jones MM (1966) The Effect of Metal Ions on Labile Phosphates. I. The Hydrolysis of Acetyl Phosphate Dianion. Biochem, 5: 2926-2931.

33 Briggs PJ, Satchell DPN, White GF (1970) Acylation. Part XXX. Metal ion catalysed hydrolysis of acetyl phosphate. J Chem Soc B, 1008-1012.

34 Mancin F, Tecilla P, Tonellato U (2000) Metallomicelles Made of Ni(II) and Zn(II) Complexes of 2-Pyridinealdoxime-Based Ligands as Catalyst of the Cleavage of Carboxylic Acid Esters. Langmuir, 16: 227-233.

35 Liu S, Hamilton AD (1997) Catalysis of phosphodiester transesterification by Cu(II)-terpyridine complexes with peripheral pendent base groups: Implications for the mechanism. Tetrahedron Lett, 38: 1107-1110.

36 Weijnen JGJ, Koudijs A, Schellekens GA, Engbersen JFJ (1992) Functionalised 1,10-phenanthroline metallocatalysts as models for hydrolytic metalloenzymes. J Chem Soc Perkin Trans, 2: 829-834.

37 Bodige S, MacDonnell FM (1997) Synthesis of free and ruthenium coordinated 5,6-diamino-1,10-phenanthroline. Tetrahedron Lett, 38: 8159-8160.

38 Li M, Xiao Z, Huan Z, Lu Z (1998) New binding state useful for attachment of dye-molecules onto TiO_2 surface. Appl Surf Sci, 125: 217-220.

5 Enzymatic Determination of Acetate *via* Acetate Kinase and RuPDO

5.1 Introduction

Short-chain fatty acids like acetate (Ac), propionate and butyrate are produced in the intestine by bacterial fermentation of indigestible carbohydrates. These degradation products are known to have positive physiological and metabolic effects and are therefore an interesting target in body fluid analysis.[1-3] This is especially true for clinical biochemistry and bioanalytics of kidney dialysis.[4] Furthermore, acetate is widely found in food mainly as product of partial oxidation of glucose and ethanol by acetic acid bacteria.[5,6] These bacteria lack the enzyme succinate dehydrogenase – a key enzyme in the citric acid cycle – prohibiting the total conversion of acetyl-CoA. Therefore, glucose is metabolized *via* the pentosephosphate pathway, i.e. formation of glyceraldehyde 3-phosphate that is oxidized to pyruvate und finally decarboxylated to yield acetate. Another metabolic pathway in these bacteria giving rise to Ac is the oxidation of ethanol.[7] Hence, acetate is a very important analyte for the determination of food quality especially for products of fermentative processes such as vine, vinegar, beer, sauerkraut or sourdough.[8,9] The bacterial oxidation of ethanol to yield acetic acid is the main reason of acidification in alcoholic beverages that can cause spoilage.[10-12] Therefore, acetate levels are routinely controlled during cultivation of microorganisms in fermenters[13,14] and in dairy industrie.[15,16] On the one hand, excessive concentrations of Ac may inhibit the growth of these microorganisms. On the other hand, acetate is an important carbon source for these organisms.[17-20]

Currently available techniques for the quantitative determination of acetate comprise the classical and well established methods like GC[21,22], GC-MS[23,24], CE[25,26] and reversed-phase liquid chromatography.[27] These methods enable sensitive, accurate, and highly reproducible determination of acetate in various biological matrices but are expensive, time consuming, and require expertise. Furthermore, also a broad spectrum of enzyme-based applications is available. These range from the well established multi-enzyme coupled reaction yielding a photometric detectable signal[28] to more sophisticated amperiometric methods using immobilized enzymes.[29] The two most common three enzyme coupled reactions for the determination of acetate are summarized in scheme 1.

Scheme 1 Enzymatic Determination of Acetate

$$\text{(1)} \quad \text{Acetate} + \text{ATP} \; \underset{}{\overset{\text{AK}}{\rightleftarrows}} \; \text{AcP} + \text{ADP}$$

A $\text{(2)} \quad \text{PEP} + \text{ADP} \; \underset{}{\overset{\text{PK}}{\rightleftarrows}} \; \text{ATP} + \text{Pyruvate}$

$$\text{(3)} \quad \text{Pyruvate} + \text{NADH} \; \underset{}{\overset{\text{LDH}}{\rightleftarrows}} \; \text{Lactate} + \text{NAD}^+$$

$$\text{(1)} \quad \text{Acetate} + \text{ATP} + \text{CoA} \; \underset{}{\overset{\text{ACS}}{\rightleftarrows}} \; \text{Acetyl-CoA} + \text{AMP} + \text{PP}$$

B $\text{(2)} \quad \text{Acetyl-CoA} + \text{Oxaloacetate} \; \underset{}{\overset{\text{CS}}{\rightleftarrows}} \; \text{CoA} + \text{Citrate}$

$$\text{(3)} \quad \text{Malate} + \text{NAD}^+ \; \underset{}{\overset{\text{MDH}}{\rightleftarrows}} \; \text{Oxaloacetate} + \text{NADH}$$
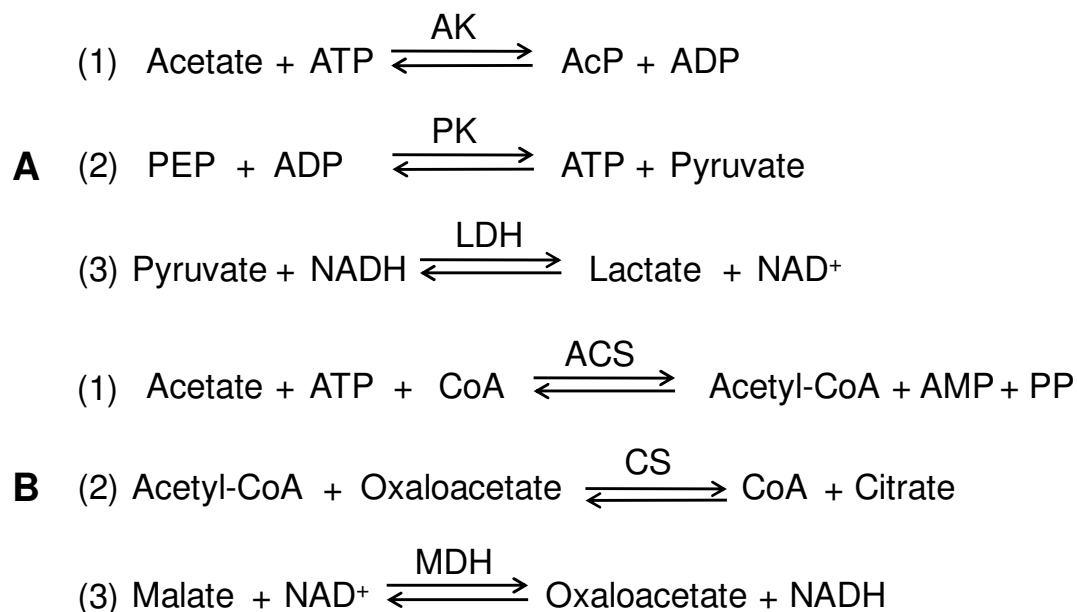
AK: Acetate kinase; PEP: Phosphoenolpyruvate; PK: Pyruvate kinase; LDH: Lactate dehydrogenase; CoA: Coenzyme A; ACS: Acetyl-CoA-Synthase; CS: Citrate synthase; MDH: Malate dehydrogenase.

In method A the acetate concentration of the sample is linked to a decrease in UV absorption of NADH at 340 nm due to its consumption. Method B utilizes the increase of this absorption peak due to formation of NADH (B 3). However, the amount of NADH in both methods is not directly proportional to the acetate concentration of the sample because the indicator reaction (A 3 or B 3) is an equilibrium reaction. Various modifications of these approaches are known in literature and are also available as commercial test kits. They all have in common that acetate is determined *via* an NAD based indicator reaction and subsequent measurement of UV absorbance.

Acetate kinase (AK) is often used as the first converting reaction in the enzymatic determination of acetate. This enzyme is highly specific towards AcP and shows only minor activity to propionyl phosphate (30%) and carbamoyl phosphate (18%) and no activity towards butyryl phosphate, glutaryl phosphate and phosphoenolpyruvate.[30] This specificity makes AK an ideal candidate for determination of acetate in real samples due to negligible cross-reactivity. Further on, the enzyme shows good long term stability when stored at 0 °C. Its activity is

restored at room temperature on addition of nucleotides within minutes. This behaviour is favourable for the applicability of test kits. A major drawback of the use of acetate kinase is that the enzymatic reaction thermodynamically greatly favours the synthesis of ATP from AcP. This results in a slow reaction kinetic for reaction A 1 (Scheme 1). Hence, a rather fast consecutive reaction that removes AcP or ADP from the equilibrium is necessary for a competitive determination of acetate.

Obviously, a multienzyme coupled system is complicated, error-prone and expensive. Moreover, the absorption signal of NADH at 340 nm is unfavourable for determination of Ac in biological samples due to the UV absorbance of numerous substances present in these matrices. Therefore, our aim was to develop a simple and inexpensive method for the determination of acetate using only reaction A 1 (Scheme 1), i.e. the quantification of acetate *via* determination of acetyl phosphate (AcP). The ruthenium based fluorogenic probe RuPDO that has already been successfully tested for the quantification of AcP in complex biological matrices (see Chapter 4) is an ideal candidate for this task.

5.2 Results and Discussion

5.2.1 Outline of the Assay Scheme

Luminescence based determination of acetate was performed by using acetate kinase and the fluorogenic probe RuPDO. The probe undergoes a strong enhancement of fluorescence accompanied by a red-shift of emission of 30 nm in the presence of acetyl phosphate within minutes (see Chapter 4). The specific reaction occurs at neutral pH in the presence of an activating cation such as Zn^{2+}. Acetate kinase catalyses the synthesis of AcP from ATP only in the presence of Mg^{2+} ions at neutral to slightly alkaline pH.[31] Herewith, the assay scheme for the enzymatic determination of acetate *via* RuPDO was clearly outlined and are summarized in scheme 2. The indicator reaction in the proposed assay is not an equilibrium-dependent reaction in contrast to the enzymatic methods described above with coupled equilibria.

Scheme 2 Enzymatic Determination of Acetate *via* RuPDO

(1) Acetate + Mg-ATP $\xrightleftharpoons{\text{AK}}$ AcP + Mg-ADP

(2) AcP + RuPDO-Zn $\longrightarrow$ AcP-RuPDO-Zn + Pi

469 nm   620 nm   469 nm   **640 nm**
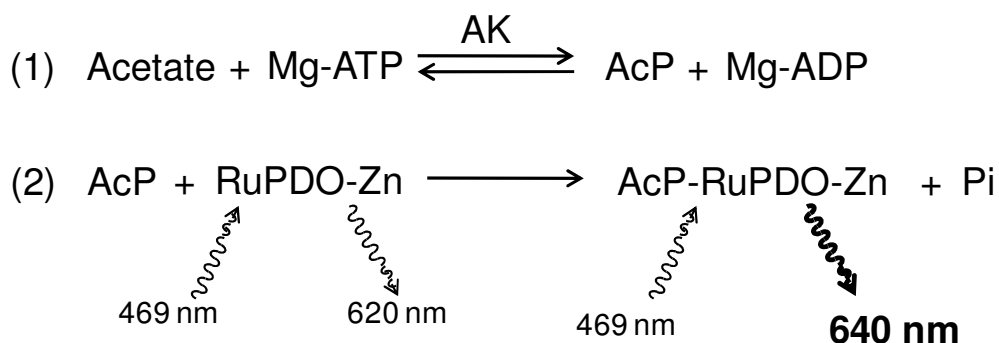
AK: Acetate kinase; AcP: Acetyl phosphate; Pi: inorganic phosphate.

5.2.2 Effect of Mg^{2+} and Optimization of Zn^{2+} concentration

The conversion of acetate and ATP into AcP and Pi is the thermodynamically unfavored direction of the acetate kinase reaction. Expectedly, micromolar concentrations of acetyl phosphate were to be determined in the presence of millimolar concentrations of ATP, ADP and Mg^{2+}. Therefore, the reaction of RuPDO-Zn (25 µM of RuPDO; 75 µM of Zn^{2+}) with 100 µM of AcP in the presence of 5 mM of ATP or ADP and up to 10 mM of Mg^{2+} in 40 mM HEPES buffer of pH 7.4 was used as a starting point for the development of the enzymatic assay. The samples were incubated for 60 min at 37 °C. Figure 5.1 shows that even 5 mM of Mg^{2+} did not interfere with the determination of AcP. A minor quenching effect (20%) was observed in samples containing 10 mM of Mg^{2+}. However, the determination of AcP in the presence of 0.25 to 5 mM of ATP or ADP, respectively, was not successful under the given assay conditions (fig. 5.2). This is due to the fact that phosphates quench the luminescence of RuPDO-Zn as shown in Chapter 4. Hence, increasing of the RuPDO concentration to 50 µM and the Zn^{2+} concentration to 500 µM was necessary. Elevated concentrations of Zn^{2+} can adequately reduce the quenching effect of phosphates on the luminescence of RuPDO as also shown in Chapter 4. The preliminary results for the determination of acetyl phosphate under the optimized assay conditions are shown in fig. 5.3. A 55% luminescence increase was observed after addition of 100 µM of AcP to the sample containing 2.5 mM of ATP, ADP, and

Mg^{2+}, respectively, in 40 mM HEPES buffer of pH 7.4 with 60 min of incubation at 37 °C. Addition of 2 mM of AcP yielded a 355 % luminescence increase.
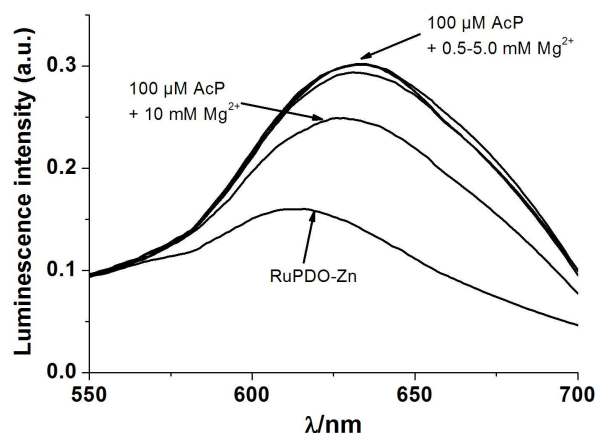
Fig. 5.1 Effect of Mg^{2+} on the luminescence of the reaction of RuPDO-Zn with AcP. 40 mM HEPES buffer of pH 7.4; 25 µM RuPDO; 75 µM Zn^{2+}; 100 µM of AcP, 0.5 – 10 mM Mg^{2+}. 60 min reaction at 37 °C. (n = 4).
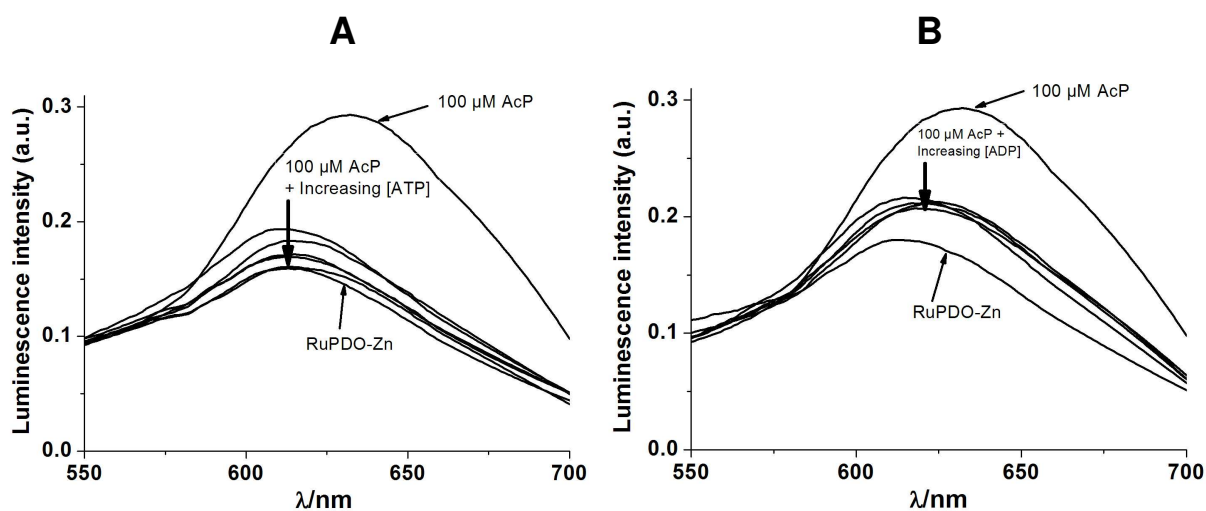
Fig. 5.2 Effect of ATP **(A)** and ADP **(B)** on the luminescence of the reaction of RuPDO-Zn with AcP. 40 mM HEPES buffer of pH 7.4; 25 µM RuPDO; 75 µM Zn^{2+}; 100 µM of AcP, 0.25 – 5 mM ATP/ADP. 60 min reaction at 37 °C. (n = 4).
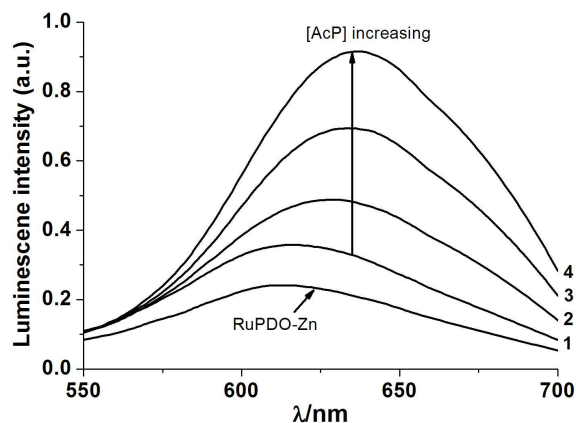
Fig. 5.3 Preliminary test of determination of AcP under the optimized enzymatic assay conditions. 40 mM HEPES buffer of pH 7.4; 50 μM RuPDO; 500 μM Zn^{2+}; 0.1 mM (1), 0.5 mM (2), 1 mM (3), 2 mM (4) AcP; 2.5 mM ATP; 2.5 mM ADP; 2.5 mM Mg^{2+}. 60 min reaction at 37 °C. (n = 4).

5.2.3 Testing of the Enzymatic Acetate Assay under the Optimized Assay Conditions

The optimal reaction conditions for the enzymatic determination of acetate regarding assay sensitivity and assay duration were empirically optimized in cuvette based tests as follows: 50 μM RuPDO, 1 mM Zn^{2+}, 3 mM ATP, 5 U/mL AK, 5 mM Mg^{2+}, and incubation at 45 °C for at least 60 min. Acetate was determined in a concentration range from 0.1 mM to 10 mM with a linear calibration range between 0.1 mM and 2.5 mM (fig. 5.4 and 5.5).
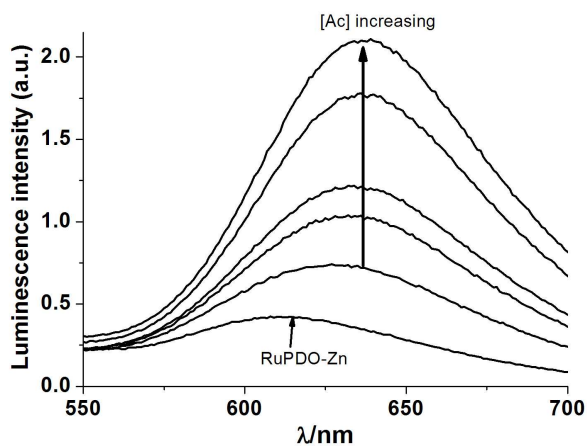
Fig. 5.4 Enzymatic determination of Ac *via* luminescence increase of RuPDO-Zn. 40 mM HEPES buffer of pH 7.4; 50 μM RuPDO; 1 mM Zn^{2+}; 0.1, 0.5, 1, 5, 10 mM Ac; 3 mM ATP; 5 mM Mg^{2+}, 5 U/mL AK. 120 min reaction at 45 °C. (n = 4).
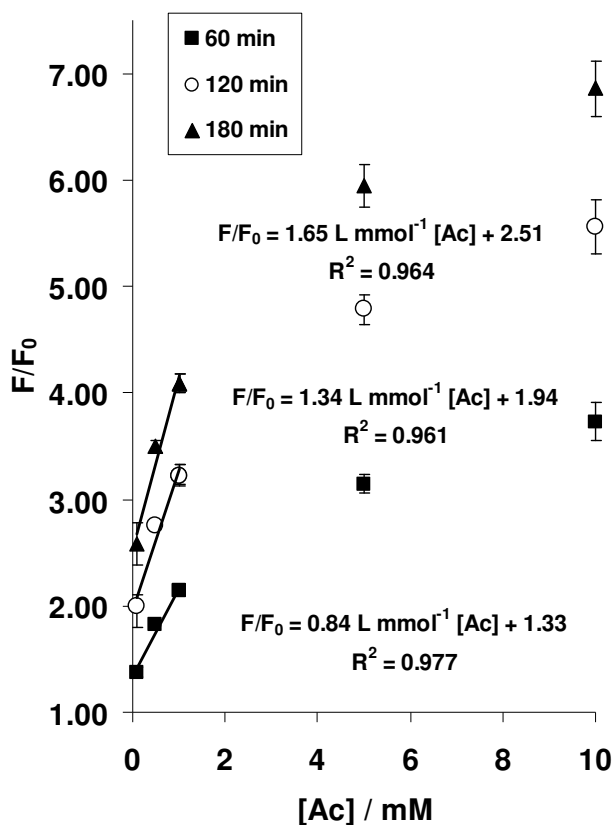
Fig. 5.5 Calibration plot for the determination of Ac *via* F/F_0 of RuPDO-Zn after 60, 120, and 180 min of reaction. 40 mM HEPES buffer of pH 7.4; 50 µM RuPDO; 1 mM Zn^{2+}; 0.1, 0.5, 1, 5, 10 mM Ac; 3 mM ATP; 5 mM Mg^{2+}, 5 U/mL AK. Reaction at 45 °C. (n = 4).

An incubation time of 90 min is clearly a sufficient compromise between signal increase (slope of the calibration plot) and assay duration. After this period the luminescent signal induced by 100 µM of acetate is distinctly distinguishable from the ground signal F_0 produced solely by RuPDO-Zn.

5.2.4 Application of the Enzymatic Assay to the Determination of Acetate in Real Samples

The practical applicability of the acetate assay was tested with three commercially available real samples, namely a Vinegar-based Cleaner, a Brandy vinegar, and a Balsamic vinegar. Additionally, the assay was transferred to the microtiter plate (MTP) format. A kinetic plot of the determination of acetate under the optimal assay conditions (carried out in a MTP) is shown in figure 5.6 for five representative concentrations of acetate.
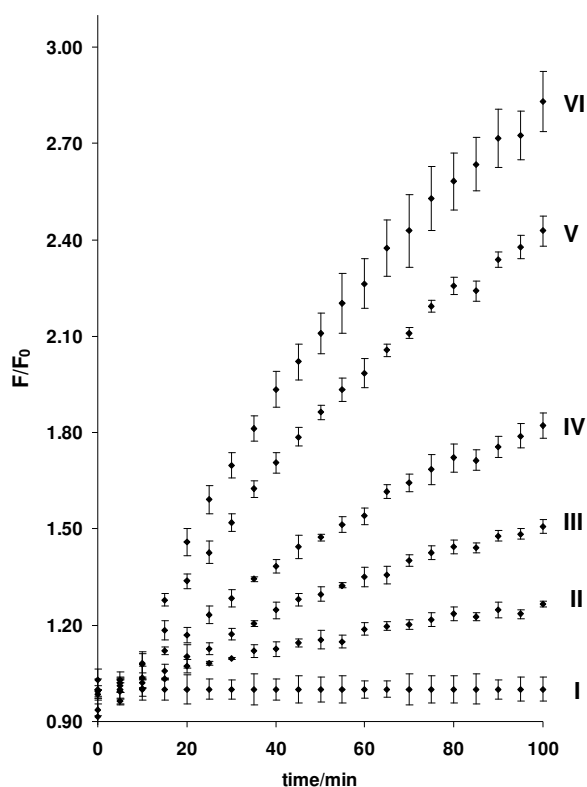
Fig. 5.6 Kinetic plot of the determination of Ac *via* F/F_0 of RuPDO-Zn carried out in a MTP under the optimal assay conditions: 40 mM HEPES buffer of pH 7.4; 50 μM RuPDO; 1 mM Zn^{2+}; 3 mM ATP; 5 mM Mg^{2+}, 5 U/mL AK. Reaction at 45 °C. [Ac]: I = 0 mM; II = 0.1 mM; III = 0.4 mM; IV = 1 mM; V = 4 mM; VI = 10 mM; (n = 4).

Again, the sufficiency of an incubation time of 90 min at 45 °C was proven also by the MTP based assay. The calibration plot (fig. 5.7) shows linearity between 0.1 and 2.5 mM of Ac. This is not unexpectedly due to the fact that only 3 mM of ATP are available for the enzymatic synthesis of AcP. Therefore, an saturation plot ($F/F_0 = 2.70 - 1.45 \cdot 0.69 \cdot L \cdot mmol^{-1[Ac]}$; acquired *via* the asymptotic fit function of Origin 8.0) was applied to the calibration data rather than the linear plot of fig. 5.7 for more accurate evaluation of the real samples.
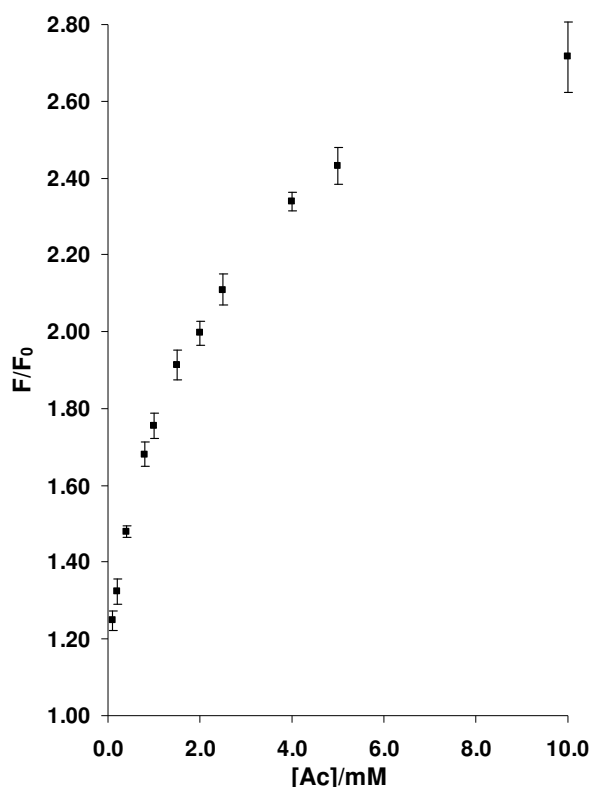
Fig. 5.7 Calibration plot for the determination of Ac *via* F/F_0 of RuPDO-Zn carried out in an MTP under the optimum assay conditions: 40 mM HEPES buffer of pH 7.4; 50 µM RuPDO; 1 mM Zn^{2+}; 3 mM ATP; 5 mM Mg^{2+}, 5 U/mL AK. Reaction at 45 °C. [Ac]: 0.1 - 10 mM; (n = 4).

The partially strong colored real samples (Brandy vinegar and Balsamic vinegar) as well as the colorless real sample (Vinegar based Cleaner) were assayed without further work up, except that they were appropriately diluted so to match the calibration range. The results are summarized in table 1.

Table 1 Evaluation of the Real Samples

Sample	F/F_0 (90 min)	SD abs	SD [%]	Dilution	[Ac] / M	[Ac] / g L^{-1}	% (w/w)	MI[a] [%]	Rec[b] [%]
Vinegar-based Cleaner	1.65	0.07	4.24	1/100	4.00	240.01	24.00	25	96
Brandy Vinegar	1.67	0.05	3.00	1/20	0.83	49.91	4.99	5	100
Balsamic Vinegar	1.85	0.03	1.62	1/20	1.05	63.29	6.33	6	106

[a] Manufacturer Information
[b] Recovery

The obtained values for the acetate concentrations are in excellent accordance to the manufacturer information. This imposingly shows the applicability of the developed assay. Furthermore, the recovery of acetate was determined by spiking of known amounts (0.2, 0.4, 0.6 mM) of Ac to the real samples. The results are summarized in Table 2.

Table 2 Recovery Rate

Sample	[Ac]/mM	$F/F_0(m)$[a]	$F/F_0(c)$[b]	Recovery [%][c]
Vinegar-based cleaner	0.88	1.65	-	-
	1.08	1.70	1.73	101.9
	1.28	1.79	1.80	100.4
	1.48	1.92	1.86	97.1
Brandy Vinegar	0.92	1.67	-	-
	1.12	1.73	1.74	100.8
	1.32	1.81	1.81	100.0
	1.52	1.88	1.88	99.8
Balsamic Vinegar	1.37	1.83	-	-
	1.57	1.89	1.89	99.8
	1.77	1.90	1.95	102.6
	1.97	2.01	2.00	99.4

[a] m: measured

[b] c: calculated; $F/F_0 = 2.70 - 1.45 \cdot 0.69 \cdot L \cdot mmol^{-1[Ac]}$

[c] Recovery rate: (m)/(c)

Recovery rates between 97% and 103% clearly show the reliability of the developed assay. The assay has a limit of detection (LOD) of 100 µM and a measuring range of 100 µM up to at least 2.5 mM that are comparable to the literature known amperiometric enzyme based methods for acetate determination.[29,32] The results obtained with the RuPDO based method are also in reach of commercially available acetate test kits (Enzytech[TM] f*luid* Acetic Acid, R-Biopharm, Darmstadt; K-ACETRM, Megazyme, Wicklow) that are based on NADH absorbance measurements.

However, the analysis time of the proposed assay is comparatively long. This drawback may be overcome by adding higher amounts of AK which would account for faster generation of AcP and, therefore, shorter assay times. This aspect was not

studied in the preliminary testing due to economic reasons. The major advantage of our assay compared to other enzymatic methods for the determination of acetate is the use of only one enzyme and four other chemicals; whereas the most common enzymatic test kits use three enzymes and at least six compounds. This renders our method rather inexpensive and easy to handle – also with respect to storage stability. The MTP format further reduces assay costs and analysis times. Further on, absorbance based methods – especially when UV absorbance is employed – suffer from undesired background signals in biological matrices. This problem can be adequately overcome when using highly specific luminescent probes, preferably with emissions peaking >600 nm, such as RuPDO, enabling measurement against almost zero background.

Obviously, the developed assay can not compete with classic instrumental analytic methods like GC and MS with regard to sensitivity. However, the aim of the development was a low-cost and simple (in handling) determination of acetate in food and biological fluids. In these samples Ac is found in micro- to millimolar concentrations with excellent recovery, where ultra trace methods are overstated.

5.3 Conclusions

A sensitive, highly selective and stable one-enzyme based fluorogenic method for the determination of acetate has been developed. The enzymatic assay was optimized and transferred into the MTP-format. Acetate was successfully determined in three different real samples – including a strongly colored balsamic acid – with excellent compliance to the manufacturer information and fine recovery rates. The combination of a selective acetyl phosphate probe RuPDO with the specificity of acetate kinase warrants a robust and unsophisticated assay compared to common commercially available test kits. Furthermore, our assay is not interfered by undesired background signals and is rather inexpensive due to the use of a luminescent signal readout, and a comparatively low amount of chemicals required (enzyme and ATP). The linear range of the method is from 0.1 mM to 2.5 mM.

5.4 Experimental

5.4.1 Materials

RuPDO was in-laboratory synthesized using the protocol given in chapter 4. All other chemicals and solvents were purchased from Sigma Aldrich (www.sigmaaldrich.com) or Acros Organics (www.acros.be). Acetate kinase, EC 2.7.2.1, (from *E.Coli*) was purchased from Sigma (A7437). Stock solutions of potassium acetate (50.0 or 1.0 mM) were prepared in HEPES buffer of pH 7.4 (40 mM) shortly before measurements. Stock solutions of RuPDO (1.0 mM) were prepared by pre-dissolving of 0.94 mg of the reagent in 10 µL of DMSO followed by dilution with HEPES buffer to 1.0 mL. The RuPDO stock solution was stored at 4 °C. Stock solutions of $ZnCl_2$ and $MgCl_2$ were prepared by dissolving 340 mg or 1.0 g of the respective salt in 50 mL of HEPES buffer (pH 7.4). Acetate kinase stock solutions were prepared by dissolving 1.0 mg of enzyme (activity: 20 U/mg) in 1.0 mL of ice-cold HEPES buffer shortly before measurements. ATP stock solutions were prepared by dissolving 10.1 mg of reagent in 1.0 mL of HEPES buffer shortly before measurements.

5.4.2 Methods

50 µL of the RuPDO stock solution (final concentration 50 µM in 40 mM HEPES buffer of pH 7.4), 20 µL of $ZnCl_2$ (final concentration 1 mM), 150 µL of ATP (final concentration 3 mM), 50 µL of $MgCl_2$ (final concentration 5 mM), and 250 µL of AK (final activity 5 U/mL) were added strictly in this order to HEPES buffer of pH 7.4 (40 mM) containing at least 0.1 mM of Ac and made up to 1.0 mL (for tests in cuvettes). One-tenth of all volumes were used for microtiter plate based experiments (final volume 0.1 mL). The same amounts of RuPDO, $ZnCl_2$, $MgCl_2$, ATP, and AK were added to the control containing no Ac. Cuvettes were vortexed for 10 s before the measurements. Microtiter plates were shaken in the preheated reader for 15 s before the measurement. The reaction vials were kept at 45 °C for 90 min before measuring luminescence. No work up of sample solutions was necessary for determination of Ac in real samples, except that they were adequately diluted (Cleaner: 1/100; Vinegar: 1/20) by addition of HEPES buffer.

5.4.3 Instrumentation

Luminescence spectra were recorded on an Aminco-Bowman AB 2 luminescence spectrometer (www.thermo.com) equipped with a 150 W continuous wave xenon lamp as excitation light source. All spectra are uncorrected. Microtiter plate experiments were performed on a Tecan Genios Plus Reader (www.tecan.de) at λ_{exc} = 485 nm and λ_{em} = 635 nm in black flat bottom 96-well plates from Greiner Bio One (www.gbo.com). pH was measured with a pH meter CG 842 from Schott (www.schott.com) at room temperature.

5.4.4 Synthesis

RuPDO was synthesized as described in chapter 4.

5.5 References

[1]   Hague A, Elder DJE, Hicks DJ, Paraskeva C (1995) Apoptosis in colorectal tumour cells: Induction by the short chain fatty acids butyrate, propionate and acetate and by the bile salt deoxycholate. Int J Cancer, 60: 400-406.

[2]   Cummings JH, Pomare EW, Branch WJ, Naylor CP, Macfarlane GT (1987) Short chain fatty acids in human large intestine, portal, hepatic and venous blood. Gut, 28: 1221-1227.

[3]   Campbell JM, Fahey Jr GC., Wolf BW (1997) Selected Indigestible Oligosaccharides Affect Large Bowel Mass, Cecal and Fecal Short-Chain Fatty Acids, pH and Microflora in Rats. J Nutr, 127: 130-136.

[4]   Hakim RM, Pontzer M-A, Tilton D, Lazarus JM, Gottlieb MN (1985) Effects of acetate and bicarbonate dialysate in stable chronic dialysis patients. Kidney International, 28: 535-540.

[5]   Stiles ME, Holzapfel WH (1997) Lactic acid bacteria of foods and their current taxonomy. Int J Food Microbiol, 36: 1-29.

[6]   Vegas C, Mateo E, González A, Jara C, Guillamón JM, Poblet M, Torija MJ, Mas A (2010) Population dynamics of acetic acid bacteria during traditional wine vinegar production. Int J Food Microbiol, 138: 130-136.

[7]   Nelson DL, Cox MM. (2008) Lehninger principles of biochemistry. 4th Edition, Freeman, New York.

[8]   Mizutani F, Sawaguchi T, Sato Y, Yabuki S, Iijima S (2001) Amperometric Determination of Acetic Acid with a Trienzyme/Poly(dimethylsiloxane)-Bilayer-Based Sensor. Anal Chem, 73: 5738-5742.

[9]   Becker T, Kittsteiner-Eberle R, Luck T, Schmidt H-L (1993) On-line determination of acetic acid in a continuous production of Acetobacter aceticus. J Biotech, 31: 267-275.

[10] Raspor P, Goranovič D (2008) Biotechnological Applications of Acetic Acid Bacteria. Crit Rev Biotechnol, 28: 101-124.

[11] Bartowsky EJ, Henschke PA (2008) Acetic acid bacteria spoilage of bottled red wine - A review. Int J Food Microbiol, 125: 60-70.

[12] Menz G, Andrighetto C, Lombardi A, Corich V, Aldred P, Vriesekoop F (2010) Isolation, Identification, and Characterisation of Beer-Spoilage Lactic Acid Bacteria from Microbrewed Beer from Victoria, Australia. J Inst Brew 116: 14-22.

[13] Yang X-M (1992) Optimization of a cultivation process for recombinant protein production by *Escherichia coli*. J Biotechnol, 23: 271-289.

[14] Hikuma M, Kubo T, Yasuda T (1979) Amperiometric Determination of Acetic Acid with immobilized *Trichosporon brassicae*. Anal Chim Acta, 109: 22-38.

[15] Vinderola CG, Mocchiutti P, Reinheimer JA (2002) Interactions Among Lactic Acid Starter and Probiotic Bacteria Used for Fermented Dairy Products. J Dairy Sci, 85: 721-729.

[16] Sharpe ME (1979) Lactic acid bacteria in the dairy industry. Int J Dairy Technol, 32: 9-18.

[17] Nieman C (1945) Influence of trace amounts of fatty acids on the growth of microorganisms. Microbiol Mol Biol Rev, 18: 147-163.

[18] Levine AS, Fellers CR (1940) Action of acetic acid on food spoilage microorganisms. 39: 499-515.

[19] Adams MR, Hall CJ (1988) Growth inhibition of food-borne pathogens by lactic and acetic acids and their mixtures. Int J Food Sci Technol, 23: 287-292.

[20] Savard T, Beaulieu C, Gardner NJ, Champagne C (2002) Characterization of spoilage yeasts isolated from fermented vegetables ans Inhibition by lactic, acetic and propionic acids. Food Microbiol, 19: 363-373.

[21] Vreman HJ, Dowling JA, Raubach RA, Weiner MW (1978) Determination of Acetate in Biological Material by Vacuum Microdistillation and Gas Chromatography. Anal Chem, 50: 1138-1141.

[22] Wittmann G, van Langenhove H, Dewulf J (2000) Determination of acetic acid in aqueous samples, by water-phase derivatisation, solid-phase microextraction and gas chromatography. J Chromatogr A, 874: 225-234.

[23] Simoneau C, Pouteau E, Maugeais P, Marks L, Ranganathan S, Champ M, Krempf M (1994) Measurement of Whole Body Acetate Turnover in Healthy Subjects with Stable Isotopes. Biological Mass Spectrometry, 23: 430-433.

[24] Ryhl-Svendsen M, Glastrup J (2002) Acetic acid and formic acid concentrations in the museum environment measured by SPME-GC/MS. Atmos Environ, 36: 3909-3916.

[25] Kuban P, Karlberg B (1997) On-Line Dialysis Coupled to a Capillary Electrophoresis System for Determination of Small Anions. Anal Chem, 69: 1169-1173.

[26] Shirao M, Furuta R, Suzuki S, Nakazawa H, Fujita S, Maruyama T (1994) Determination of organic acids in urine by capillary zone electrophoresis. J Chromatogr A, 680: 247-251.

[27] Skelly NE (1982) Ion-suppression reversed-phase liquid chromatographic determination of acetate in brine. J Chromatogr A, 250: 134-137.

[28] Clarke P, Payton MA (1983) An Enzymatic Assay for Acetate in Spent Bacterial Culture Supernatants. Anal Biochem, 130: 402-405.

[29] Mieliauskiene R, Nistor M, Laurinavicius V, Csöregi E (2006) Amperiometric determination of acetate with a tri-enzyme based sensor. Sensors and Actuators B, 113: 671-676.

[30] Spector LB (1980) Acetate kinase: A triple-displacement enzyme. Proc Natl Acad Sci USA, 77: 2626-2630.

[31] Anthony RS, Spector LB (1971) Exchange Reactions Catalyzed by Acetate Kinase. J Biol Chem, 246: 6129-6135.

[32] Tang X-M, Johansson G (1997) A Bioelectrochemical Method for the Determination of Acetate with Immobilized Acetate Kinase. Anal Lett, 30: 2469-2483.

6 Chromogenic Sensing of Biogenic Amines Using a Chameleon Probe and the RGB Readout of Digital Camera Images

6.1 Introduction

Biogenic amines (BAs) are defined as low-molecular organic bases with aliphatic, aromatic, or heterocyclic groups and, in contrast to alkaloids, have at least one non-heterocyclic amino group. The presence of BAs can be expected in virtually all foods and beverages that contain proteins or free amino acids. They are mainly generated during storage or processing of protein-rich seafood, fish, meat, and fermented products by thermal or bacterial enzymatic decarboxylation of the respective amino acids.[1] The total amount of biogenic amines formed strongly depends on the nature of the food and the present microbial flora, but, as a mater of fact, this amount is rising during storage. Histamine, tyramine, putrescine, cadaverine, spermidine, spermine, and ethanolamine are primarily found in foods and referred to as exogeneous amines. Hence, they are important indicators of food quality and hygiene.[2,3] Histamine poisoning with its allergy-like symptoms is a health risk for sensitive individuals. Its adverse effects are even potentiated in the presence of other BAs due to synergistic effects.[4-6] Low concentrations of biogenic amines can be degraded in healthy individuals by monoaminoxigenases (MAO) and diaminoxigenases (DAO) to inhibit exceeding resorption. However, alcohol and certain types of drugs are able to inhibit MAO and DAO.[7] The metabolic origin and the structure of the five biogenic amines that were mainly studied in this work are shown in figure 6.1.

Nevertheless, BAs occur regularly in metabolic pathways in low concentrations and have numerous functions in physiology and in the cell and are therefore referred to as endogeneous amines. They are found in ribosomes (cadaverine, putrescine) and sperm (spermine, spermidine), and form building blocks of phosphatides (ethanolamine), vitamins and coenzymes (aminopropanol being a building block of vitamin B12 and cysteamine; β-alanine being a building block of coenzyme A). Elevated levels of biogenic amines are presumably biomarkers for certain tumors[8-11] and for a number of diseases.[12,13]
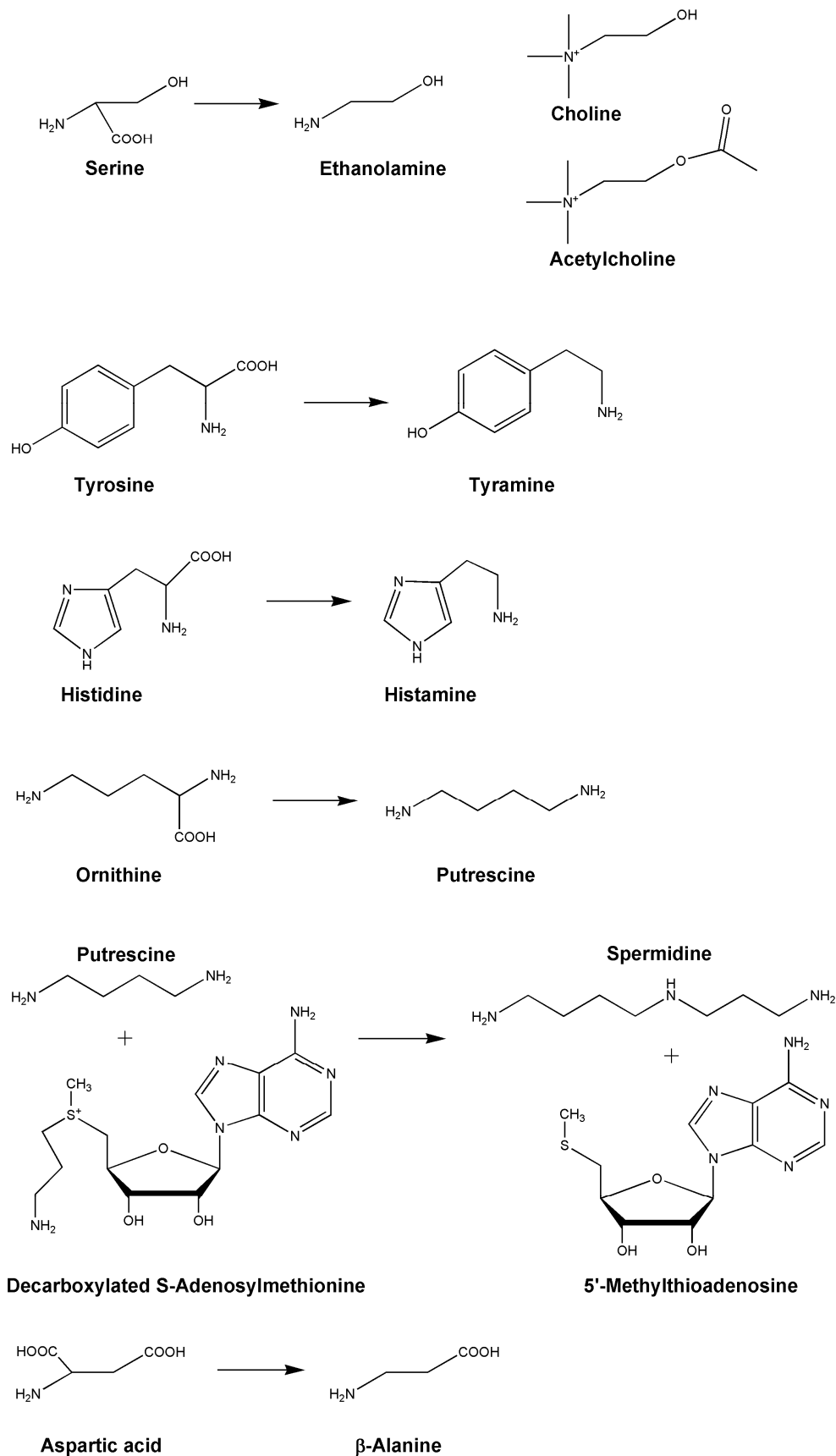
Fig. 6.1 Formation and Structure of Ethanolamine (EA), Tyramine (TY) Histamine
(HI), Putrescine (PU), Spermidine (SP), and β-Alanine (βAL).

Hence, research on the simultaneous and rapid analysis of BAs in a variety of biological matrices is of widest interest, and inexpensive, rapid and simple methods are sought. High performance liquid chromatography (HPLC)[14], capillary electrophoresis (CE)[15] and gas chromatography (GC)[16] in combination with various derivatization procedures are among the most important instrumental methods for precise quantitative analysis of biogenic amines. However, these methods often are time-consuming and require considerable skill. Thin layer chromatography (TLC)[17] and enzymatic[18] and immuno-enzymatic[19] methods are quite common and suitable for routine analysis with semi-quantitative and quantitative determination of BAs.

Most commercially available test kits for histamine rely on immuno-enzymatic techniques. Recently, an interesting concept using polymer layers with different changes in absorption due to interaction with aliphatic, aromatic, and polyamines was reported.[20] Few colorimetric methods using test spots are known.[21,22] These can be semi-quantitatively evaluated by visual readout of the originated color in comparison to a reference color scale. However, quantitative determination of BAs with this method requires sophisticated reflectance based readout (see also the respective section in the Background). Further, colorimetric sensor arrays consisting either of several amine-sensitive dyes[23,24] or organic liquid crystals[25] have been used for the determination of volatile amines. Computer based methods are required for qualitative (pattern recognition) as well as for quantitative (principal component analysis) evaluation. The recent progress in sensor technologies involves the use of very simple and easy accessible light sources like computer screens in combination with low-tech mobile phone cameras[26-28] or light-emitting diodes (LEDs) and commercially available digital cameras with subsequent readout of the red-green-blue (RGB) information (see also the respective section in the Background).[29]

New chromogenic and fluorogenic dry-chemistry sensing spots are presented here that are based on filter paper containing an amine-reactive chromogenic probe and fluorescein as a green fluorescent (but amine insensitive) reference dye incorporated in a hydrogel matrix. These test spots can quantitate biogenic amines upon dipping into the sample. The test spots were evaluated with six different biogenic amines at concentrations between 0.01 and 10 mM using the RGB readout option of a digital camera.

6.2 Results and Discussion

6.2.1 Design and Optimization of the Sensing Spots

The sensing spots are composed of four components: The chromogenic probe (Py-1), the reference dye (fluorescein), the polymer matrix (Hypan) to both incorporate Py-1 and shield it from larger molecules such as proteins, and the filter paper acting as a mechanical support (figure 6.2). The concentration of all components was empirically optimized.
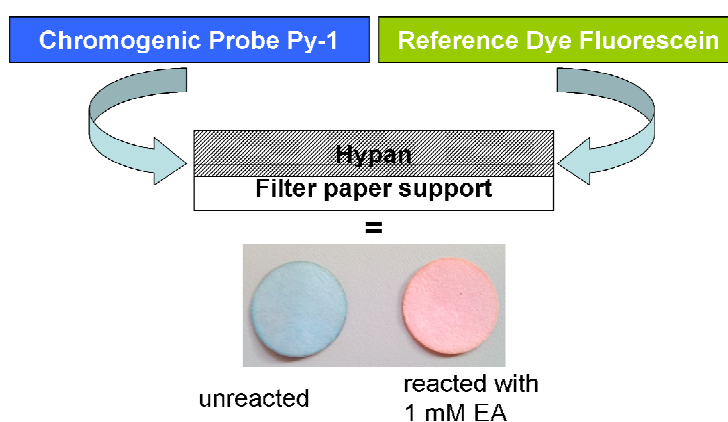
Fig. 6.2 Composition of the sensing paper and photo of unreacted blue test spot and a spot after a reaction time of 15 min with 1 mM of EA in CHES buffer.

6.2.1.1 Choice of Amine Reactive Dye

The amine-reactive label Py-1 has been developed a while ago.[32] It was chosen as amine-sensitive probe because of its chromogenic and fluorogenic properties. It is blue and virtually non-fluorescent in its non-conjugated form but shows a dramatic color change to red accompanied by a strong increase in fluorescence intensity when covalently reacted with primary amino groups. The label is therefore referred to as chameleon label. Its reactivity towards proteins was studied in great detail.[30-32] Py-1 previously has been used as a sensitive pre-staining label for proteins (LODs as low as 98 pM of HSA were achieved using a LIF-CE setup)[31] and quantities as low as 20 pg were detectable *via* poly(acrylamide) gel electrophoresis.[33] The structure of Py-1 and of its amine conjugate is shown in fig. 6.3; their respective spectral properties are summarized in Table 1. Interferences of the determination of BAs with Py-1 are

known – as a matter of fact – from proteins. Furthermore, the reaction of the label with biogenic amines occurs only in organic solvents like methanol or dimethylformamide (DMF).

Py-1
blue, very weak red fluorescence

Py-1-amine-conjugate
red, fairly strong orange fluorescence
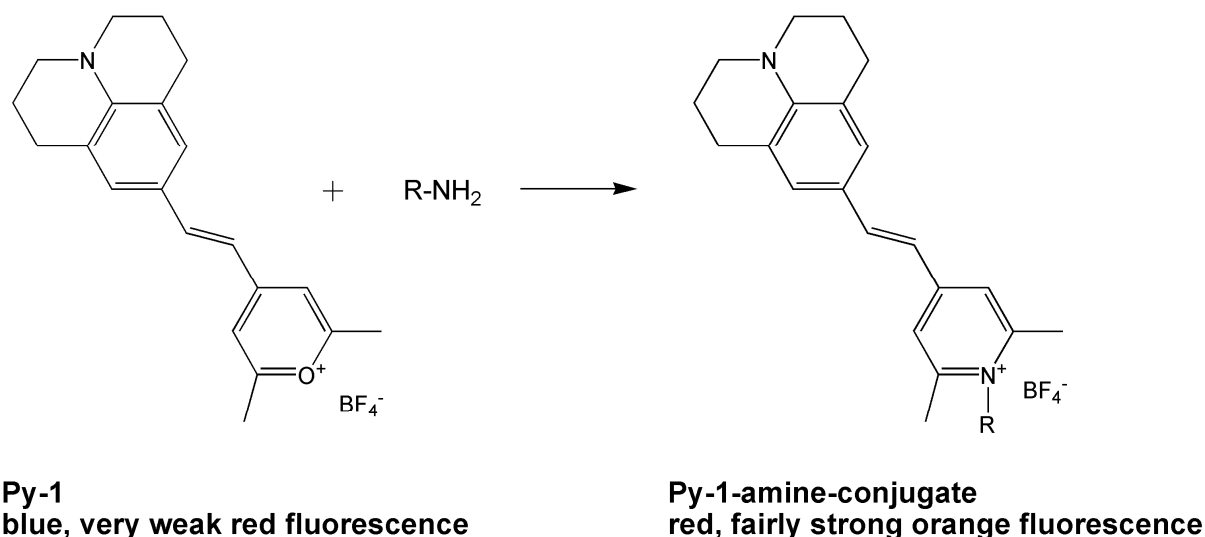
Fig. 6.3 Structure of Py-1 and its amine conjugate.

Table 1 Spectral Properties of Py-1 and its Amine Conjugate

	Free Label	**Conjugate**
λ_{abs}^{max} / **nm**	611	490 - 510
λ_{em}^{max} /**nm**	665	610 - 625
ε_{MeOH} / (**L cm^{-1} mol^{-1}**)	70000	20000 – 25000
color	deep blue	brilliant red

6.1.2.2 Choice of Polymer

In order to overcome this "interference problem" with proteins on determination of biogenic amines, several hydrogels (Hypan, poly-HEMA, D4) were investigated for their protein-shielding or BA-selective-filtering features, respectively. Finally, the poly(acrylonitrile)-based hydrogel Hypan was chosen as polymer matrix, first, because it is a good solvent for the amine probe and the reference dye. Second, and most importantly, there is virtually no undesired reaction of proteins with the amino

reactive probe when combining Hypan and Py-1 as shown with HSA as model protein (vide infra). Furthermore, Hypan HN80 is able to absorb up to 80% wt of analyte solution.[34] Another interesting feature of this polymer is that it is a block-co-polymer composed of polyacrylonitrile (PAN) and polyacrylamide (PAA) (figure 6.4). The PAN hard blocks are hydrophobic and provide an ideal non-nucleophilic environment for Py-1. However, the PAA soft blocks are hydrophilic and contain high amounts of water (sample solution) in the swollen form of the polymer.[35] Both types of blocks are in close proximity within the polymer matrix supplying an ideal reaction sphere for Py-1 with biogenic amines.
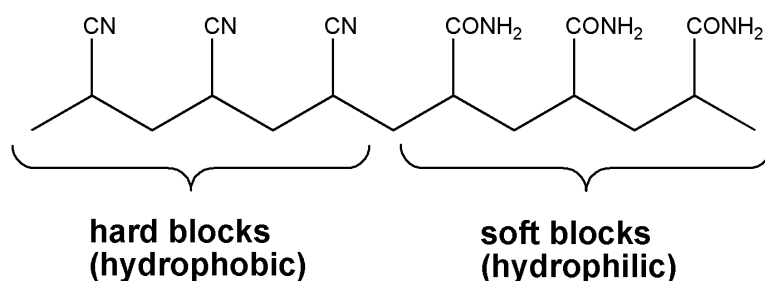
Fig. 6.4 Structure of the hydrogel Hypan.

6.1.2.3 Choice of Reference Dye

Polymeric sensor films often suffer from inhomogeneous distribution of the sensor dye, dye leaching, light scatter by the sensor (or sample), irregular illumination or fluctuations of the intensity of the excitation source, and of the detector. Therefore, an additional dye that is not sensitive towards biogenic amines was incorporated in the sensor cocktail. Fluorescein was chosen as reference fluorophore because it can be excited at the same wavelength as Py-1 and its emission peaks at 510 nm which is spectrally well separated from the emission of the BA Py-1 conjugates with their emissions peaking at 620 nm.

Ratiometric sensing is accomplished by dividing the signals of the red peak (dependent on the amine concentration) and the green peak (independent of amine concentration). This also increases the dynamic range and provides a built-in correction for above mentioned environmental effects.

6.1.2.4 Choice of Mechanical Support

The polymer solution containing the dyes had to be spread on a mechanical support to warrant reproducible applicability. First of all, a common plastic support (Mylar) was investigated. A film of the sensor cocktail was spread over a piece of Mylar *via* knife coating (fig. 6.5). However, it was not possible to reproducibly create a stable and homogeneous sensor film on the synthetic material. The elevated temperatures required for evaporation of the solvent (DMSO) from the sensor layer caused curling of the plastic support. This resulted in inhomogeneous film distribution.

Fig. 6.5 Photograph of a knife coated sensor film on Mylar.

Therefore, different types of filter paper were tested for their applicability as mechanical support for the sensor cocktail. It was empirically found that Schleicher and Schüll 589[1] and Whatman Grade 42 filter paper is most suitable for preparation of the sensing spots with homogenous distribution of the sensor cocktail. Other types of filter paper showed deterioration of the amine-label during drying of the sensor strips presumably due to special surface coatings of the paper by the manufacturers (fig. 6.6).

Fig. 6.6 Photograph of different filter papers immersed in the sensor cocktail.

Another advantage of a filter paper support over Mylar is that sample solution is absorbed by the cellulose matrix upon dipping the sensing strip into the solution. Hence, pre-concentration of analyte is enabled.

6.2.2 Testing of the Home-Built RGB Readout Setup

The home-built setup and the sensing spots were tested with the following six biogenic amines: ethanolamine (EA), histamine (HI), tyramine (TY), putrescine (PU), spermidine (SP), and β-alanine (βAL)); each at 14 different concentrations (0.01, 0.02. 0.04, 0.05, 0.1, 0.25, 0.5, 0.75, 1, 1.5, 2, 4, 8 and 10 mM); and with four replicates for each concentration. All measurements were conducted as described in the Experimental Section. The amines were chosen so to cover mono- and polyamines from the aliphatic, aromatic, and hetero-aromatic class of BAs to show the universal applicability of the method towards all biogenic amines (fig. 6.1). It is obvious from table 2 that there are – not unexpectedly – differences in the sensitivity of Py-1 towards the various BAs (slope of the regression equation). The clinically relevant concentration range of BAs is between 0.3 and 1.0 mM.[20] Biogenic amines in concentrations below 1.0 mM are not detectable by the human nose in most cases but may be indicative of food spoilage and, hence, represent a health risk. The linear

range for the quantitative determination of the amines tested with our setup matches this critical range of interest (table 2). Figure 6.7 shows a calibration plot of TY obtained with the standard operation protocol.

Table 2 Regression (expressed as the ratio R/G) of the calibration plots (n = 4), limits of detection (LODs; in mM), and linear ranges (in mM)

Amine	Regression	R	LOD	Linear Range
TY	0.93 L mmol^{-1} [TY] + 1.30	0.950	0.02	0.040 - 1.0
HI	0.35 L mmol^{-1} [HI] + 1.41	0.970	0.10	0.25 - 2.0
PU	0.60 L mmol^{-1} [PU] + 1.24	0.959	0.04	0.050 - 1.0
EA	0.31 L mmol^{-1} [EA] + 1.04	0.970	0.25	0.50 - 2.0
βAL	0.07 L mmol^{-1} [βAL] + 1.23	0.965	0.50	0.75 - 2.0
SP	0.57 L mmol^{-1} [SP] + 1.49	0.962	0.05	0.10 - 1.0

$$y = 0.934x + 1.303$$
$$R^2 = 0.949$$
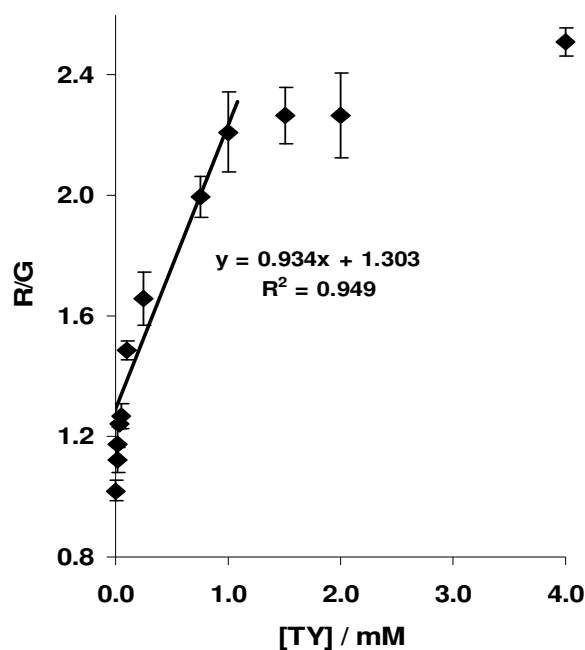
Fig. 6.7 Calibration plot for TY from 0 to 4 mM. (n = 4). The plot was obtained from the photo shown in figure 6.8 after digital data processing.

The sensing spots are greenish (the prevailing color of fluorescein) at the lowest amine concentrations of this range. At a concentration of 1 mM of amine, however, the spots show a pink color, and at even higher concentrations of BA, the color changes to a deep red (figure 6.8). This would clearly indicate a potentially toxic amine concentration, even to the untrained home user. Most biogenic amines can be visually verified down to 0.25 mM. The BAs are instrumentally detectable with high sensitivity and limits of detection (LOD) below 0.1 mM, except for β-Al and EA. β-Al has a carboxy group that probably interferes with the binding of its amino group to Py-1. This observation is similar to those of the interference tests with amino acids (vide infra).
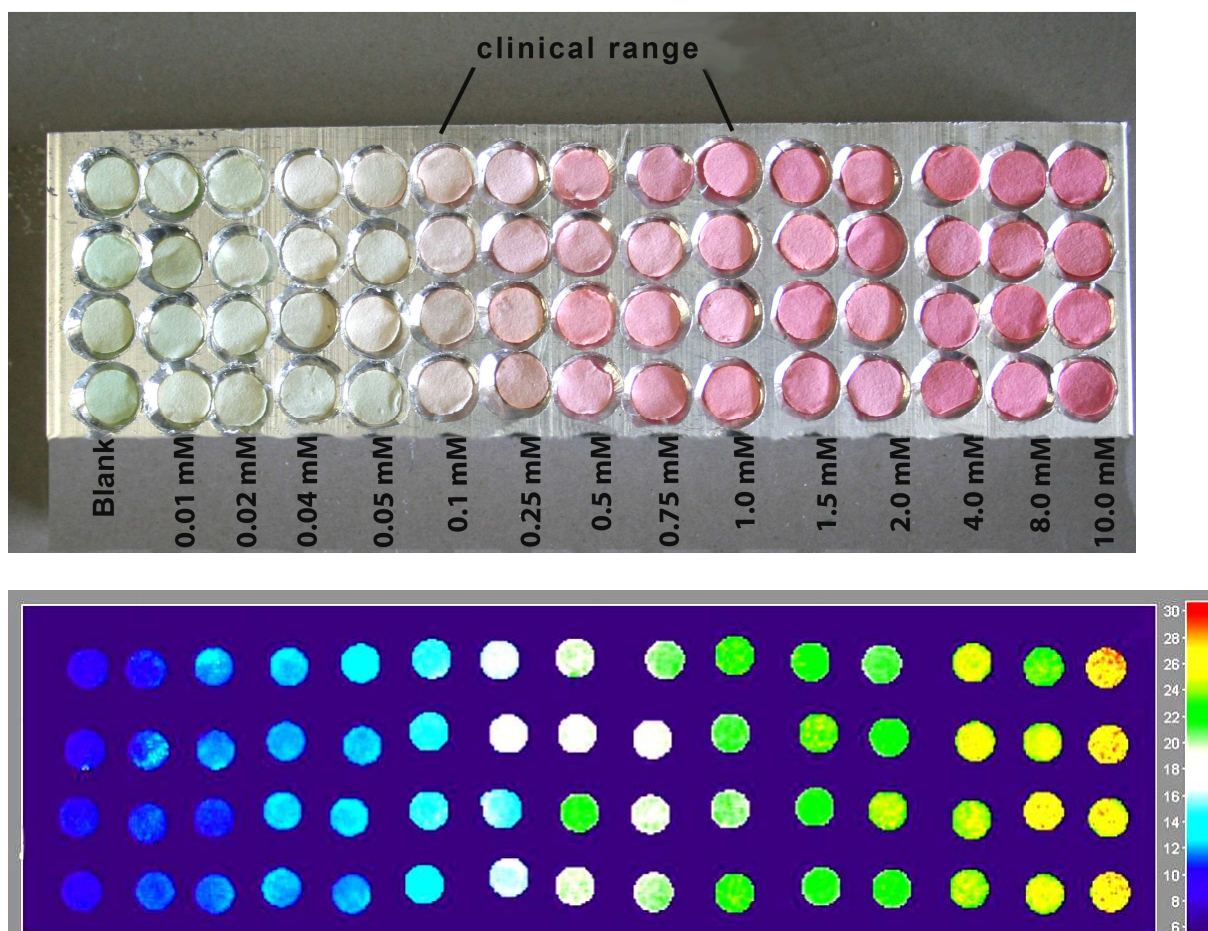
Fig. 6.8 *Top:* Photograph of the sensing spots aligned in the black box and showing calibration series of TY from 0 to 10 mM. (n = 4). *Bottom:* Pseudo color picture of the photo after RGB readout and digital processing.

The LOD is defined as the analyte concentration yielding a red/green (R/G) signal equal or higher than the average value produced by the blank sample, plus three standard deviations. The linear calibration range covers 1 to 2.5 decades of [BA]. Saturation of the red color is observed at concentrations of BA above 2 mM. This is most likely due to the limited quantity of Py dye available for the reaction. At least four test spots from the same batch were used in each experiment. The overall accuracy was 10% ± 2.5%.

6.2.3 Testing of Conceivable Interferents

Next, the reaction of the sensor spots with amino acids, thiols, proteins, secondary amines, tertiary amines, and ammonia in a 1 mM and 10 mM concentration, each, was investigated. Additionally, the response of the spots was also tested in the presence of 1 mM EA and 10 mM of the above-mentioned potential interfering agents. The results are summarized in Table 3. Secondary and tertiary amines like dimethylamine (DMA) and trimethylamine (TMA) are not able to form a red conjugate with Py-1 (as do primary amines). They slowly react (compared to primary amines) to yield a rather sallow colored and non-fluorescent reaction product. A 10-fold molar excess of DMA quenches the R/G value of EA only by 33%. TMA decomposes the label to a higher degree compared to DMA (negative values of the blank-corrected R/G value). Nevertheless, EA can be determined even in the presence of 10-fold molar excess of TMA (fig. 6.9).
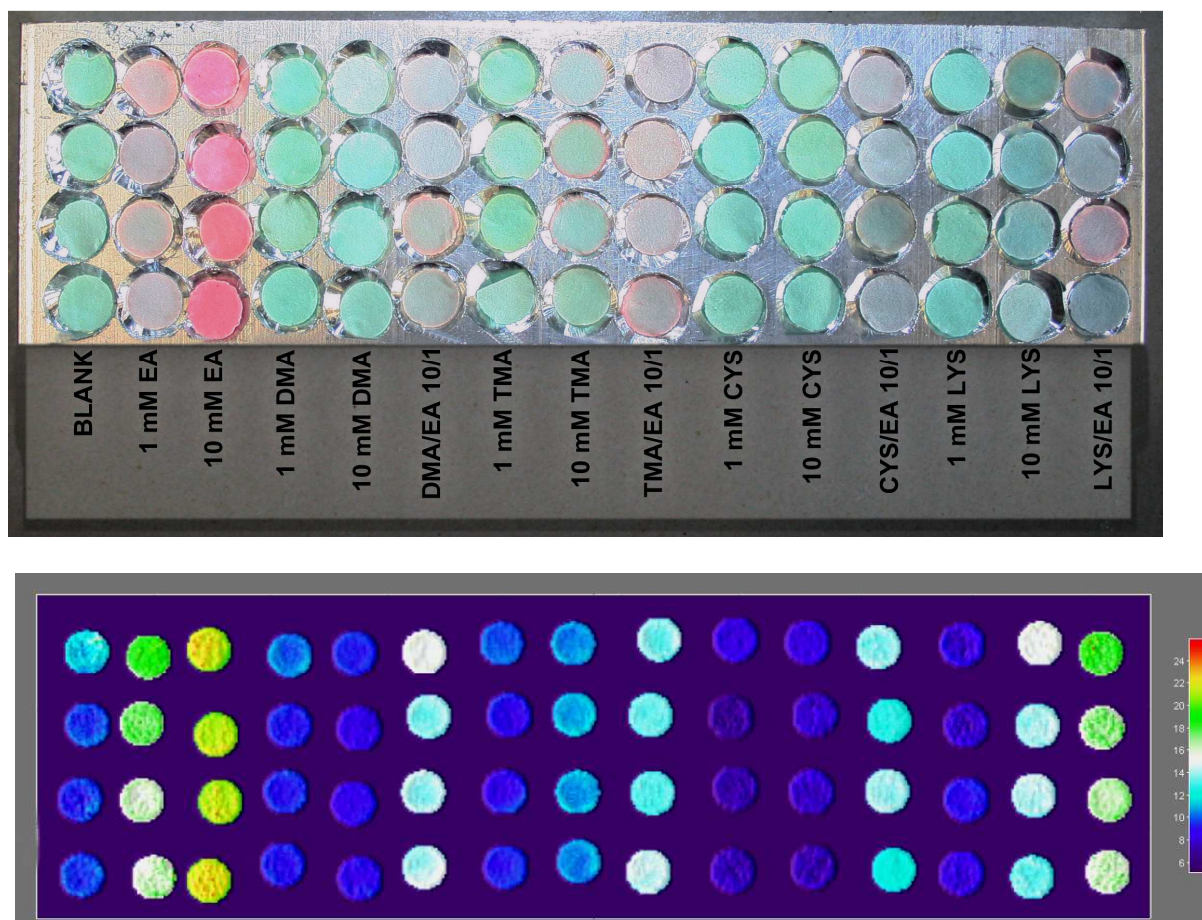
Fig. 6.9 *Top:* Photograph of the sensing spots aligned in the black box and showing potential interferents. (n = 4). *Bottom:* Pseudo color picture of the photo after RGB readout and digital processing.

The amino acids cysteine (CYS), lysine (LYS) and serine (SER) show weak interference on the determination of EA only at concentrations of >10 mM. LYS contains an ε-amino group that conceivably can react like an amino group of a biogenic amine and, therefore, yield the highest fluorescence signal of all three amino acids tested. However, the R/G ratio at a concentration of 10 mM of LYS is not as high as the R/G ratio of a 1 mM solution of EA. Dithiothreitol (a dithiol) also showed virtually no reaction with the sensing spots. HSA was used as model protein but gave no color change. Obviously, the polymer matrix is capable of shielding off the protein even at concentrations as high as 1 mg/mL. Finally, ammonia was tested for interference with the sensing spots. The red/green ratios in the presence of 1 mM and 10 mM ammonia are comparable to those of TMA. However, EA was successfully determined even in the presence of a 10-fold molar excess of ammonia.

The operational stability of the sensing spots is at least 3 months when stored in the dark in sealed glass vials at ambient temperature. The color intensity of reacted sensing spots is stable for 24 h at least.

Table 3 Effects of conceivable Interferents

Sample	Concentration / mM	R/G	R/G[a]
Blank	-	1.00	0.00
EA	1	1.74	0.73
EA	10	2.19	1.19
DMA	1	1.00	-0.06
DMA	10	0.94	-0.12
DMA/EA	10/1	1.55	0.49
TMA	1	0.92	-0.14
TMA	10	0.69	-0.37
TMA/EA	10/1	1.21	0.15
CYS	1	0.97	-0.09
CYS	10	1.42	0.36
CYS/EA	10/1	1.61	0.55
LYS	1	0.99	-0.07
LYS	10	1.66	0.60
LYS/EA	10/1	1.92	0.86
SER	1	0.83	-0.17
SER	10	1.44	0.44
SER/EA	10/1	1.72	0.72
DTT	1	0.95	-0.05
DTT	10	0.89	-0.11
DTT/EA	10/1	1.43	0.43
HSA	1	0.93	-0.07
HSA	10	1.08	0.07
HSA/EA	10/1	1.37	0.37
ammonia	1	0.75	-0.25
ammonia	10	0.79	-0.21
ammonia /EA	10/1	1.32	0.32

[a] corrected for blank

6.2.4 Application of the Test Strips to the Determination of the Total Amine Content (TAC) in Real Samples

The optimized test strips were considered for monitoring biogenic amines in real samples. Differentiation between the various biogenic amines present in the samples is obviously not possible due to the fact that Py-1 shows no specific selectivity towards a single amine. However, the total amine content (TAC) can be evaluated with this method. Conceivably, the TAC can report more comprehensively on the hygienic state of food than monitoring the concentration of a single amine, for example histamine. Four different samples, beef and pork steak, salmon filet, and shrimp, were stored for six days at 4 °C and 20 °C, respectively. The samples were assayed in the fresh state and after one, three, and six days of storage. The extraction procedure is described in detail in section 6.4.5. Briefly, 5 g of each sample were mixed and extracted with 5% (w/w) trichloroacetic acid (TCA) using a homogenizer. The extracts were filtered and appropriately diluted with 40 mM CHES buffer of pH 9. The dilution of the sample was adjusted so to match the linear range of determination of HI (0.25 - 2.5 mM). The total amine content of the sample was evaluated with the standard addition method. The amine determination and data evaluation was performed as described in sections 6.4.4 and 6.5.7.

The samples were spiked each with standard solutions of histamine in concentrations from 0.1 to 1 mM. The TAC was then evaluated as equivalents of histamine (µmol HI / g sample). This is possible and reasonable due to the fact that (1) histamine is one of the predominant biogenic amines in protein rich food;[36,37] (2) the mean molar mass of BAs found in food (histamine, tyramine, putrescine, cadaverine, spermidine) equals the molar mass of histamine. Four typical spiking plots are shown in fig. 6.10 and the results of the spiking experiments are summarized in table 4. The corresponding recoveries are displayed in table 5. It is notable that for most of the results a standard deviation of <10% was achieved with fairly good correlation coefficients (keeping in mind that sampling was done via test strips) ranging from 0.954 to 0.999. The recoveries ranged in total from 89% to 121% with most of them situated between 94% and 109%, which is acceptable for filter paper-based test strips. Better statistical data can be achieved by using more than four sensing spots per spiking solution. Though, this was not possible for the presented experiments due to time constrains and economic reasons.
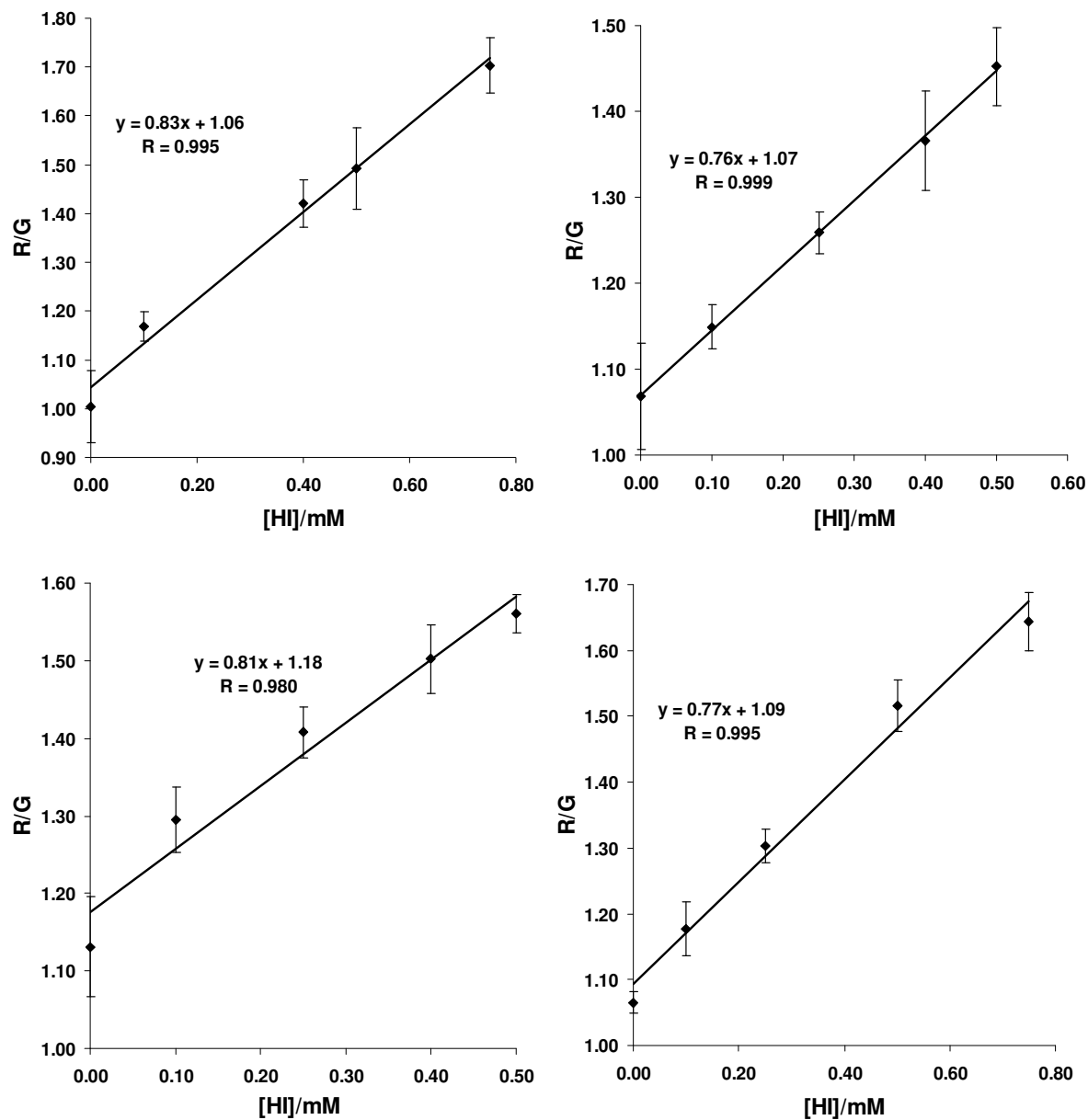
Fig. 6.10 Spiking plots. *top left:* beef steak after 6 days of storage at 4 °C; *top right:* pork steak after 1 day of storage at 20 °C; *bottom left:* salmon filet after 1 day of storage at 4 °C; *bottom right:* shrimp after 3 days of storage at 20 °C.

Table 4 Regression (expressed as the ratio R/G) of the spiking plots (n = 4), total amine content (TAC; µmol HI / g sample), and standard deviation (SD, in a) µmol/g b) and %)

	Sample	Regression	R	TAC	SD[a)]	SD[b)]
Beef 4 °C	Fresh	0.78 L mol^{-1} [HI] + 1.04	0.990	2.13	0.62	29.0
	Day 1	0.78 L mol^{-1} [HI] + 1.10	0.990	5.64	0.90	16.0
	Day 3	0.80 L mol^{-1} [HI] + 1.10	0.970	5.52	0.28	5.0
	Day 6	0.83 L mol^{-1} [HI] + 1.06	0.995	10.16	0.20	2.0
Beef 20 °C	Day 1	0.75 L mol-^{1} [HI] + 1.12	0.980	5.96	0.12	2.0
	Day 3	0.82 L mol^{-1} [HI] + 1.13	0.985	5.52	0.11	2.0
	Day 6	0.69 L mol^{-1} [HI] + 1.10	0.990	12.72	0.25	2.0
Pork 4 °C	Fresh	1.06 L mol^{-1} [HI] + 1.00	0.980	1.50	0.01	0.4
	Day 1	1.18 L mol^{-1} [HI] + 0.99	0.975	5.68	0.45	8.0
	Day 3	0.72 L mol^{-1} [HI] + 1.08	0.975	6.00	0.36	6.0
	Day 6	1.01 L mol^{-1} [HI] + 1.00	0.985	9.04	0.18	2.0
Pork 20 °C	Day 1	0.76 L mol^{-1} [HI] + 1.04	0.999	5.64	0.34	6.0
	Day 3	0.71 L mol^{-1} [HI] + 1.15	0.990	6.48	0.19	3.0
	Day 6	0.87 L mol^{-1} [HI] + 1.07	0.999	9.84	0.79	8.0
Salmon 4 °C	Fresh	0.55 L mol^{-1} [HI] + 0.96	0.995	2.80	0.06	2.0
	Day 1	0.81 L mol^{-1} [HI] + 1.18	0.980	5.84	0.12	2.0
	Day 3	0.67 L mol^{-1} [HI] + 1.11	0.990	6.64	1.20	18.0
	Day 6	0.89 L mol^{-1} [HI] + 1.02	0.999	9.20	0.09	1.0
Salmon 20 °C	Day 1	0.41 L mol^{-1} [HI] + 1.08	0.995	10.52	1.58	15.0
	Day 3	1.04 L mol^{-1} [HI] + 1.20	0.959	9.20	1.56	17.0
	Day 6	1.46 L mol^{-1} [HI] + 1.18	0.964	32.40	2.27	7.0
Shrimp 4 °C	Fresh	0.26 L mol^{-1} [HI] + 1.21	0.980	7.44	1.04	14.0
	Day 1	0.68 L mol^{-1} [HI] + 1.20	0.985	7.04	0.49	7.0
	Day 3	0.54 L mol^{-1} [HI] + 1.22	0.995	9.04	0.36	4.0
	Day 6	0.60 L mol^{-1} [HI] + 1.20	0.995	16.00	0.16	1.0
Shrimp 20 °C	Day 1	0.91 L mol^{-1} [HI] + 1.03	0.995	9.36	0.28	3.0
	Day 3	0.77 L mol^{-1} [HI] + 1.09	0.995	11.36	0.11	1.0
	Day 6	1.00 L mol^{-1} [HI] + 1.04	0.954	41.60	2.50	6.0

Table 5 Recovery Rate

	Sample	HI added / mM	HI found / mM	SD / %	Mean of Recovery / %
Beef 4 ℃	Fresh	0	1.33	11.76%	-
		0.25	1.59	3.23%	103
	Day 1	0	1.41	8.49%	-
		0.1	1.53	5.04%	115
	Day 3	0	1.38	3.85%	-
		0.75	2.08	1.81%	93
	Day 6	0	1.27	5.51%	-
		0.75	2.04	1.76%	103
Beef 20 ℃	Day 1	0	1.49	2.65%	-
		0.25	1.74	4.58%	101
	Day 3	0	1.38	5.50%	-
		0.5	1.87	2.61%	98
	Day 6	0	1.59	0.92%	-
		0.75	2.29	1.90%	93
Pork 4 ℃	Fresh	0	0.94	4.17%	-
		0.4	1.31	5.04%	92
	Day 1	0	1.42	6.32%	-
		0.4	1.79	4.20%	93
	Day 3	0	1.50	2.97%	-
		0.75	2.19	3.16%	93
	Day 6	0	1.13	3.09%	-
		0.4	1.58	3.01%	101
Pork 20 ℃	Day 1	0	1.41	5.61%	-
		0.5	1.91	1.28%	100
	Day 3	0	1.62	7.96%	-
		0.75	2.35	3.16%	98
	Day 6	0	1.23	8.41%	-
		0.4	1.63	3.97%	101

Table 5 Recovery Rate (Continuation)

	Sample	HI added / mM	HI found / mM	SD / %	Mean of Recovery / %
Salmon 4 °C	Fresh	0	1.75	4.21%	-
		0.25	2.02	11.71%	109
	Day 1	0	1.46	5.31%	-
		0.25	1.74	2.13%	114
	Day 3	0	1.66	10.81%	-
		0.75	2.39	4.38%	98
	Day 6	0	1.15	4.85%	-
		0.75	1.90	1.18%	100
Salmon 20 °C	Day 1	0	2.63	14.15%	-
		0.25	2.87	5.08%	98
	Day 3	0	1.15	10.43%	-
		0.4	1.51	7.14%	89
	Day 6	0	0.81	3.60%	-
		0.4	1.19	2.75%	96
Shrimp 4 °C	Fresh	0	4.65	6.50%	-
		0.4	5.07	1.52%	106
	Day 1	0	1.76	5.98%	-
		0.5	2.23	3.95%	94
	Day 3	0	2.26	7.44%	-
		0.75	3.04	2.44%	104
	Day 6	0	2.00	4.20%	-
		0.75	2.75	1.82%	100
Shrimp 20 °C	Day 1	0	1.17	2.00%	-
		0.1	1.29	4.39%	121
	Day 3	0	1.42	1.87%	-
		0.25	1.69	2.31%	109
	Day 6	0	1.04	6.91%	-
		0.5	1.50	3.08%	92

Figure 6.11 shows the spoilage of all four samples over six days at both storage temperatures. The maximum legally accepted limit for histamine in food products is 100–200 mg/kg (0.9–1.8 µmol/g), and a concentration of 1000 mg/kg (9.0 µmol/g) is evidently toxic.[38] All fresh samples tested showed a TAC of 1.5 to 3 µmol/g, except for the shrimp sample that exceeded this value three fold. A TAC between 1 and 5 µmol/g can be referred to as toxicological safe, assuming that the samples were bought fresh and showed negligible bacterial activity on the very first sampling day. Consequently, a total amine content above 15 µmol/g is defined toxic in this context.

The amine concentration was increasing by about a factor of three within the first days of storage in all samples, except for the shrimp sample that showed a high, but almost stable concentration. A lower amount of amines in the 4 °C samples than in the 20 °C samples is found but not as pronounced as expected. The TAC of the 20 °C samples of beef and pork persisted well below the toxic limit (15 µmol/g) over three days of storage; whereas the salmon and shrimp samples reached the limit of 15 µmol/g within about four days. Beef and pork samples became toxic after six days of storage at 20 °C. This is in good correlation to observations of daily life. Furthermore, the seafood samples showed a more pronounced increase of the TAC over the total experiment duration than the other samples. Finally, the salmon and shrimp samples exceeded the toxic amine limit two times after six days of storage at room temperature. This is also in good agreement with the odor and consistency of these samples. The observed progress of spoilage and increase of the total amine content of the seafood samples correlates with previous data on TAC determination in fish.[38,39]
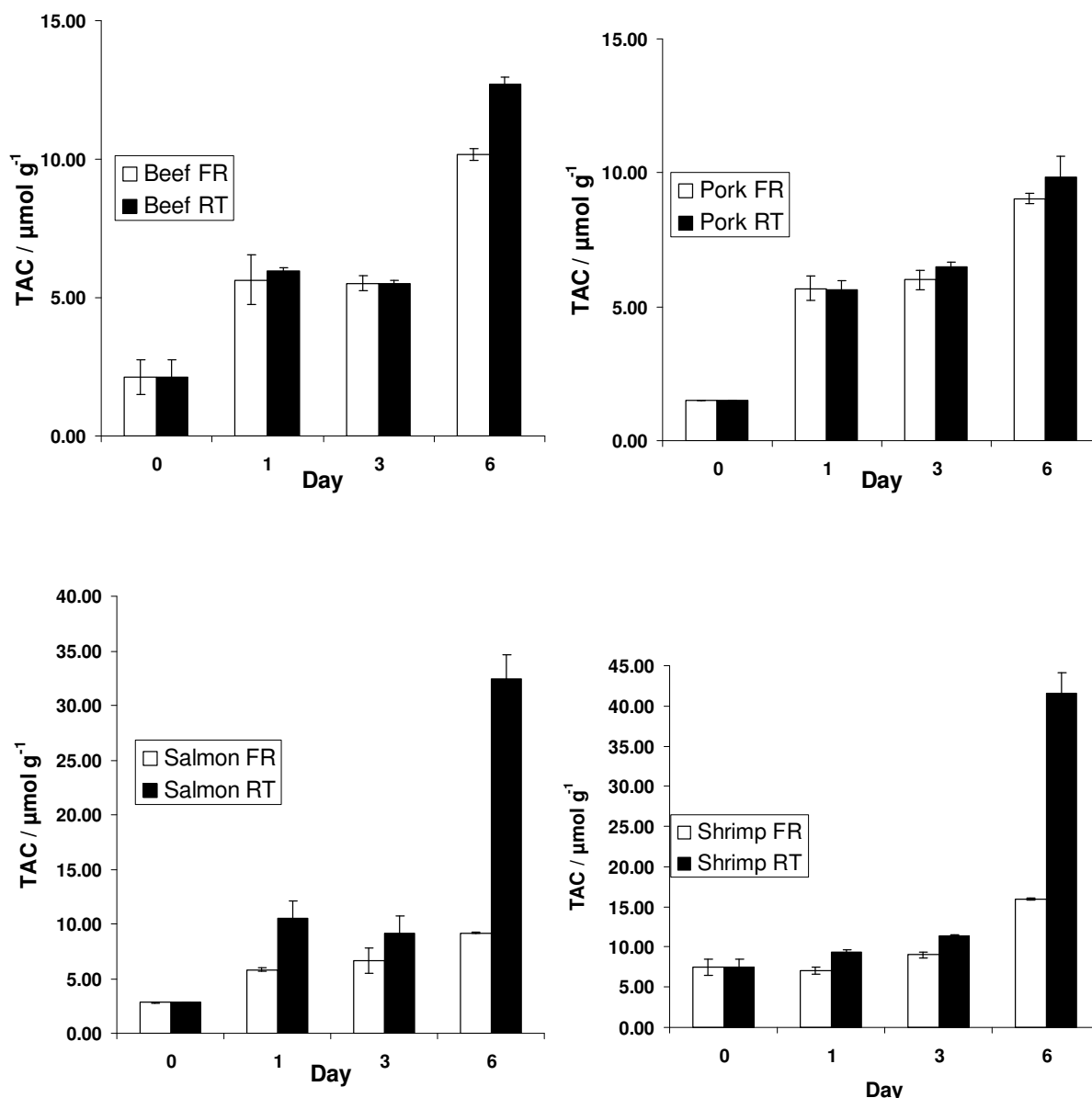
Fig. 6.11 Monitoring of the spoiling of real samples at 4 °C (white column) and 20 °C (black column). *top left:* beef steak; *top right:* pork steak; *bottom left:* salmon filet; *bottom right:* shrimp.

6.3 Conclusions

A self-referenced portable and rapid test for biogenic amines is presented here that is based on a hydrogel matrix and an amine-reactive dye. On one hand, the sensing spots can be visually evaluated semi-quantitatively *via* comparison to a calibration color scale. On the other hand, sensitive and more precise quantitative analysis of

the spots can be performed *via* an inexpensive home-built setup using a RGB readout method of a digital image taken with a commercial digital camera. The sensor spots show high selectivity for biogenic amines, only minor interferences of ammonia and secondary or tertiary amines and no sensitivity to proteins. The sensing system was successfully applied to the rapid determination of the total amine content (TAC) in four different kinds of meat. The spoilage of the samples at 4 °C and 20 °C was monitored over six days. The obtained data showed reasonable results. Determination of the TAC represents a substantial advantage over the common immuno-enzymatic method that focuses on the determination of a single BA (mostly HI) because the spoilage of food is a process that is not restricted to the formation of only one single BA. Thus, the sensor spots represent an attractive alternative to existing schemes for sensing biogenic amines.[40] Its digital read-out makes it more robust, and the use of conventional cameras goes along current trends towards simplified methods for absorption-based and emission-based detection schemes.[26,41] The method also may enable high-throughput analysis and in-field examinations and does not require sophisticated instrumentation or trained personnel.

6.4 Experimental

6.4.1 Materials

Ethanolamine (EA), putrescine (PU) and DMSO were obtained from Merck (www.merck.com) as liquids. The hydrochlorides of β-alanine (βAL), tyramine (TY), histamine (HI), spermine (SE), dimethylamine (DMA), and trimethylamine (TMA) were from Sigma (www.sigmaaldrich.com). Serine (SER), lysine (LYS), cysteine (CYS), human serum albumin (HSA) and fluorescein also were from Sigma. The buffer N-Cyclohexyl-2-aminoethanesulfonic acid (CHES) was from Roth (www.carl-roth.de). Hypan (type HN 80) was from HyMedix International. Py-1 was from ActiveMotif Chromeon (www.activemotif.com). All solvents and reagents were of analytical grade and used without further purification. The 40 mM CHES stock buffer of pH 9 was prepared by dissolving 4.15 g (0.02 mol) of CHES in 500 mL deionized water and adjusting the pH to the desired value with 1.0 M NaOH. The dark blue

stock solution of Py-1 was obtained by dissolving 5.0 mg of Py-1 in 1.0 mL of DMSO.
The green fluorescent stock solution of the reference dye was prepared by dissolving
6.6 mg of fluorescein in 1.0 mL of DMSO. A 5% (w/w) hydrogel stock solution was
prepared by dissolving 1.00 g of Hypan in 20.0 mL of DMSO. Stock solutions of all
samples (10.0 or 1.00 mM; 1.0 mg/mL or 0.1 mg/mL for HSA) were prepared in 40
mM CHES buffer of pH 9.0 shortly before measurements. Schleicher and Schüll 589[1]
or Whatman Grade 42 (www.whatman.com) filter paper was used for preparation of
the sensing spots, throughout.

6.4.2 Preparation of Sensor Spots

A "sensor cocktail" was prepared by adding 300 µL of the Py-1 stock solution (final
concentration 1.5 mg/mL), 45 µL of fluorescein stock solution (final concentration 0.4
mg/mL), 200 µL of the Hypan stock solution (final concentration 1% (w/w) and 455 µL
of dimethylsulfoxide (DMSO) to an Eppendorf cup (final volume 1 mL). The mixture
was shaken for 20 min at 60 °C in an Eppendorf Thermomixer Comfort
(www.eppendorf.com). The dark blue sensor cocktail was then transferred into a
glass bowl with flat bottom. Square pieces of filter paper (35 x 35 mm) were
immersed in this solution until saturation and put on a glass plate. The plate was then
placed in an oven at 80 °C for 45 min to evaporate the DMSO, whereby the blue
color of the test spots became slightly brighter. After this first drying step, each side
of the square paper strip was washed with 50 mL of distilled water in order to remove
an excess of blue Py-1 that may adhere to the surface of the sensing paper. The
paper strips were dried again on a glass plate in the oven at 80 °C for 30 min (fig.
6.12). Finally, round sensing paper spots with a diameter of 6 mm were cut from the
square filter paper *via* a metal hole puncher. The spots were then stored at room
temperature in a closed vial in the dark.
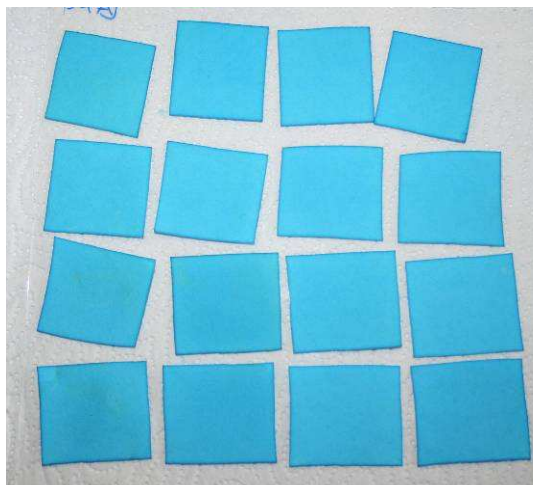
Fig. 6.12 Photograph of the square pieces of sensing paper after the final drying.

6.4.3 Home-built Setup for Fluorescence-Readout via the RGB-Signals of a Digital Camera

A Canon EOS 350D digital camera was used for instrumental readout, throughout. It was equipped with a standard 18-55 mm objective with image stabilization and an orange glass filter directly mounted on the filter thread. The photos were taken in the M(anual)-Mode with an shutter speed of 1/20 s, aperture of 3.5, resolution of 8 MPixel, ISO 100, and a focal distance of 18 mm. The camera was fixed on top of a black box (Fig 6.13 A). The template to hold the test spots was centered in this box and illuminated from the top with six turquoise high power (1 W) LEDs (Lumileds Luxeon Star, www.luxeon.com) with peak emissions at 505 nm (fig. 6.13 B/C). Both the amine-Py-1 conjugate and the reference dye (fluorescein) are excited at this wavelength. Their emissions are peaking at 620 nm and 510 nm, respectively. A schematic of the complete setup is shown in Scheme 1 and the spectral match of dye absorptions with LED excitation and dye emissions with the red and green channel of the camera, together with the transmission of the filter are shown in fig. 2.9 in the Background.
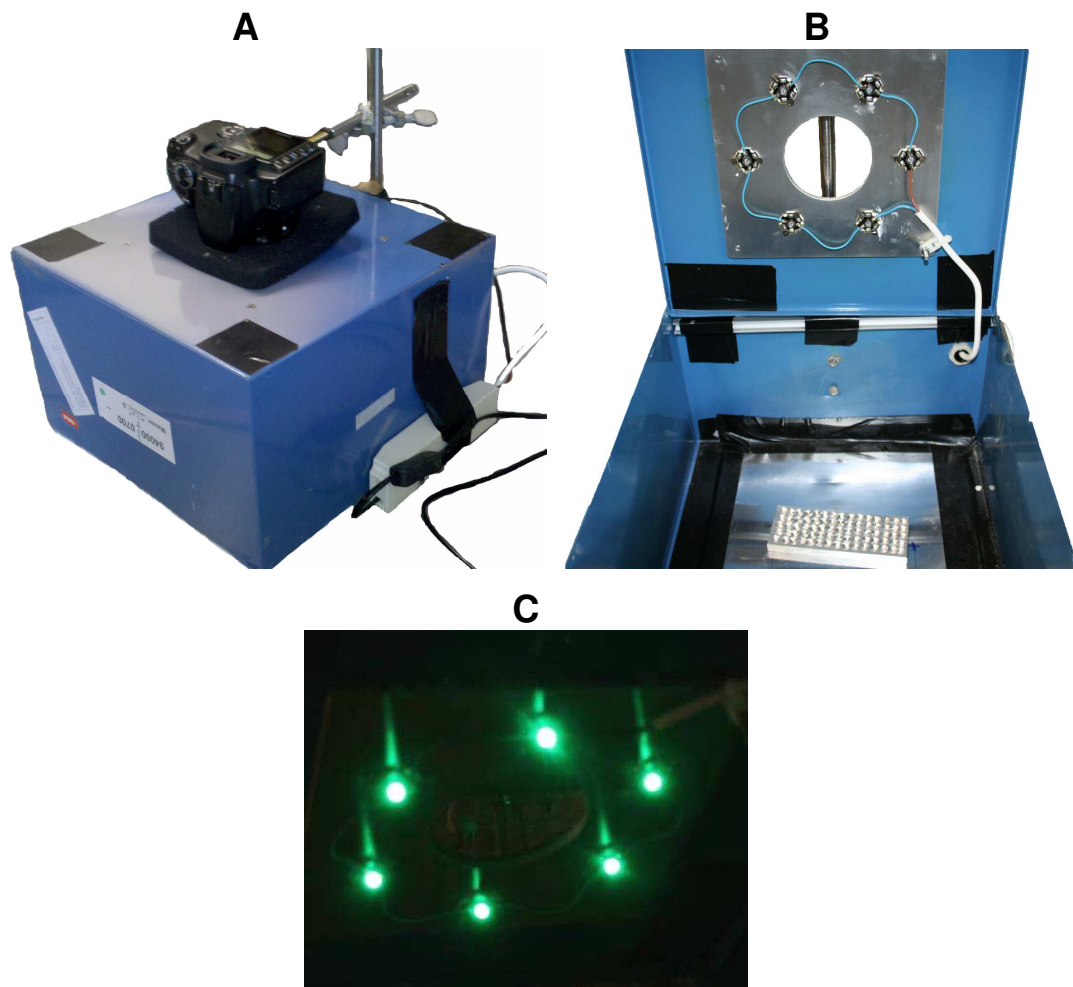
Fig. 6.13 Photographs of the home-built setup. **(A)** Photo of the blackbox with aligned
digital camera; **(B)** Photo of the inside of the box; measuring template at the bottom;
light source at the top; **(C)** Photo of the six green high power LEDs in operation.

Scheme 1 Home-built Setup for RGB Readout
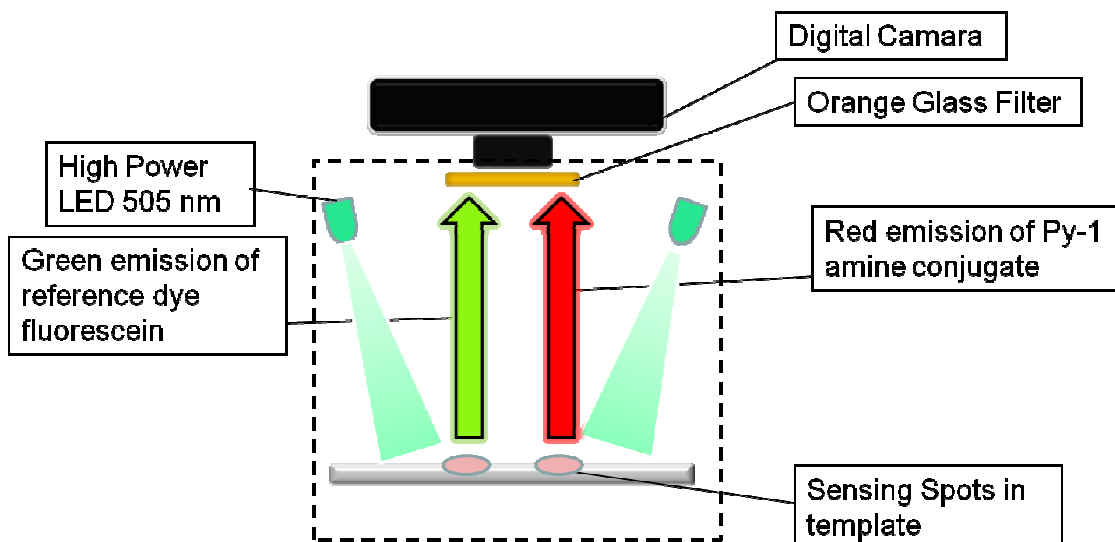
6.4.4 Standard Procedure for Determination of Biogenic Amines

The dry, blue colored round sensing spots were dipped into 200 µL of a pH 9.0 sample containing the BA for 30 s. The color was allowed to develop for 15 min on a glass plate. The spots were dried on a paper towel for ca. 5 min and then immediately submitted to photography. Stable fluorescence signals are obtained after this period.

6.4.5 Preparation of the Real Samples

Shrimp, salmon filet, beef and pork steak were purchased from a local supermarket and stored at -18 °C prior to analysis. The samples were thawed in a microwave using the defrost setting for 5 min. Approximately 200 g of each type of meat was divided in two parts, put into plastic bags that were tightly sealed, and stored at 4 °C or 20 °C, respectively. Biogenic amines were extracted from the fresh samples and after one, three, and six days of storage from both temperature fractions. A 5 g portion of each meat was minced, put into a falcon tube and blended with 40 mL of 5 % (w/w) trichloroacetic acid (TCA). The mixture was cooled in an ice-bath and homogenized with an IKA Ultra-Turrax (IKA, Germany, www.ika.de) for one minute at maximum speed. The extract was then filtered through Schleicher&Schüll Nr. 589[2] filter paper. Aliquots (1 mL) of the filtrate were pipetted into eppendorf tubes and stored at -18 °C until analysis.

6.4.6 Determination of Total Amine Content (TAC) in Extracts of Real Samples

The extracts were thawed within 1 min in a microwave using the defrost setting. Each sample was diluted with 40 mM CHES buffer of pH 9 according to table 6. The samples were then spiked with histamine using a 100 mM histamine stock solution in CHES buffer. This yielded 5 histamine-spiked solutions per sample. The following histamine concentrations were used for the spiking plots depending on the sample: 0, 0.1, 0.25, 0.4, 0.5, 0.75, and 1 mM. The spiking solutions were analysed with the sensing strips in quadruplets as described in section 6.4.4. Finally, the TAC was evaluated as equivalents of histamine (µmol HI per gram of sample.

Table 6 Dilution factors of extracts from meat samples

Day/Storage Temperature	Salmon		Beef		Pork		Shrimp	
	4 ℃	20 ℃	4 ℃	20 ℃	4 ℃	20 ℃	4 ℃	20 ℃
0	20	20	20	20	20	20	20	20
1	50	100	50	50	50	50	50	100
3	50	100	50	50	50	50	50	100
6	100	500	100	100	100	100	100	500

6.4.7 Data Evaluation

The general procedure for data evaluation is shown in figure 6.11. Data evaluation and processing was accomplished by a slightly modified method described by Wang et al.[29] Briefly, the photos of the LED-illuminated sensing spots acquired in RAW format (figure 6.14-A) were processed with Adobe Photoshop CS4, in particular by placing a black mask layer around the sensing spots to suppress undesired light scattering. The color temperature was set to 2550 K and the tint value was set to zero for all photos. Then, the image was stored as a 16-bit color TIF file (figure 6.14-B). This file was then split into the red, green and blue channel *via* ImageJ software (NIH, Bethesda, MD), available free of charge at http://rsbweb.nih.gov/ij/. The blue channel contained virtually no information due to the almost zero transmittance of the orange glass filter. Data of the red channel contained the emission intensity information of the amine-Py-1 conjugate. The green channel contained the emission intensity information of the reference dye fluorescein (figure 6.14-C). The data of the red channel were divided by the data of the green channel to give pseudo color images that were visually evaluated (figure 6.14-D, left). A circular region of interest (ROI) with a diameter of 48 pixels was drawn around each sensing spot, (both in the red and green channel split color picture) for quantitative determinations. The histogram of each of these ROI delivered a mean color value that was used for quantitative determinations and calibration plots (figure 6.14-D, right).
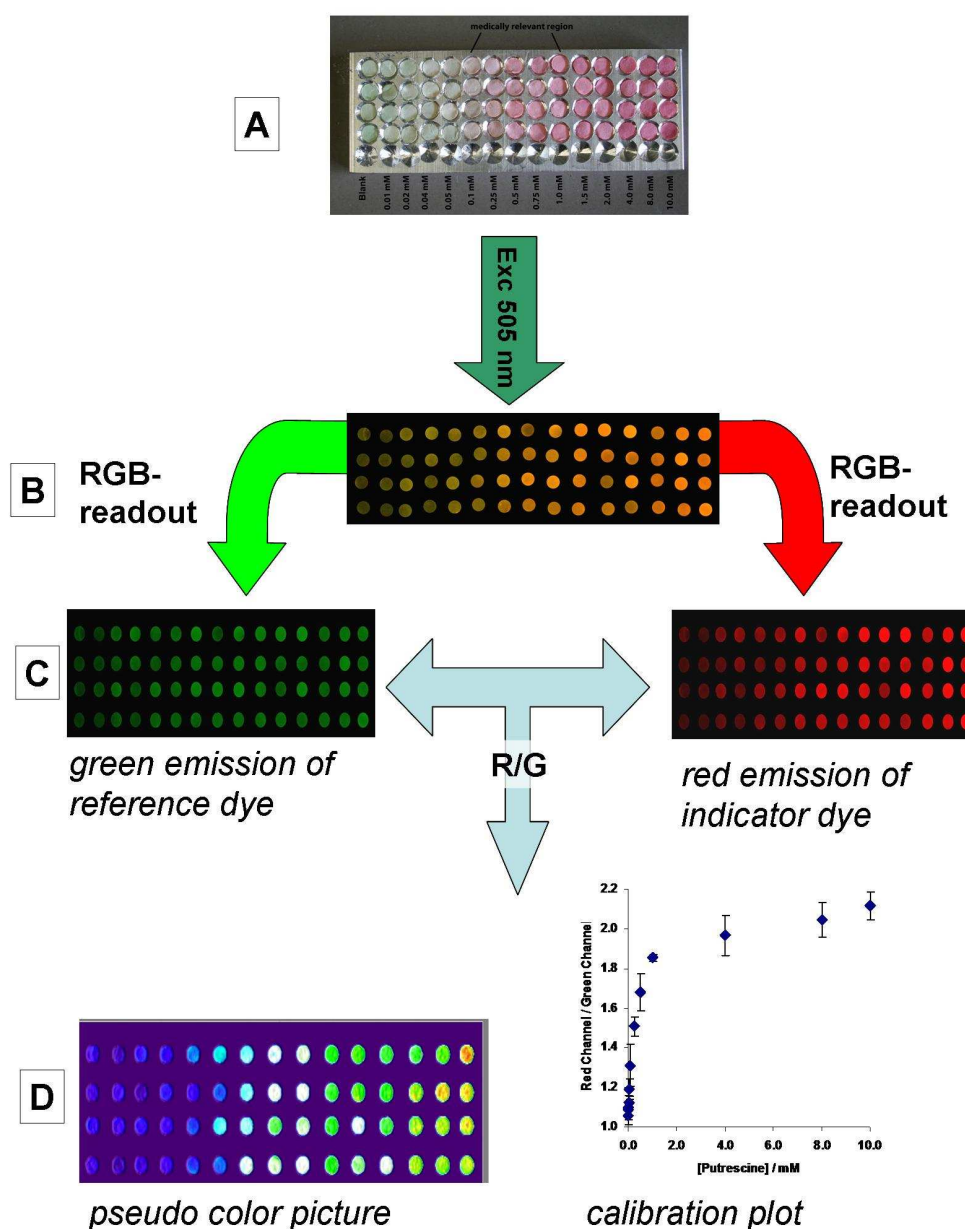
Fig. 6.14 Readout scheme. **(A)** Photograph of sensing paper. Calibration of tyramine (TY; n = 4); 15 concentrations from 0 to 10 mM; photo taken after 20 min; **(B)** Photo taken with illumination *via* 505 nm LEDs and orange glass filter. Adjustment of color temperature to 2550 K and masking; **(C)** RGB readout; the green channel contains the intensity information of fluorescein, while the red channel contains that of the Py-1-TY conjugate; **(D)** Direct picture calculation (red channel picture divided by green channel picture) delivers pseudo color picture (*bottom left*). Evaluation of the histographic information of each sensor spot of the red and green channel picture yields calibration plots (*bottom right*).

6.5 References

[1] Silla Santos MH (1996) Biogenic amines: their importance in foods. Int J Food Microbiol, 29: 213-231.

[2] Paleologos EK, Kontominas MG (2004) On-Line Solid-Phase Extraction with Surfactant Accelerated On-Column Derivatization and Micellar Liquid Chromatographic Separation as a Tool for the Determination of Biogenic Amines in Various Food Substrates. Anal Chem, 76: 1289-1294.

[3] Önal A (2007) A review: Current analytical methods for the determination of biogenic amines in foods. Food Chem, 103: 1475-1486.

[4] Taylor SL, Stratton JE, Nordlee JA (1989) Histamine poisoning (scombroid fish poisoning): an allergy-like intoxication. Clin Toxicol, 27: 225-240.

[5] García-Acosta B, Comes M, Bricks JL, Kudinova MA, Kurdyukov VV, Tolmachev AI, Descalzo AB, Marcos MD, Martínez-Máñez R, Moreno A, Sancenón F, Soto J, Villaescusa LA, Rurack K, Barat JM, Escriche I, Amorós P, (2006) Sensory hybrid host materials for the selective chromo-fluorogenic detection of biogenic amines. Chem Comm, 21: 2239-2241.

[6] Latorre-Moratalla ML, Bosch-Fusté J, Lavizzari T, Bover-Cid S, Veciana-Nogués MT, Vidal-Carou MC (2009) Validation of an ultra high pressure liquid chromatographic method for the determination of biologically active amines in food. J Chromatogr A, 1216: 7715-7720.

[7] Guggenheim M (1924) Die Biogenen Amine. Von Julius Springer Verlag, Berlin

[8] Eccleston D, Crawford TBB, Ashcroft GW (1963) Tryptamine in the Blood and Urine of a Patient with a Carcinoid Tumour. Nature, 197: 502-503.

[9] Toninello A, Pietrangeli P, De Marchi U, Salvi M, Mondovì B (2006) Amine oxidases in apoptosis and cancer. Biochim Biophys Acta, 1765: 1-13.

[10] Kubota S, Okada M, Imahori K, Ohsawa N (1983) A new simple enzymatic assay method for urinary polyamines in humans. Cancer Res, 43: 2363-2367.

[11] Medina MA, Urdiales JL, Rodríguez-Caso C, Javier Ramírez F, Sánchez-Jiménez F (2003) Biogenic amines and polyamines: similar biochemistry for different physiological missions and biomedical applications. Crit Rev Biochem Mol Biol, 38: 23-59.

[12] Xu CX, Marzouk SAM, Cosofret VV, Buck RP, Neuman MR, Sprinkle RH (1997) Development of a diamine biosensor. Talanta, 44: 1625-1632.

[13] Banchaabouchi MA, Marescau B, D'Hooge R, Engelborghs S, De Deyn PP (2000) Consequences of renal mass reduction on amino acid and biogenic amine levels in nephrectomized mice. Amino Acids, 18: 265-277.

[14] Özdestan Ö, Uren A (2009) A method for benzoyl chloride derivatization of biogenic amines for high performance liquid chromatography. Talanta, 78: 1321-1326.

[15] Steiner M-S, Meier, RJ Spangler C, Duerkop A, Wolfbeis OS (2009) Determination of biogenic amines by capillary electrophoresis using a chameleon type of fluorescent stain. Microchim Acta, 167: 259-266.

[16] Awan MA, Fleet I, Thomas CLP (2008) Determination of biogenic diamines with a vaporisation derivatisation approach using solid-phase microextraction gas chromatography–mass spectrometry. Food Chem, 111: 462-468.

[17] Lapa-Guimarães J, Pickova J (2004) New solvent systems for thin-layer chromatographic determination of nine biogenic amines in fish and squid. J Chromatogr A, 1045: 223-232.

[18] Alonso-Lomillo MA, Domínguez-Renedo O, Matos P, Arcos-Martínez MJ (2010) Disposable biosensors for determination of biogenic amines. Anal Chim Acta, 665: 26-31.

[19] Rogers PL, Staruszkiewicz WF (2000) Histamine test kit comparison. J Aquat Food Prod Tech, 9: 5-17.

20 Nelson TL, Tran I, Ingallinera TG, Maynor MS, Lavigne JJ (2007) Multi-layered analyses using directed partitioning to identify and discriminate between biogenic amines. Analyst, 132: 1024-1030.

21 Hall M, Eldridge DB, Saunders RD, Fairclough DL, Bateman Jr RC (1995) A rapid dipstick test for histamine in tuna. Food Biotech, 9: 39-57.

22 Patange SB, Mukundan MK, Ashok Kumar K, (2005) A simple and rapid method for colorimetric determination of histamine in fish flesh. Food Control, 16: 465-472.

23 Rakow NA, Avijit S, Janzen MC, Ponder JB, Suslick KS (2005) Colorimetric sensor arrays for volatile organic compounds. Angew Chem Int Ed, 44: 4528-4532.

24 Tang Z, Yang J, Yu J, Cui B (2010) A Colorimetric Sensor for Qualitative Discrimination and Quantitative Detection of Volatile Amines. Sensors, 10: 6463-6476.

25 Sutarlie L, Quin H, Yang K-L (2010) Polymer stabilized cholesteric liquid crystal arrays for detecting vaporous amines. Analyst, 135: 1691-1696.

26 Filippini D, Alimelli A, Di Natale C, Paolesse R, D'Amico A, Lundström I (2006) Chemical Sensing with Familiar Devices. Angew Chem Int Ed, 45: 3800-3803.

27 Lim SH, Feng L, Kemling JW, Musto CJ, Suslick KS (2009) An optoelectronic nose for detection of toxic gases. Nature Chem, 1: 562-567.

28 Rakow NA, Suslick KS (2000) A colorimetric sensor array for odour visualization. Nature, 406: 710-713.

29 Wang X-D, Meier RJ, Link M, Wolfbeis OS (2010) Photographing Oxygen Distribution. Angew Chem Int Ed, 49: 4907-4909.

30 Hoefelschweiger BK, Duerkop A, Wolfbeis OS (2005) Novel type of general protein assay using a chromogenic and fluorogenic amine-reactive probe. Anal Biochem, 344: 122-129.

31 Craig DB, Wetzl BK, Duerkop A, Wolfbeis OS (2005) Determination of picomolar concentrations of proteins using novel amino reactive chameleon labels and capillary electrophoresis laser-induced fluorescence detection. Electrophoresis, 26: 2208-2213.

32 Wetzl BK, Yarmoluk SM, Craig D, Wolfbeis OS (2004) Chameleon labels for staining and quantifying proteins. Angew Chem Int Ed, 43: 5400-5402.

33 Meier RJ, Steiner M-S, Duerkop A, Wolfbeis OS (2008) SDS-PAGE of proteins using a chameleon-type of fluorescent prestain. Anal Chem, 80: 6274-6279.

34 Stoy VA (1988) New type of hydrogel for controlled drug delivery. J Biomater Appl, 3: 552-604.

35 Ramseyer P, Meagher-Villemure K, Burki M, Frey P (2007) (Poly)acrylonitrile-based hydrogel as a therapeutic bulking agent in urology. Biomater, 28: 1185-1190.

36 Maynor MS, Nelson TL, O'Sullivan C, Lavigne JJ (2007) A Food Freshness Sensor Using the Multistate Response from Analyte-Induced Aggregation of a Cross-Reactive Poly(thiophene). Org Lett, 9: 3217-3220.

37 Hwang D-F, Chang S-H, Shiau C-Y, Cheng C-C (1995) Biogenic Amines in the Flesh of Sailfish (Istiophorus platypterus) Responsible for Scombroid Poisoning. J Food Sci, 60: 926-928.

38 Chemnitius GC, Bilitewski U (1996) Development of screen-printed enzyme electrodes for the estimation of fish quality. Sens Act B, 32: 107-113.

39 Niculescu M, Nistor C, Frébort I, Pec P, Mattiasson B, Csöregi E (2000) Redox Hydrogel-Based Amperiometric Bienzyme Electrodes for Fish Freshness Monitoring. Anal Chem, 72: 1591-1597.

40 McDonagh C; Burke CS; MacCraith BD (2008) Optical chemical sensors. Chem Rev, 108: 400-422.

41 Wang X, Chen H, Zhao Y, Chen X, Wang X (2010) Optical oxygen sensors move towards colorimetric determination. Trends Anal Chem, 29: 319-338.

7 Summary

7.1 In English

Fluorescent probes for the determination of biologically relevant anions like acetate (Ac), and acetyl phosphate (AcP) were investigated. Two known probes for anions were screened for their spectral responses towards these target molecules. With the insights obtained, new luminescent probes based on ruthenium complexes were designed, synthesized, and characterized with respect to selectivity towards AcP in organic solvents and highly competitive aqueous solutions and response towards other biologically important anions.

The determination of acetyl phosphate was successfully accomplished using the fluorogenic probe RuPDO. This complex contains two oxime groups that are activated *in situ* by the addition of Zn^{2+}. The rapid and direct determination of acetyl phosphate was conducted in highly biocompatible aqueous solutions at neutral pH. The metal complex itself is almost non-fluorescent (λ_{exc} = 469 nm , λ_{em} = 610 nm). The intensity of emission undergoes ca. 30-fold enhancement upon reaction with AcP in low mM concentrations in HEPES buffer at pH 7.4. An incubation time of 60 min at 37 °C is required. Upon reaction with AcP, the probe shows a 30 nm-longwave shift of emission to 640 nm. Most importantly, and unlike in common methods for determination of AcP, the presence of millimolar inorganic phosphate only weakly reduces sensitivity. Successful determination of AcP in complex biological matrices like cell medium and bacterial growth medium (even in presence of lysed cells) was shown.

Furthermore, a combination of RuPDO with the enzyme acetate kinase (AK) yielded a microplate assay for the determination of the important target acetate. The analyte was successfully determined with the developed assay in various real samples (even in strongly colored samples) with excellent compliance to the manufacturer information. The linear range of the method is from 100 µM to 2 mM. The LOD of the assay is comparable to commercially available enzymatic acetate kits. Though, the acetate assay developed is more robust and inexpensive due to the use of only one enzyme.

Sensing strips for biogenic amines containing an amine-reactive dye are described in Chapter 6. These additionally contain a green fluorescent (amino-insensitive) reference dye incorporated in a hydrogel matrix that is deposited on a

paper strip. Such strips enable rapid and direct determination of primary amines – especially biogenic amines (BA). A color change from blue to red occurs on addition of the test strips to a slightly alkaline sample containing primary amines in a concentration range from 0.01 to 10 mM within 15 min, thus enabling rapid qualitative and semi-quantitative evaluation. The color shift is accompanied by a strong increase of the fluorescence intensity of the dye, with a peak at 620 nm after photo-excitation at 505 nm with LEDs. A home-built setup was used for quantitative readout of the strips containing high-power 505-nm LEDs in a black box and a digital camera. The strips are photographed and the digital color information stored in the camera is extracted *via* a red-green-blue (RGB) readout. By referencing the red channel to the green channel, a quantitative signal is obtained that was used to create pseudo-color pictures of the sensor spots and for calculation of calibration plots. Finally, the sensing system was also successfully applied to the monitoring of the spoilage of different kinds of meat.

7.2 In German

Diese Arbeit beschreibt neue fluoreszente Sonden für den Nachweis der biologisch wichtigen Anionen Acetat und Acetylphosphat. Dabei wurde zuerst das Ansprechen zweier literaturbekannte Sonden auf die Zielanalyten evaluiert. Mit Hilfe der gewonnenen Erkenntnisse konnten neue, fluoreszierende Sonden auf Basis von Ruthenium-Komplexen entworfen, synthetisiert und charakterisiert werden. Insbesondere wurden die Sonden auf selektive Erkennung von Acetylphosphat in organischen Lösungsmitteln und kompetitiven wässrigen Lösungen untersucht.

Die Experimente mit den Anionensonden führten zur Entwicklung der Sonde RuPDO für den Nachweis von AcP. Die Sonde trägt zwei vicinale Oxim-Gruppen, die *in situ* durch Zn^{2+}-Ionen aktivierbar sind. Der schnelle und direkte Nachweis von Acetylphosphat konnte in biokompatiblen, wässrigen Lösungen bei neutralem pH-Wert erfolgen. Der Metall-Liganden-Komplex selbst ist nicht fluoreszent (λ_{exc} = 469 nm, λ_{em} = 610 nm). Seine Emission verstärkt sich aber durch die Reaktion mit AcP in niedrigen mM Konzentrationen in neutralem HEPES Puffer ca. um das 30-fache. Während der Reaktion von 60 min bei 37 °C verschiebt sich das Emissionsmaximum der Sonde um 30 nm langwelliger auf 640 nm. Bemerkenswerterweise und im Gegensatz zu anderen üblichen Methoden zum Nachweis von Acetylphosphat ist in

Gegenwart millimolarer Konzentrationen von anorganischem Phosphat eine kaum reduzierte Selektivität beobachtbar. AcP wurde auch erfolgreich in komplexen biologischen Matrices wie z.B. Zellmedium und Bakterienwachstumslösung, die sogar lysierte Zellen enthielt, nachgewiesen.

Eine Kombination aus RuPDO und dem Enzym Acetatkinase (AK) ermöglichte die Entwicklung eines enzymatischen und fluoreszenzbasierten Assays für den Analyten Acetat. Dieses wurde mit dem Assay in unterschiedlichen (und auch stark gefärbten) Realproben in Mikrotiterplatten in ausgezeichneter Übereinstimmung zu den Herstellerangaben bestimmt.

Des Weiteren wurden Teststreifen zum Nachweis biogener Amine (BA) entwickelt, die einen aminreaktiven Farbstoff und einen grün fluoreszierenden (nicht aminreaktiven) Referenzfarbstoff enthalten. Beide sind in eine Hydrogelmatrix eingebettet, welche auf Papierstreifen aufgetragen wird. Diese Teststreifen ermöglichen den schnellen und direkten Nachweis von primären Aminen – vor allem von biogenen Aminen. Es erfolgt ein Farbwechsel von blau nach rot, wenn der Teststreifen in eine schwach basische und aminhaltige Lösung getaucht wird. Amine können rasch quantitativ und mit dem bloßen Auge semi-quantitativ in einem Konzentrationsbereich von 0.01 bis 10 mM innerhalb von 15 min bestimmt werden. Gleichzeitig mit dem Farbumschlag erfolgt ein starker Anstieg der Fluoreszenz des aminreaktiven Farbstoffs bei 620 nm nach LED-Anregung bei 505 nm. Für den quantitativen fluorometrischen Nachweis von biogenen Aminen und deren bildgebende Darstellung wurde ein apparativer Eigenbau zur Auswertung der Teststreifen eingesetzt. Dieser besteht aus einer lichtundurchlässigen Messkammer in der 505 nm Hochleistungs-LEDs als Lichtquelle dienen und eine digitale Spiegelreflexkamera zur Messung benutzt wird. Die Teststreifen werden in dieser Kamera fotografiert und die digitale Farbinformation mittels rot-grün-blau (RGB) Ausgabe extrahiert. Durch die Referenzierung des Signals des roten zum grünen Farbkanal erhält man ein quantitatives Signal, das benutzt werden kann, um Falschfarbenbilder der Sensorfläche und Kalibrationskurven zu ermitteln. Das Messsystem wurde schließlich auch erfolgreich zur Beobachtung des Verderbens verschiedener Lebensmittelproben eingesetzt.

8 Curriculum Vitae

Mark-Steven Steiner

born on July 15, 1983 in Vienna (Austria)

Education

10/2007 - present	**PhD Thesis at the Institute of Analytical Chemistry, Chemo- and Biosensors, Prof. Otto S. Wolfbeis:**
	„Optical Detection of Acetyl Phosphate and Biogenic Amines"
09/2007	**Diploma degree in Chemistry (equivalent to M. Sc.)**
10/2002 - 09/2007	**Chemistry Studies, Diploma, Regensburg University**
	Diploma Thesis at the Institute of Analytical Chemistry, Chemo- and Biosensors, Prof. Otto S. Wolfbeis:
	"Fluorogenic Label for Biogenic Amines, and Their Determination via Laser Induced Fluorescence Capillary Electrophoresis"
06/2002	**General qualification for university entrance ("Abitur")**
	Gabelsberger Gymnasium, Mainburg

Work Experience

07/2000 - 09/2009	**Regular Summer Jobs at Nat-Labs GmbH (Siegenburg) (Manufacturer of dietary supplement and diagnostics)**
10/2006 - present	**Regular Tasks as Student and Graduate Assistant:**
	Supervision of laboratory courses for medical, dentistry and chemistry students, tutorial in inorganic chemistry for medical and dentistry students, supervision of a bachelor student, supervision of three apprentices (lab technician), supervision of exchange students
10/2007 - present	**Private lessons in inorganic chemistry for medical and dentistry students**

Language Skills

German   native

English   fluent

Publications

M.-S. Steiner, R. Meier, C. Spangler, A. Duerkop, O.S. Wolfbeis, **Determination of Biogenic Amines by Capillary Electrophoresis Using a Chameleon-Type of Fluorescent Stain**, *Microchim. Acta* 2009, 167, 259-266.

R. J. Meier, M.-S. Steiner, A. Duerkop, O. S. Wolfbeis, **SDS-PAGE of Proteins Using a Chameleon-Type of Fluorescent Prestain**, *Anal. Chem.* 2008, 80, 6274-6279.

M.-S. Steiner, A. Duerkop, **Luminescent ruthenium probe for the determination of acetyl phosphate in complex biological matrices**, *Analyst, 2010,* DOI: 10.1039/c0an00439a.

M.-S. Steiner, A. Duerkop, O. S. Wolfbeis, **Chromogenic Sensing of Biogenic Amines Using a Chameleon Probe and the RGB-Readout of Digital Camera Images**, *Analytical Chemistry 2010,* 82, 8402-8405.

M.-S. Steiner, A. Duerkop, O. S. Wolfbeis, **Glucose Sensing and Glucose Determination Using Fluorescent Probes,** in J. Popp**, Handbook of Biophotonics,** *accepted*

M.-S. Steiner, A. Duerkop, O.S. Wolfbeis O. S., Review: **Glucose Sensing and Glucose Determination,** Chem. Soc. Review (invited), *in preparation.*

G.M. Khairy, M.-S. Steiner, A. Duerkop, H.A. Azab, S.A. El-Korashy, Z.M. Anwar, **High-Throughput Sensor Microtiter Plate for Determination of Biogenic Amines in Sea Food using fluorescence or eye-vision**, *in preparation*.

Posters and Presentations

Conference Methods and Applications of Fluorescence MAF-11 2009, Budapest, (Poster):

"Ruthenium Complex with Oxime Ligand as Luminescent Probe for Acetyl Phosphate"

6th International Students Conference 'Modern Analytical Chemistry' 2010, Prague, (Oral Presentation):

"Sensing strip for biogenic amines using a chromogenic (chameleon) probe, a reference dye, and RGB optical readout"

Conferences

European Association for Chemical and Molecular Sciences EuCheMS 2008, Turin

Methods and Applications of Fluorescence MAF-11 2009, Budapest

6th International Students Conference 'Modern Analytical Chemistry' 2010, Prague